IIT RESEARCH INSTITUTE
Technology Center
Chicago, Illinois 60616

IITRI Project No. M6066
Summary of Research Report

DEBRIS DISTRIBUTION

by

D. I. Feinstein

Contract No. OCD-PS-64-50
OCD Work Unit 3322B

Office of Civil Defense
Washington, D. C.

March, 1966

DEBRIS DISTRIBUTION
SUMMARY

INTRODUCTION

This study is a continuation of the "DEBRIS CLEARANCE STUDY."* That study developed methods of estimating gross debris accumulation in various types of urban areas, based on total structural demolition and uniform distribution of the debris over a given size area.

The present study intends to improve the degree of sophistication of predicting debris distribution. The modus operandi of this improvement was to divide debris into two categories; stationary and transportable. Application of fragmentation and trajectory models was made on the transportable debris and distribution was based on this type of debris. Although transportable debris may originate from such sources as buildings, automobiles, communication equipment, public utilities, and any other exposed object, this report addresses itself exclusively to buildings. To be specific, brittle wall elements of buildings were studied in detail. Because of blast orientation, thermal effects and material properties, brittle wall elements were considered to be one of the primary sources of transportable debris.

A descriptive outline for estimating debris distribution, in an area of interest, was developed. It was shown that if one can specify the relationship between load and fragment piece size distribution (i.e., fragmentation) then area-wide debris distributions may be developed with a fair degree of confidence.

In order to predict the fragmentation of a brittle wall element an analytical model was developed. This model was based on a probabilistic approach and the basic underlying assumptions were verified by experimentation. Debris profiles of transportable debris were developed utilizing the analytical fragmentation model and a trajectory analysis.

*Ahlers, E. B., "Debris Clearance Study," IIT Research Institute, for the Office of Civil Defense, OCD-PS-62-202, Subtask 3322-A, September 1962.

FINDINGS

In order to demonstrate the feasibility of the techniques developed a hypothetical structure was analyzed. This structure consisted of a single wall composed of similar masonry wall panels. The individual panels were 8 ft-6 in. high and 6 in. thick. This panel when suitably idealized and uniformly loaded yielded the fragmentation characteristics as shown in Fig. S. 1. This curve illustrates that fragmentation occurs at about 8 psi and total fragmentation is achieved at about 20 psi. Figure S. 2 illustrates the transport characteristics of the resulting panel fragments under similar loading conditions and at various heights above ground. Information obtained from Fig. S. 1 and S. 2, together with some knowledge of wall dimensions are sufficient to develop a debris profile for the entire wall as shown in Fig. S. 3. Walls of various heights and fragmentation characteristics were investigated and the results summarized in Table S. 1.

Table S. 1

SENSITIVITY OF DEBRIS CONTOURS TO BUILDING HEIGHT AND PARTICLE SIZE

Building Height	All Small		Predicted		All Large	
	x^*	y^*	x^*	y^*	x^*	y^*
40	514	0.003	200	0.036	200	0.085
35	496	0.0027	180	0.035	180	0.080
30	460	0.0023	165	0.032	130	0.075
25	425	0.019	155	0.029	---	---
20	400	0.015	135	0.026	130	0.060
15	350	0.012	125	0.023	125	0.055
10	300	0.009	75	0.018	90	0.045
5	175	0.006	50	0.015	40	0.040

x^*, y^* are the coordinates of the peak value of the debris profile.

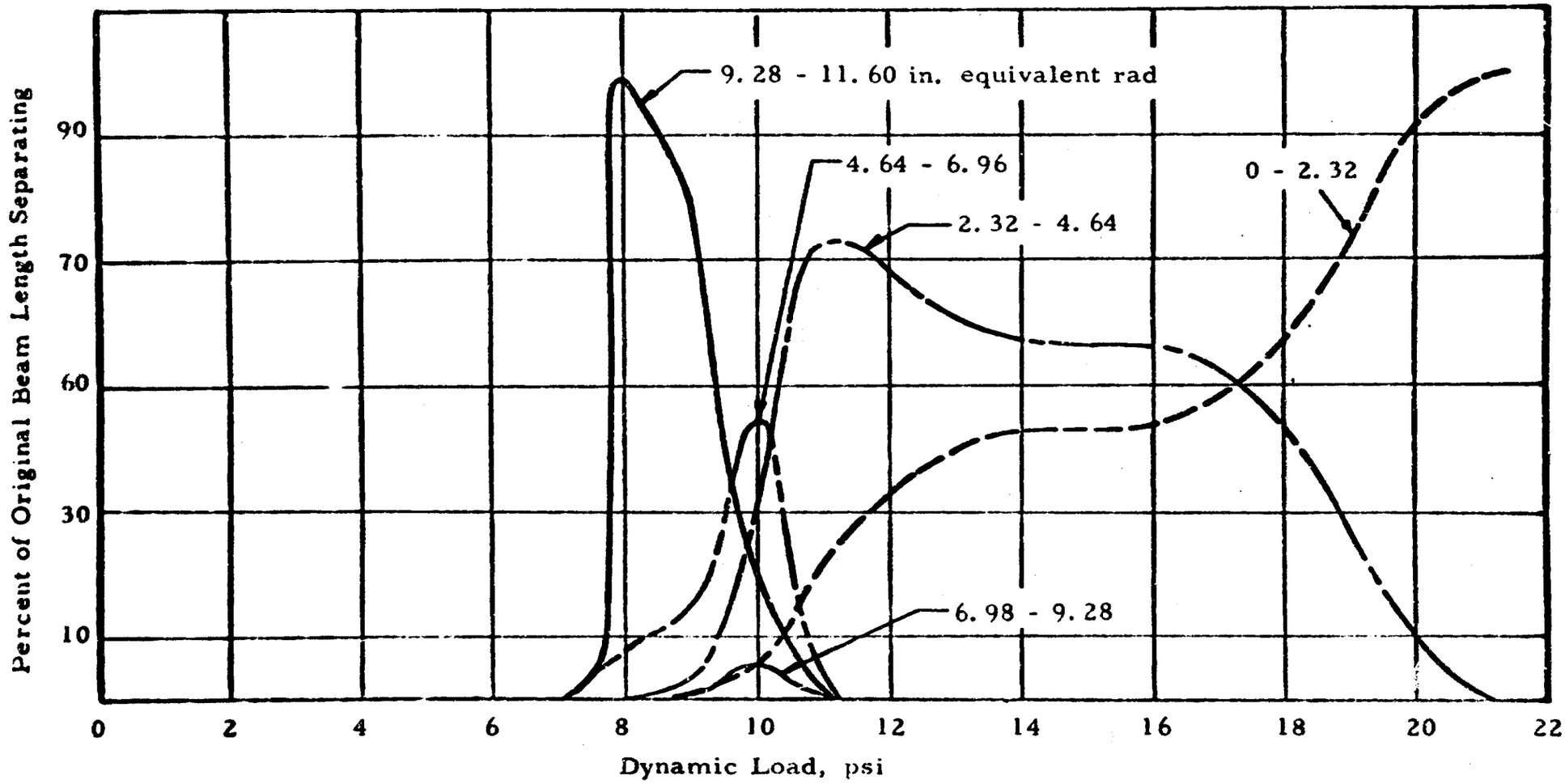

Fig. S.1 FRAGMENTATION CURVE FOR MASONRY PANEL

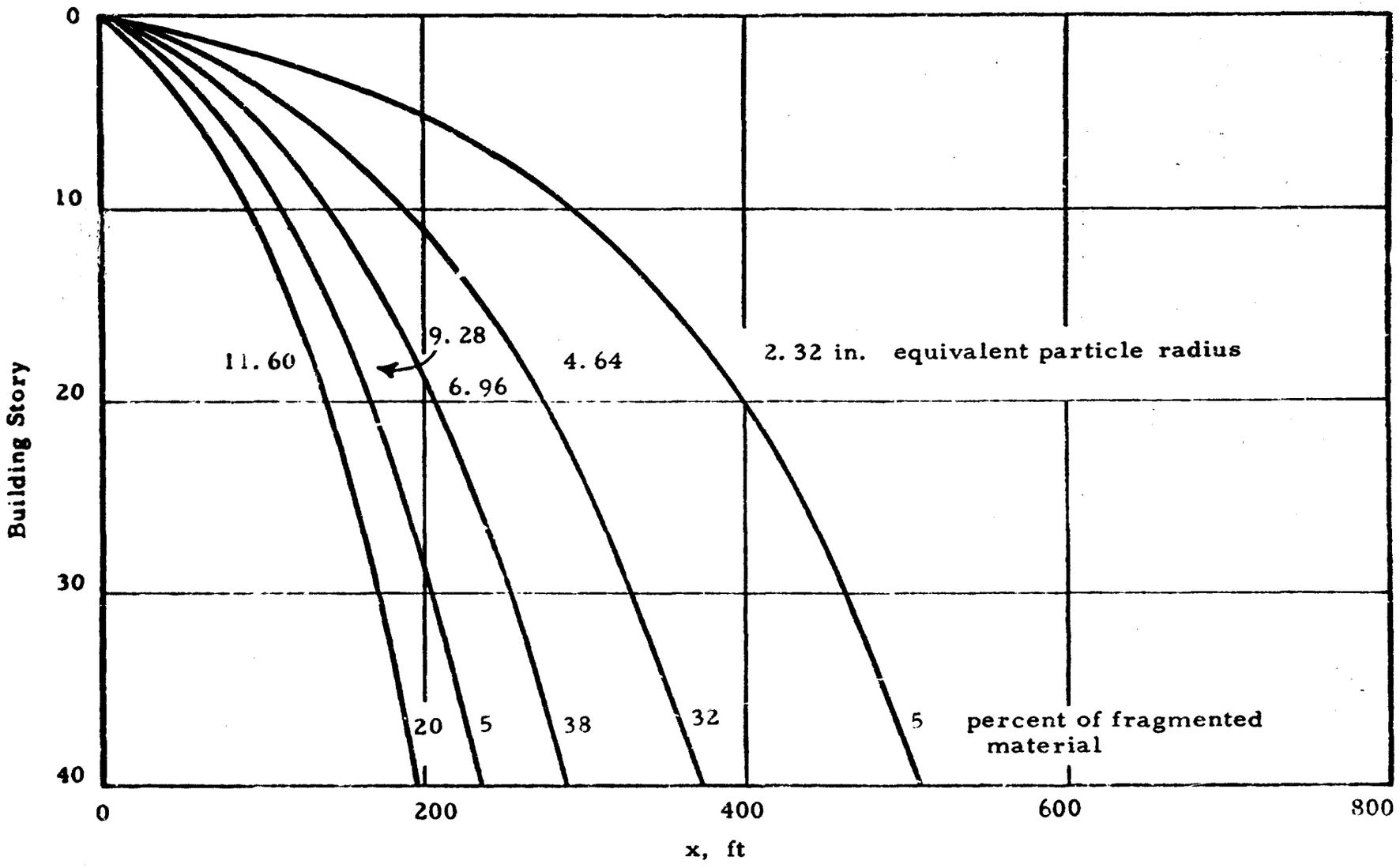

Fig. S. 2 FRAGMENTATION AND TRANSPORT CHARACTERISTICS FOR MODEL PANEL

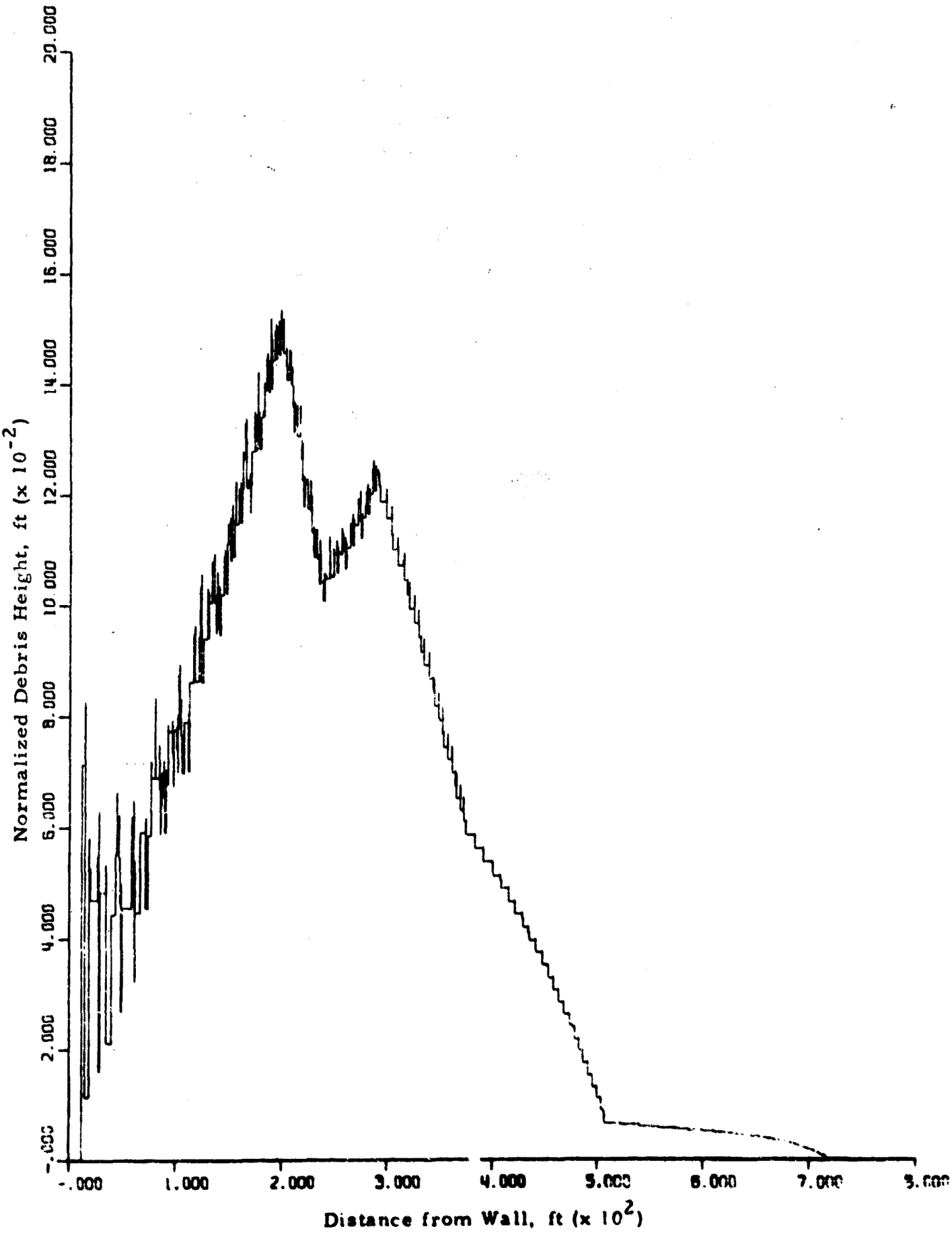

Fig. S. 3 DEBRIS PROFILE FOR A WALL HEIGHT OF 40 STORIES EXPOSED TO 10 psi AT 1 MT

The findings of this study may be summarized as follows.

1. Debris may be divided into two categories, offsite and onsite. Onsite debris prevents no impedance to logistic activity other than localized shelter rescue operations.

2. In order to characterize offsite debris profiles, the piecesize distribution of the fragments must be known. This is in order to characterize the particle's trajectory.

3. Low level dwellings must be included as potential debris producing structures. Even elements at 10 ft above ground may be transported significant distances (e. g., into the street) at moderate overpressure levels (10 psi).

4. In general, smaller particles from higher initial heights will be transported greater distances than larger particles at lower heights. As overpressure increases the size of the particle fragmenting will be smaller.

5. Particles fragmenting and being transported offsite from their original position will have an extremely high terminal velocity (i. e., at least 50 ft per sec). For this reason, offsite debris must be considered an extremely dangerous secondary effect of blast. This effect must be evaluated in light of its damage producing capabilities to structures as well as a casualty producing mechanism to unsheltered populence.

6. The assumption that the maximum dynamic stresses introduced into the various unit segments are independent of the fracture characteristics has been shown both experimentally and analytically. This establishes the theoretical development of the fragmentation model.

7. The statistical strength characteristics of typical unit segments have been expressed by their cumulative distribution function, $F(p)$. This function gives the probability of fracturing the unit at a load magnitude equal to or less than p and for computational purposes has been expressed in Weibull form. It is to be emphasized that this form was chosen for convenience. At present, Weibull parameters are not known for many common construction materials and must be determined.

8. Debris profiles from multistory walls may be generated. The profiles are typically unimodal in shape and of course are very sensitive to piecesize distribution. For walls at 5, 10, 15 stories in height profiles exist for each of three piecesize distributions, all large, predicted, and all small. It is interesting to note that the large particles generally lend most of the shape to the predicted size profile. That is, up to the peak the large size particles predominate. This, of course, is in part due to the method of developing these profiles. Large particles are distributed over much less area than small ones and hence tend to produce much greater depths.

9. The profiles have their ordinate normalized with respect to volume and packing. (Packing corresponds to a void ratio of 1.0). If the ordinate were multiplied by the unit width volume of material at one story height and then again by a suitable void ratio, then the profile would express the true depth of the building's transported debris at all points along its transported distance.

The analytical methods of fragmentation and subsequent transport did not consider either the effects of orientation of the structure to the blast or shielding of one building by another. It is therefore recommended that any follow on study should:

1. Continue to develop analytical methods for additional structural materials and elements as well as complete structures. These analytical models should be suitably verified by appropriate experimental investigation.
2. The individual building debris contours must be combined to give a cumulative debris contour for an entire subarea of contiguous structures.
3. Effects of blast orientation and structural shielding should be accounted for in specifying the load on the structure.
4. Finally, all methods developed should be combined to yield a single computational model.

DEBRIS DISTRIBUTION

ABSTRACT

This study is a continuation of the "DEBRIS CLEARANCE STUDY."[1*] That study developed methods of estimating gross debris accumulation in various types of urban areas, based on total structural demolition and uniform distribution of the debris over a given size area.

The present study makes use of several of the tools developed in the previous report and expanded herein to more accurately predict the debris distribution. Structural fragmentation is defined for a particular set of blast and structural parameters. The trajectories of the transportable material are calculated, and the distribution of this material is found by size as well as mass. In order to establish the credibility of the fragmentation theories which were developed, a series of experiments were conducted on brittle beams under dynamic loading.

A sample problem is worked out that utilizes the above techniques on a hypothetical building to illustrate how the building's debris distribution may appear under various conditions of building height and fragment size distribution.

*All references will be numbered and listed together at the end of this report.

CONTENTS

CONTENTS (Cont'd)

LIST OF ILLUSTRATIONS

LIST OF ILLUSTRATIONS (Cont'd)

LIST OF ILLUSTRATIONS (Cont'd)

INTRODUCTION AND ORGANIZATION

If there is to be any simulation of the postattack environment of any given locale, certain input information must be available to the simulation model. Among this input may be such things as specifying an urban area analytically, defining clearance priorities, and specifying debris distributions.

This report, although it is a continuation of the previous postattack report: "DEBRIS CLEARANCE STUDY,"[1] intends to improve the degree of sophistication of predicting debris distribution. The modus operandi of this improvement was to divide debris into two categories: stationary and transportable. Application of the fragmentation and trajectory models was made on the transportable debris and distribution will be based on this type of debris.

As an example of the application of the techniques developed, a hypothetical exterior masonry wall was represented by an equivalent beam analogy and debris profiles computed for various heights and size distributions.

The report is organized into five chapters. Chapter One is a descriptive outline or plan of attack for estimating debris distribution in a given area of interest. It will be shown here that if one can specify the relationship between load and fragment piecesize distribution (i.e., fragmentation) then area-wide debris distributions may be developed with a fair degree of confidence.

The phenomena of structural fragmentation of brittle materials (e.g., masonry and concrete) is discussed in Chapter Two. The fragmentation model for various brittle beam conditions is presented and the application of its results are discussed. Review of the transport model is covered here too.

Chapter Three attempts to establish the validity of the fragmentation theory discussed above. Brittle beams with various end conditions were subjected to a variety of external dynamic loadings.

An example of a hypothetical masonry wall is investigated, utilizing the methods of the previous chapters, in Chapter Four. Also developed is a procedure which allows one to develop debris profiles.

Finally, Chapter Five contains a summary, conclusions and recommendations concerning the work done in this report.

CHAPTER ONE

A MODEL FOR PREDICTING DEBRIS DISTRIBUTION

1. GENERAL

In order to predict the distribution of offsite debris in a metropolitan area, a great deal of information must be known. Lack of this information does not preclude the possibility of using intuitive assumptions. These assumptions, of course, must be pointed out as such and some qualitative, if not quantitative, check should be made on them.

In this report we wish to investigate the quantity and composition of offsite debris (e.g., debris which is transported from its original location) which hampers postattack logistical missions. Although such debris may originate from such sources as buildings, automobiles, communication equipment, public utilities, and any other exposed object, this report will address itself exclusively to buildings. To be specific, brittle wall elements of buildings will be studied in detail. Because of blast orientation, thermal effects, and material properties, brittle wall elements are considered to be one of the primary sources of the transportable debris.

The following sections of this chapter describe a step-by-step approach by which a postattack analyst might map the debris distributions for an entire metropolitan area. This approach is not to be considered unique. Any other rational method of analysis is not precluded.

1.1 Division of Metropolitan Areas by Representative Building Types

By use of aerial photographs, Sandborne maps, or some other convenient source the investigator will find that most metropolitan areas may be broken down into sub-areas which may be represented by one or, at most, only a few different types of structures. Such a sub-area may be considered homogeneous from the standpoint of potential debris production. It now becomes necessary to investigate the different types of building construction in order to evaluate the condition of each sub-area.

1.2 Specification of Blast Loading on a Single Building Type

When one investigates the formulation and transportation of debris from a single source the loading, due to primary weapon effects, must be

available in a manner such as the following:

$$P_o = P_o (W, X_o, h_b, k)$$

where,

P_o = Peak Overpressure

W = Weapon Yield

X_o = Distance from Ground Zero

h_b = Height of Burst

k = Shielding Factor

The description of the above relationship has been the subject of many investigators.[2, 3] One of the less highly investigated areas is the relationship between the shielding factor, k, and the degree of structural density at the distance X_o.

1.3 Debris Production for a Single Building

The next step in establishing debris levels for structures is to describe the actual distribution of material in a particular building. This may be shown in the manner illustrated in Fig. 1.1. Each curve is symbolic of different types of materials and might include concrete, masonry, plaster, etc.

It becomes necessary, next, to be able to predict the piecesize distribution of these materials as a function of the loading on the structure. Such a relationship is shown in Fig. 1.2.

1.4 Final Deposition of Debris Material for a Single Building

If the initial position and size of debris is known, it is possible to accurately predict its transported position on the ground by computing its trajectory. In order to get a picture of how the debris accumulates or distributes something must be known about the available open area surrounding the debris particle's final transported position. That is, in an open region debris can spread out and not be as deep as it might be under more crowded conditions.

It is possible, therefore, to draw the distribution curve of offsite debris, for a single structure, if a one to one correspondence between

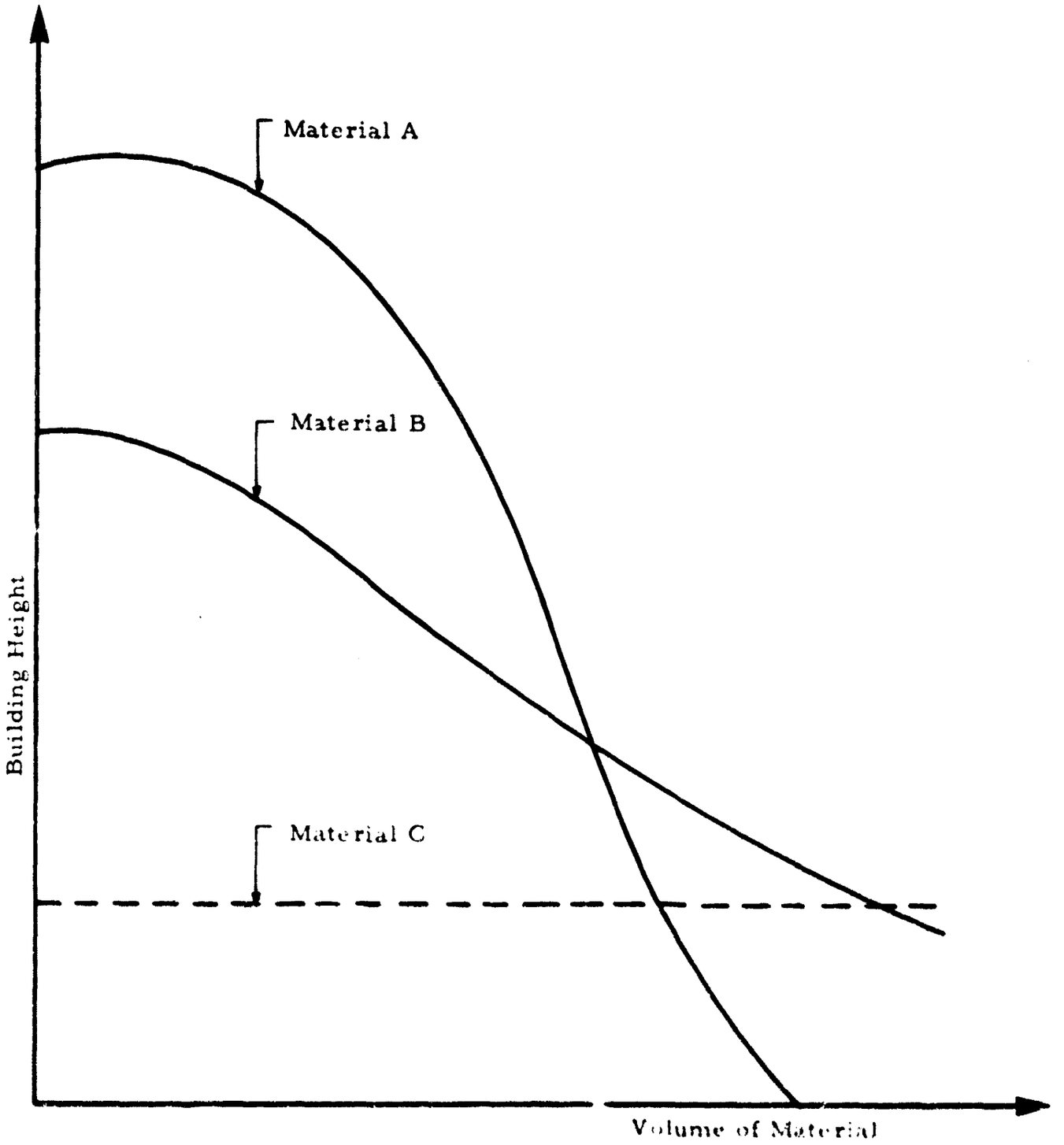

Fig. 1.1 DISTRIBUTION OF BUILDING MATERIAL

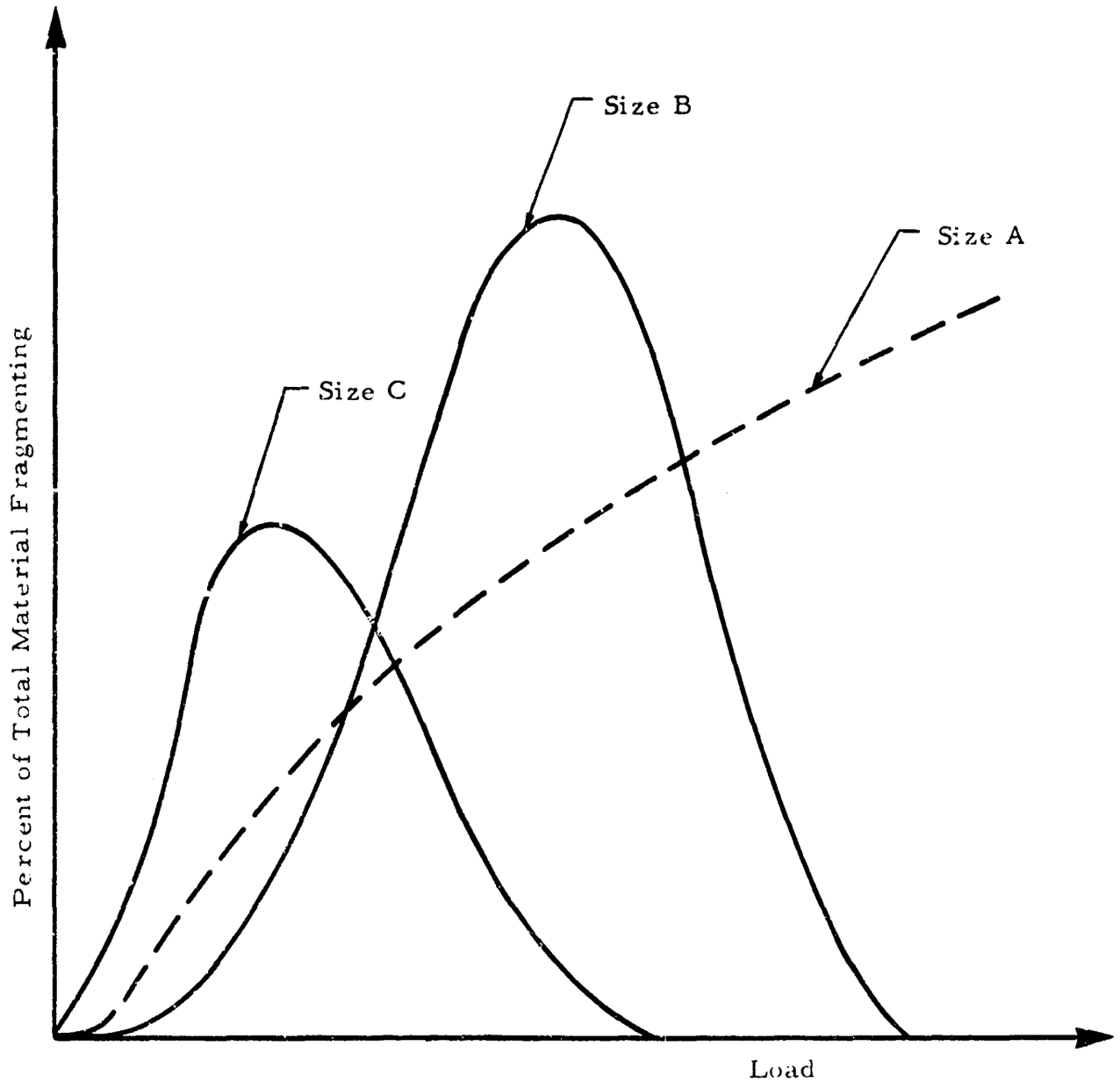

Fig. 1.2 PIECESIZE DISTRIBUTION FOR MATERIAL B

debris produced and final ground position is known. Such a curve may very well turn out to look like the one shown in Fig. 1.3. It is observed that the maximum debris level, y^*, occurs at some distance, x^*, from the structure for a particular loading.

1.5 Estimating Level of Constant Debris for Sub-Area

Now that debris profiles, as shown in Fig. 1.3, are available for each building type in a particular sub-area, a single cumulative debris height may be determined from the envelope of the superimposed individual profiles. Such a relationship is shown in Fig. 1.4.

If x^*_{max} represents the maximum debris level distance for an individual debris profile making up the cumulative curve, then this distance will represent the inner boundary of the original sub-area. Within the inner sub-area there will be a constant level of debris equal to the cumulative debris height, y^*_{max}. This is shown in Fig. 1.5 and is a conservative estimate. Figure 1.6 represents these "islands" of constant debris height within the overall area. It remains to interpolate the debris depths between the islands.

1.6 Interpolation Based on Blast Angle of Incidence

Up to this point it has been assumed that the blast impinges at normal incidence on the structure. This assumption was made to simplify the loading analysis. At this point, however, the blast angle of incidence (i.e., to each "debris island") may now be introduced to help weight the process of interpolation of the debris level between islands. The final result of such a process leads to a map of debris level for the entire area under investigation. Such a map is pictured in a qualitative manner in Fig. 1.7.

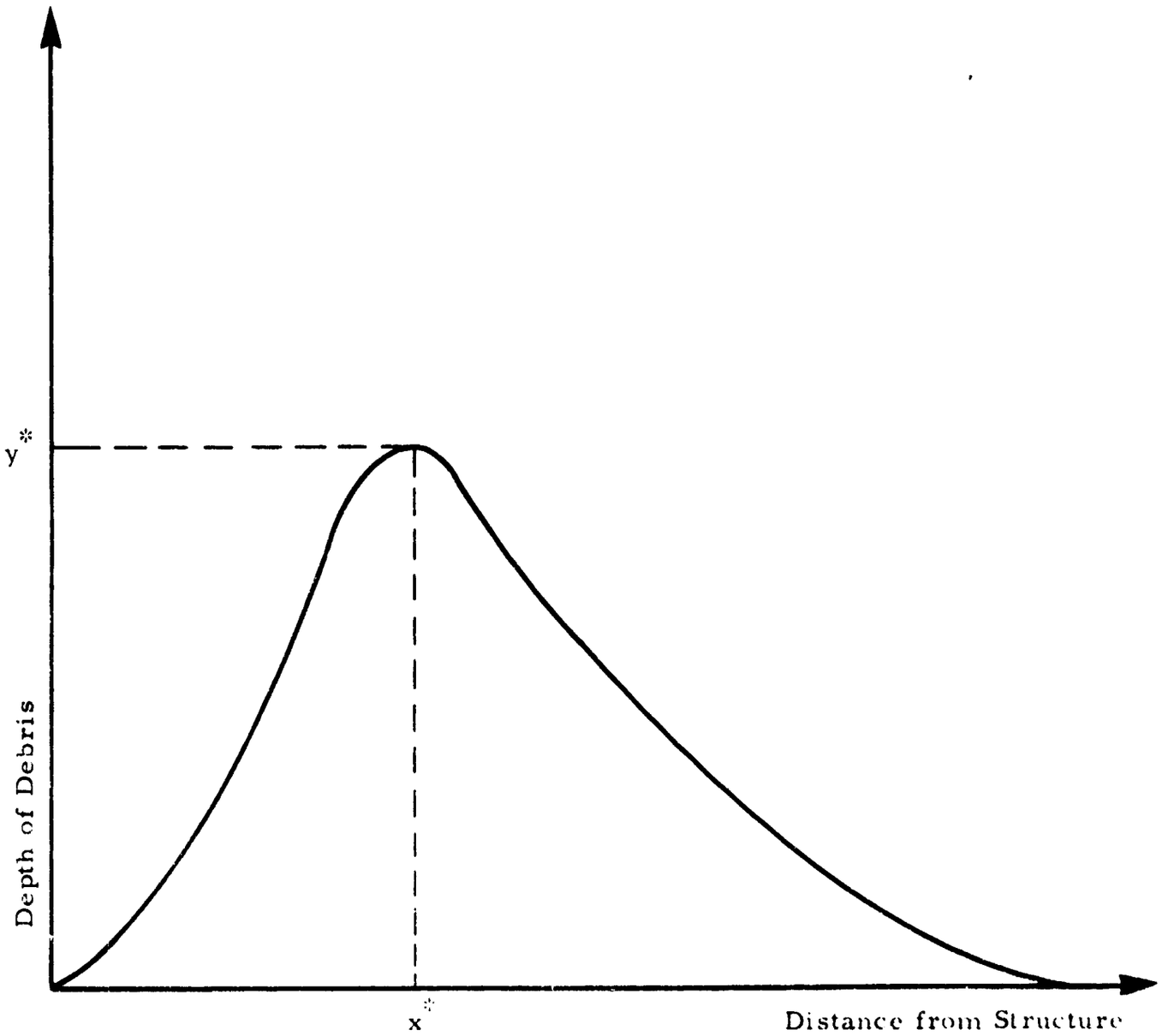

Fig. 1.3 OFFSITE DEBRIS PROFILE FOR A SINGLE STRUCTURE

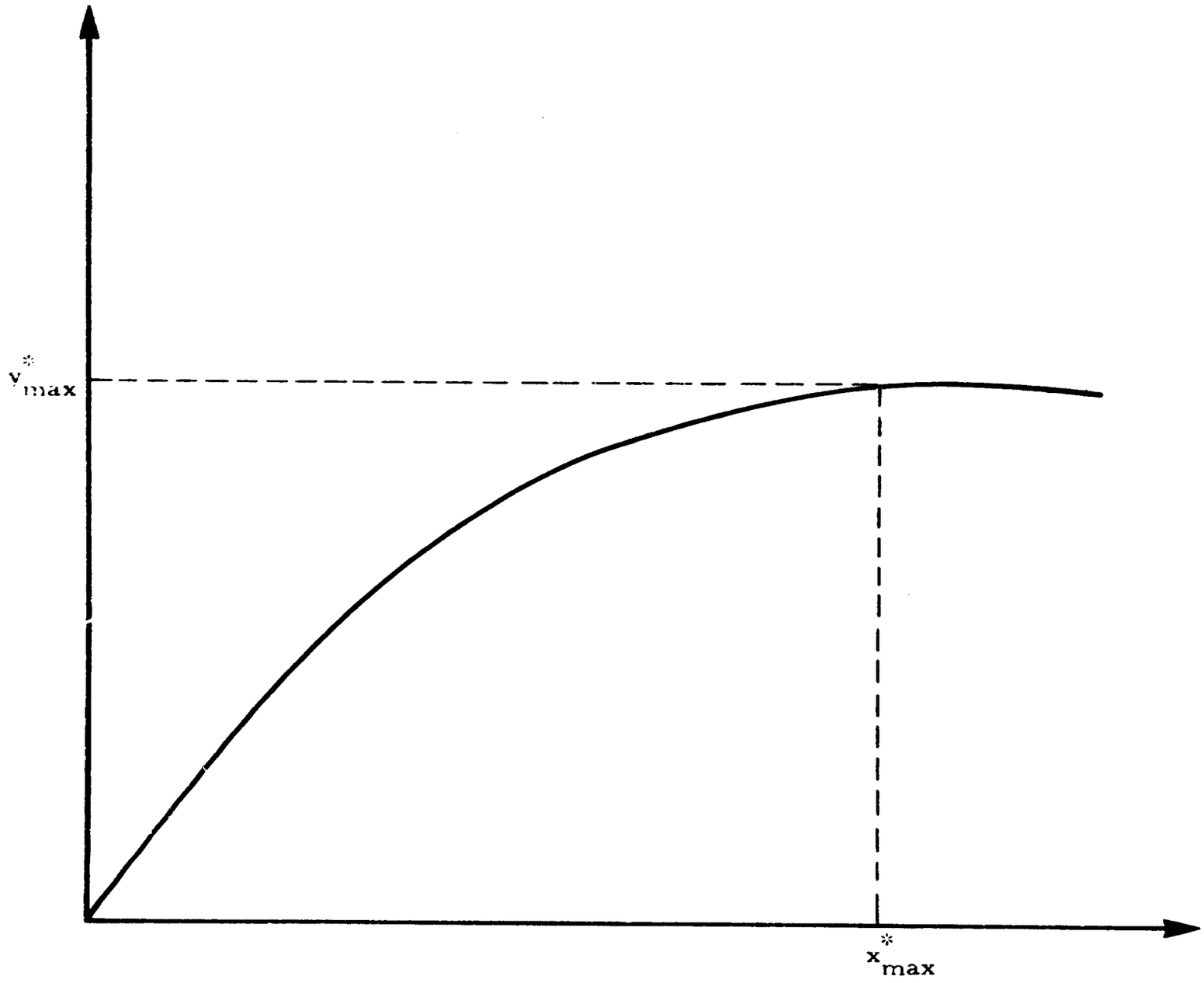

Fig. 1.4 CUMULATIVE OFFSITE DEBRIS PROFILE FOR A SUB-AREA

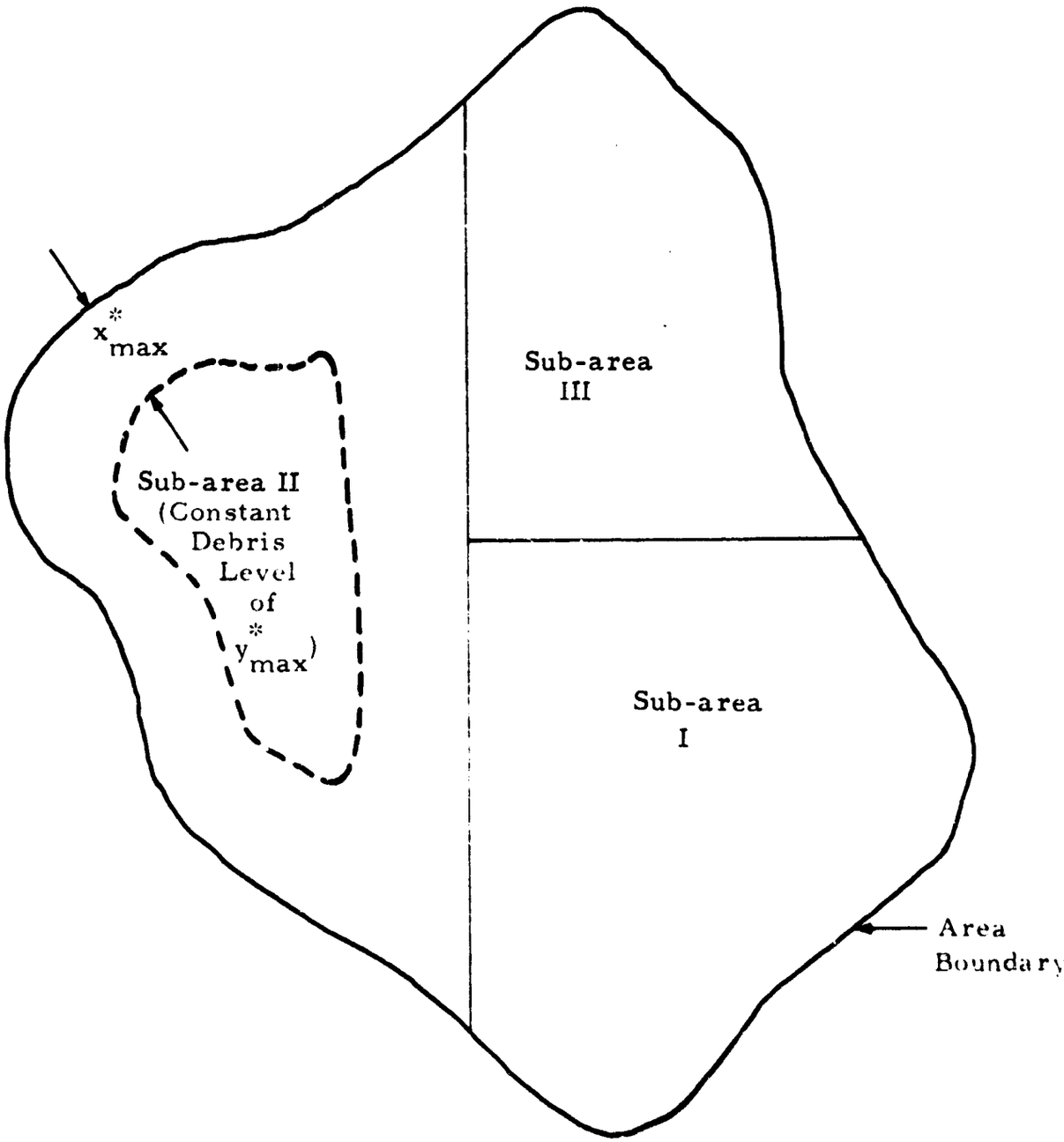

Fig. 1.5 FORMATION OF "DEBRIS ISLAND" WITHIN A SUB-AREA

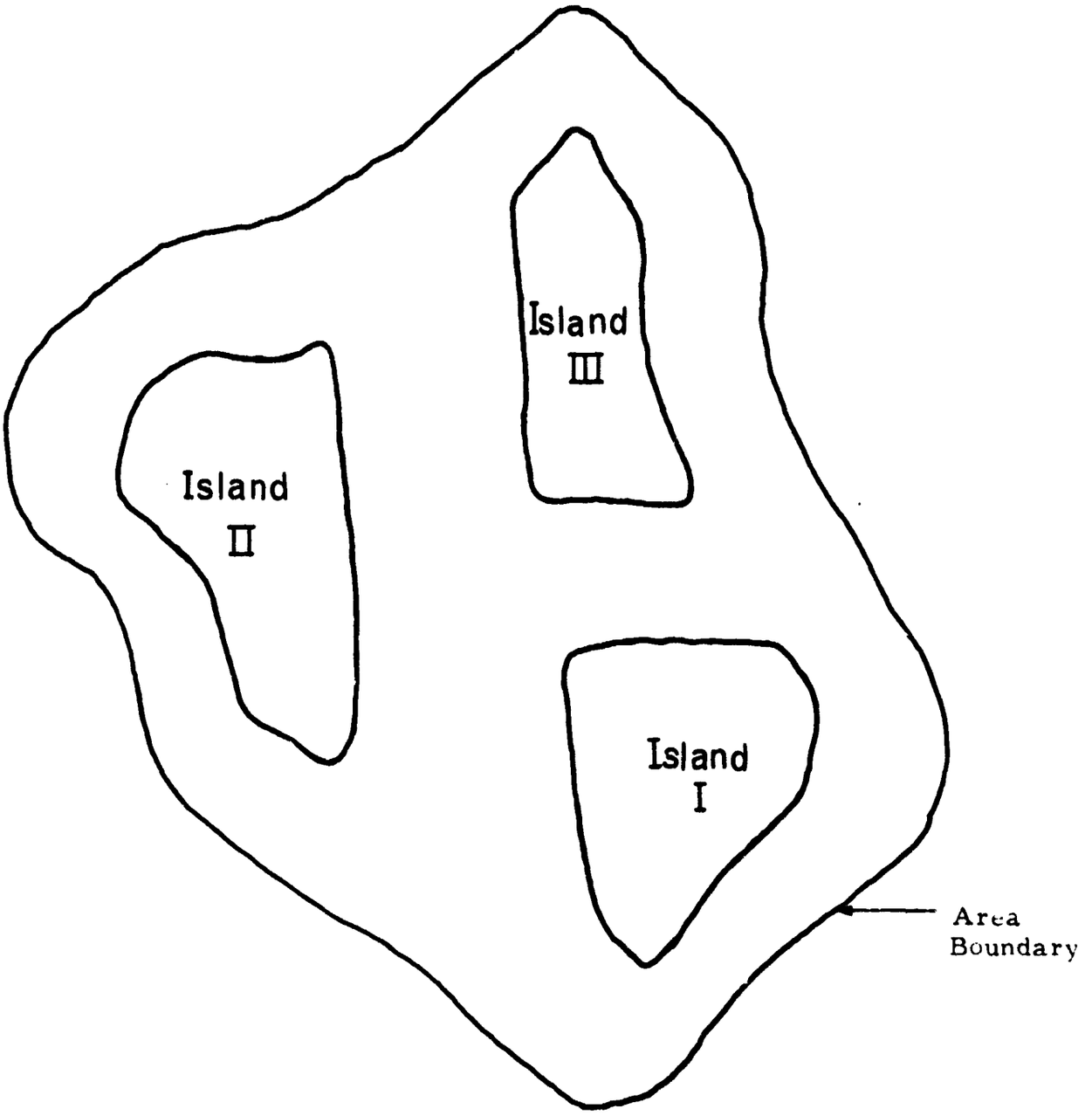

Fig. 1.6 "ISLANDS" OF CONSTANT DEBRIS DEPTH

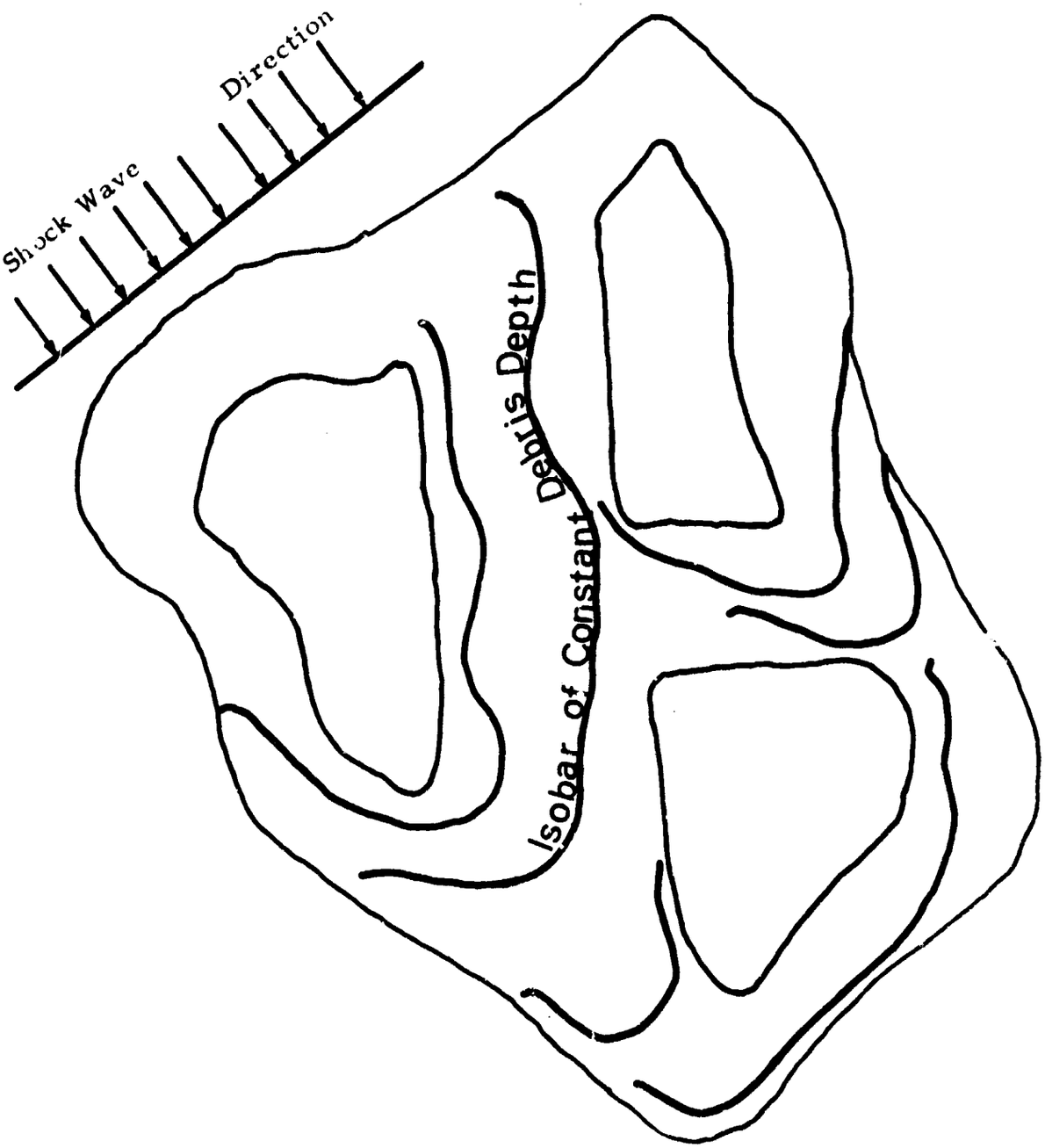

Fig. 1.7 MAP OF AREA DEBRIS DISTRIBUTION

CHAPTER TWO

AN ANALYTICAL APPROACH TO PREDICTING SIZE AND TRANSPORT OF OFFSITE DEBRIS

2. GENERAL APPROACH

This chapter deals with a problem that is fundamental in any analytical model of the postattack environment. As has been discussed in the first chapter of this report, one of the most predominant forms of offsite debris will be masonry and other forms of frangible rubble. In order to predict the final deposition of known sources of this offsite debris the actual mode of fracture must be investigated as well as the subsequent motion of the fragmented element.

As has been outlined previously[1] the prediction of the formation and transport of offsite debris is a four step process that includes:

1) The prediction of the reflected and drag pressures resulting from a given set of attack parameters.
2) Determination of the reflected and drag pressures on various structural elements.
3) The prediction of when and how a brittle structural element will fail.
4) The motion of the displaced element in space under gravitational and wind forces.

The problem posed by the first two steps of the description above has been taken up satisfactorily in a number of well known documents.[2, 3, 4] The final two steps are of a more fundamental nature and will be dealt with here in detail.

Having modeled the actual formation and transport of offsite debris it becomes evident that a one-to-one correspondence can be established between materials in the target and their final position on the ground surface.

2.1 A Simple Fragmentation Model

2.1.1 Introduction

The ultimate strengths obtained from the repeated static testing of nominally identical brittle specimens will exhibit a characteristic scatter. Furthermore, the locations of the resulting fractures will vary from one specimen to another. Because the disposition of ultimate strengths is usually very large for brittle materials, it is generally not possible to predict the behavior of a single element with any useful accuracy regardless of the amount of accumulated experience with similar elements. It is possible, however, through the use of statistics, to predict the composite behavior of a large group of nominally identical brittle components from a knowledge of the characteristics of still another large group of similar components.

Adopting a statistical viewpoint, we shall consider the fragmentation of a brittle beam structure such as the cantilever shown in Fig. 2.1. Under a sufficiently high static loading, the statistical theory of fracture allows that fracture may occur anywhere in the span. The likelihood of fracture will be greatest at the fixed end where the stress level is highest. It can be observed that the probability of fracture occurring at a specified station along the beam is zero. Any finite probability of failure at the various beam stations would always result in the physical contradiction that the survival probability of the beam is zero. Consequently, it is meaningless to seek fragments of a given size; and indeed, the number of fragments which occur within a given range of sizes should be sought.

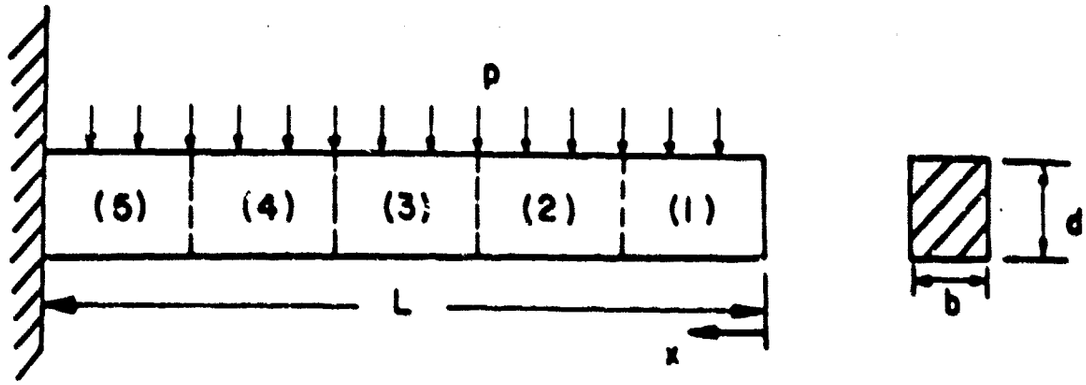

Fig. 2.1 BRITTLE CANTILEVER UNDER UNIFORM LOAD

2.1.2 Method of Attack

To obtain a finite probability of fracture, we must consider a region along the beam rather than a specific station. Therefore, we shall imagine the beam to be divided into n units of equal length. To each of these units will be assigned a measure of its statistical strength characteristics. This will take the form of a cumulative distribution function, F (p), which is a measure of the probability of fracturing the unit at a load magnitude equal or less than a load p. It remains to investigate the probability of obtaining any size element resulting from single or multiple fractures occurring within any of the n subunits of the beam. It will be seen that the problem of predicting fracture is an analogy of the classical "run" probability problem.[5]

2.1.3 Dynamic Stresses

The fundamental assumption in the development of the fragmentation model is that the maximum dynamic stresses introduced into the various unit segments are independent of the fracture characteristics of these segments. This would, of course, be the case if the loading was sufficiently rapid to fully stress the unit before any fracture occurred. This important assumption leads to the simplification that the units can be treated as being stochastically independent. For static loading, this assumption is clearly invalid since fracture in a unit segment would immediately relieve the stresses in other segments. This implies that only one fracture can occur in a statically loaded statically determinate beam. On the other hand, even the crudest dynamic loading experiments with statically determinate brittle beams produce multiple fracture.

Taking the dynamic beam loading in the form

$$p\, f(x)\, g(t)$$

where the effects of magnitude, load distribution, and pulse shape are explicitly delineated the maximum dynamic stresses can be estimated for a typical unit by multiplying the static stresses associated with p f (x) by the maximum dynamic load factor (DLF) for the first mode of vibration. Thus, the stress distribution for a given unit segment has the form

$$p\, h(x, y, z)\, (DLF) \qquad \text{(See Appendix A)}$$

2.1.4 Statistical Strength of Unit Segments

The statistical strength characteristics of a typical unit segment are described by its cumulative distribution function, F (p). This function gives the probability of fracturing the unit at a load magnitude equal to or less than p. The distribution function may be determined by physically testing many unit segments or by appealing to one of the "weakest link" statistical fracture theories. Of these, Weibull's[6] is the most famous theory and is shown below in a form which is appropriate for the unit segment.

$$\left.\begin{aligned} F(p) &= 1 - e^{-\int_V \left[\frac{\sigma - \sigma_u}{\sigma_o}\right]^m dV} && \sigma \geq \sigma_u \\ &= 0 && \sigma < \sigma_u \end{aligned}\right\} \qquad (2\text{-}1)$$

where σ is the stress distribution in the segment of the form $ph(x, y, z)(DLF)$; σ_u, σ_o, and m are constants of the material; and where the integration is taken over the volume of the unit segment. The distribution parameters σ_u, σ_o, and m are usually determined from simple bending or tension specimens. (Appendix B)

The practical application of the Weibull function takes advantage of certain mechanical properties normally found in most brittle materials. For example, the linearity of the stress-strain relationships up to rupture greatly simplifies the stress analysis. Also the insensitivity of the strength of the brittle materials to wide variations in strain-rate enables the determination of a unique set of distribution parameters from static test results. Finally, since the tensile strength is generally much smaller than the compressive or shear strength, a consideration of tensile bending stresses alone is usually sufficient for the determination of the strength of normally proportioned beams.

2.1.5 The Problem of Runs

When a beam undergoes multiple fracture along its span, different size elements occur due to the proper combination of fractures taking place. If one were to examine each combination of possible fracture this would involve $2^n - 1$ possibilities. The result of the investigation would lead to being able to predict the probability of getting an element, of a given size

range, from a particular part of the loaded beam. If it is sufficient to only know the probability of getting an element, with a given size range, from an unspecified point along the original beam, the fragmentation problem is directly analogous to the problem of runs.

A run of exactly r successes will be said to occur if it is possible to find a sequence of r consecutive successes which is not part of a sequence of more than r successes. Thus a run of exactly r successes can occur either at the beginning of the series in which case it must be followed by a failure, or at the end in which case it must be preceded by a failure, or elsewhere in which case it must be both preceded and followed by a failure.

No difficulty arises in calculating the probability that a run of exactly r successes will occur in n trials so long as $r \geq 1/2\ n$, (i.e., so long as it is not possible for two or more separate runs to occur in the same series). For example, a run of exactly five successes in eight trials can occur as follows, where p denotes success, q denotes failure and X denotes an unspecified result:

p p p p p q X X,	probability $p^5 q$,
q p p p p p q X,	probability $q\ p^5 q$,
X q p p p p p q,	probability $q\ p^5 q$,
X X q p p p p p,	probability $q\ p^5$

These four ways are mutually exclusive and exhaustive and the required probability is thus the sum of the four separate probabilities (i.e., $2\ p^5 q\ (1 + q)$). In general, if $r \geq 1/2\ n$, the probability of a run of exactly r successes beginning at the initiation of the series or ending at the end of the series is $p^r q$ in each case, while the probability of such a run elsewhere in the series in a specified position is $p^r q^2$. As there are $(n - r - 1)$ possible positions apart from the beginning and end, the probability $p(r)$ say of a run of exactly r successes is given by

$$p(r) = 2\ p^r q + (n - r - 1)\ p^r q^2 \qquad (2\text{-}2)$$

provided $1/2\ n \leq r < n$. If $r = n$, $p(n) = p^n$ obviously.

It is easy to see that Eq. (2-2) always gives the expected number of runs of exactly r successes in a series of n trials, whether or not $r \geq 1/2\ n$.

First, suppose that $r \geq 1/2\ n$; then the probability that there is exactly 1 run is given by Eq. (2-2), while the probability of any higher number of runs is zero, so that Eq. (2-2) is the expected number of runs. Suppose that $r < 1/2\ n$ so that more than one run of exactly r successes may occur in a series of n trials. Then in a series, the number of runs beginning at the first trial is obviously either 0 or 1, and the probability that it is 1 is $p^r q$. Similarly, the expected number of runs beginning at the first trial is $p^r q$. Similarly, the expected number beginning at the second trial is $q\ p^r\ q$, as it is for the third, fourth, ..., (n - r + 1) th trial (i.e., a run at the end of the series is $p^r q$). Thus the expected number of runs in the series is Eq. (2-2). Of course, some of these possibilities are mutually exclusive, but this is immaterial since we are finding the expected number of runs in the series and not the probability that a run will occur.

For the purposes of analysis, it is assumed that the beam is subdivided into n equal segments and that cracks can occur only at the n + 1 joints shown in Fig. 2.2.

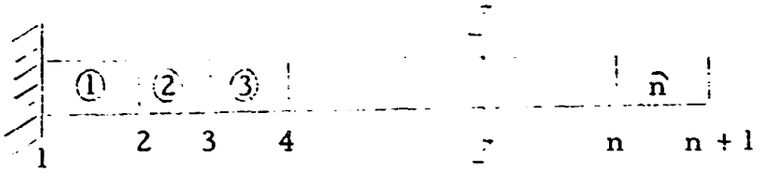

Fig. 2.2 BEAM NUMBERING SYSTEM

The expected number of fragments, r segments in length, is equal to the sum of the expectations of such fragments starting at each of the joints 1, 2, ... n - r + 1. That is,

$$E(r) = \sum_{k=1}^{n-r+1} J_k \qquad (2\text{-}3)$$

where

$$J_k = q_k q_{k+1} \quad \text{for} \quad r = 1, \text{ and}$$

$$J_k = q_k \left(\prod_{j=k+1}^{k+r-1} P_j \right) q_{k+r} \quad \text{for} \quad r > 1 \qquad (2\text{-}4)$$

in which p_i and q_i are the probabilities of the ith joint not having or having a crack, respectively. Of course, $p_{n+1} = 0$ and $q_{n+1} = 1$.

In the case of a simple beam, Eq. (2-3) and (2-4) still hold, but of course here we have $q_1 = 1$ as well as $q_{n+1} = 1$. Where the analysis is to be made on a fixed-fixed beam formulas (2-3) and (2-4) hold with no restrictions on p_{n+1} and q_{n+1} or q_1.

The recursive relation (Eq. 2-3) predicts the expected number of segments of each elemental size where an elemental size , r, consists of r unit segments. (i. e. r = 1, 2, 3. . . . . , n segments in length) Because fracture may occur anywhere in a unit segment rather than at the assumed joints as shown in Fig. 2. 2, any elemental fragment size (e. g. r = 1, 2, 3, ... , n) actually represents the midpoint of a range of sizes which may differ from the indicated size by as much as one unit length ($\pm \frac{L}{n}$). It is apparent that the elemental fragment size ranges overlap considerably as shown in Fig. 2. 3, and as a consequence, they cannot be used directly for classifying sizes. To circumvent this problem we will group the elemental sizes into broader physical size intervals Now, since E(r) represents the expected number of segments of elemental size, r E(r) x r x L /n represents the total physical length devoted to elements of elemental size r. To convert this to a fraction of the original beam length, F(r), we divide by L, thus,

$$F(r) = \frac{r}{n} E(r) \qquad (2-5)$$

The expected fractions of the beam, as determined by Eq. (2-5) may be grouped into broader subdivisions in such a way that the effect of overlapping may be made as small as desired.

It is clear from Fig. 2. 3 that the relative amount of overlap decreases with increasing n. The effect of overlap on the accuracy of the fragmentation predictions can be seen from Table 2-1 which indicates little improvement after n passes 30 trials.

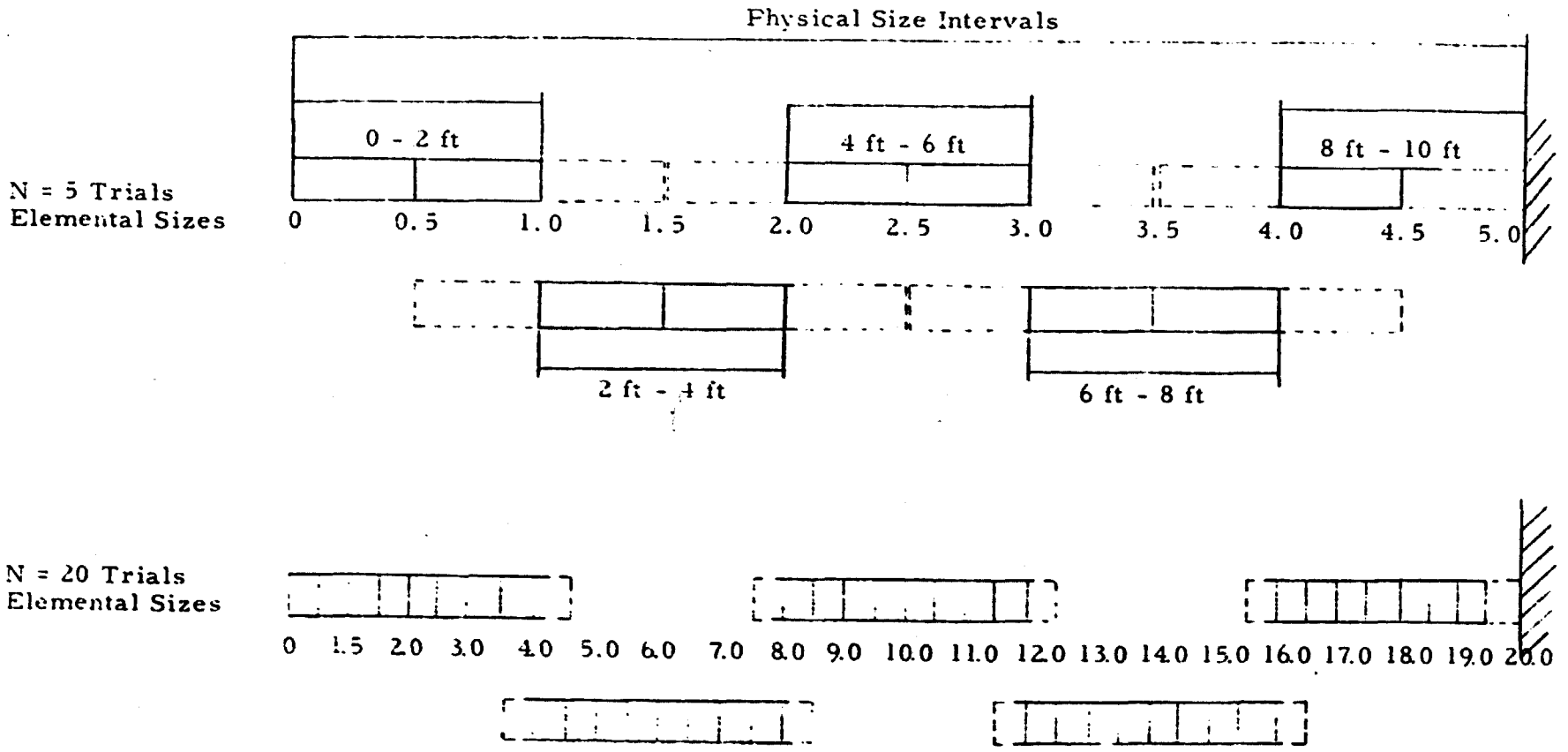

Fig. 2.3 ELEMENTAL AND PHYSICAL SIZE INTERVALS

Table 2.1

THE EFFECT OF OVERLAP ON THE ACCURACY OF FRAGMENTATION PREDICTIONS (P_o = 20 psi)

Size Range, ft	n = 5	15	30	50	100
6-2	25.8	31.63	32.05	32.13	32.16
2-4	0	0.10	0.16	0.19	0.23
4-6	14.6	6.87	4.58	3.77	3.22
6-8	49.6	61.49	63.36	64.07	64.59
8-10	0	0	0	0	0

2.1.6 Hydrostone Cantilever Results

As a test case of the analytical procedure described above the same hydrostone beam studied in the overlap considerations of the previous section was analyzed for a constant n (i.e. n = 15) over a complete range of loads. Figure 2.4 shows the results of this analysis as well as an insert of the beam itself. The results consist of fragmentation expectation as a function of overpressure over a range of physical size ranges. It is interesting to note that the results verify what one would intuitively expect: that is, under low load the cantilever beam will fail near its support while as the pressure is increased the possibility of getting smaller and smaller size particles becomes increasingly more probable. Each particle size range reaches a peak at a particular load level (not necessarily predominating). At a certain load, there is no chance of getting any size other than the smallest size range considered. This leads to the possibility of achieving a pulverization pressure if a small enough size range is considered. At any specific load level (e.g. 20 psi) some physical size intervals may dominate (e.g. 8-10 ft, 6-8 ft, and 0 to 2 ft) while others may have been phased out or have not been developed yet. (e.g. 2-4 ft and 4-6 ft) This is wholly dependent on the statistical nature of the material (i.e. the Weibull parameters in this case M = 7, σ_o = 50, and σ_u = 1500).

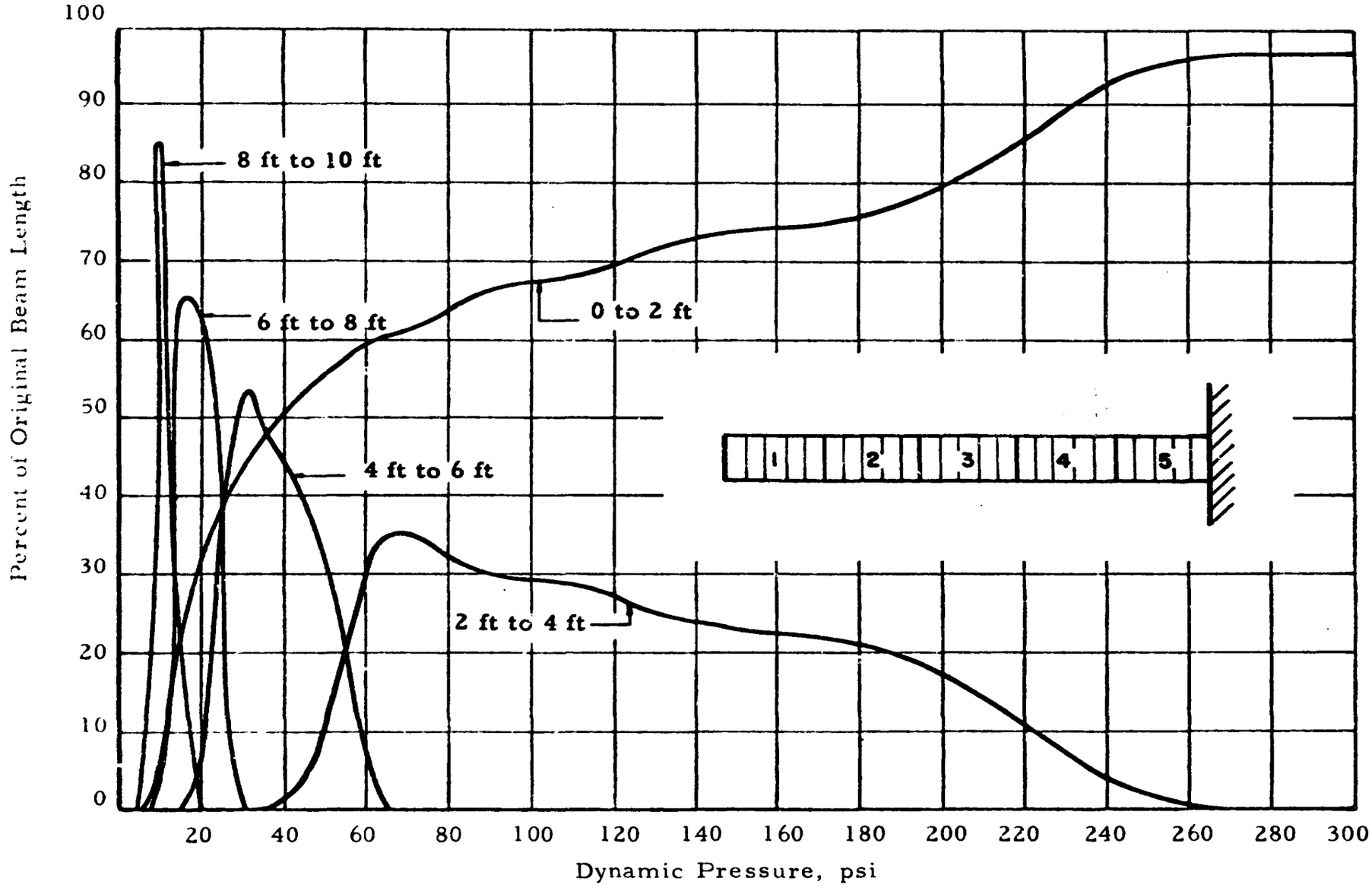

Fig. 2.4 HYDROSTONE CANTILEVER RESULTS

2.2 Fragment Trajectory Analysis

Trajectory analysis for structural fragments starts with the equation-of-motion of a particle acted upon by drag forces. This is a second-order nonlinear differential equation, which can be solved in a series of steps as the fragment is followed through its horizontal translation. The flight time of the particle is determined by its initial height, depending on its location in the structure under consideration. Families of trajectories can be found for a range of particle sizes, each set corresponding to some combination of weapon yield and ground range. An indication of debris distribution can then be made by combining all the sets of trajectories corresponding to a specific weapon yield.

The initial conditions required for the use of this transport model are characterized by three results of the fragmentation solution, namely: time of failure, size of fragment, and initial fragment velocity. Solutions are obtained for particle sizes consistent with those examined in the fragmentation model and with the conservative assumption that time of failure and failure velocity are zero. We now discuss the transport model in some detail.

2.2.1 Trajectory of a Particle

Consider the motion of a particle through air such that the drag force acting on the particle is proportional to the square of the relative velocity between the particle and the medium. It is assumed that the vertical and horizontal motion of the debris particle are uncoupled. This is true if the center of pressure of the particle coincides with its centroid for all orientations so that no rotation occurs, and further that the horizontal component of relative velocity between the air and particle be significantly greater than the vertical component.

The horizontal equation of motion is then

$$\ddot{x} = \frac{k \rho}{2} (\dot{x} - u)^2 \qquad (2\text{-}6)$$

where

x = horizontal coordinate

y = vertical coordinate, positive downward

($\dot{}$) = differentiation with respect to time

α = aerodynamic coefficient, $\frac{\text{(projected area x drag coefficient)}}{\text{mass}}$

ρ = mass density of air

u = air particle velocity

g = gravitational constant

$$k = \begin{cases} -1; & u \geq \dot{x} \\ +1; & u < \dot{x} \end{cases}$$

$$k = \begin{cases} +1; & \dot{y} \leq o \\ -1; & \dot{y} > o \end{cases}$$

This is a Riccati type nonlinear differential equation and can be linearized by a simple transformation of coordinates.

Let
$$\dot{x} = \beta \frac{\dot{s}}{s} \tag{2-7}$$

Then
$$\ddot{x} = \beta \frac{\ddot{s}}{s} - \beta \left(\frac{\dot{s}}{s}\right)^2 \tag{2-8}$$

Making the substitution into Eq. (2-6)

$$\beta \frac{\ddot{s}}{s} - \beta \left(\frac{\dot{s}}{s}\right)^2 = \frac{k}{2} \alpha \rho \left[u^2 - 2u \beta \frac{\dot{s}}{s} + \beta^2 \left(\frac{\dot{s}}{s}\right)^2 \right] \tag{2-9}$$

The value of β can be determined to make the $\left(\frac{\dot{s}}{s}\right)^2$ term vanish.

Thus
$$\beta = - \frac{2}{k \alpha \rho} \tag{2-10}$$

and then

$$\beta \frac{\ddot{s}}{s} - \beta \left(\frac{\dot{s}}{s}\right)^2 = - \beta^{-1} u^2 + 2u \frac{\dot{s}}{s} - \beta \left(\frac{\dot{s}}{s}\right)^2$$

$$\beta \frac{\ddot{s}}{s} = - \beta^{-1} u^2 + 2u \frac{\dot{s}}{s} \tag{2-11}$$

$$\beta^2 \ddot{s} = -u^2 s + 2 \beta u \dot{s}$$

$$\beta^2 \ddot{s} - 2 \beta u \dot{s} + u^2 s = 0$$

Treating u as a constant, a closed form solution to Eq. (2-11) can be obtained in the form

$$s = (C_1 + C_2 t) e^{\frac{u}{\beta} t} \tag{2-12}$$

from which follows

$$\dot{s} = \frac{u}{\beta} (C_1 + C_2 t) e^{\frac{u}{\beta} t} + C_2 e^{\frac{u}{\beta} t} \qquad (2\text{-}13)$$

where C_1 and C_2 are constants of integration.

From the substitution

$$\dot{x} = \beta \frac{\dot{s}}{s}$$

It can be shown that

$$\dot{x} = u + \frac{C_3 \beta}{1 + C_3 t} \qquad (2\text{-}14)$$

where the two constants of integration C_1, C_2 have been combined to form the single constant C_3 through the relation

$$C_3 = \frac{C_2}{C_1}$$

The horizontal displacement follows by an integration of Eq. (2-14) and it is given by

$$x = C_4 + ut + \beta \log_e (1 + C_3 t) \qquad (2\text{-}15)$$

It will be noted that a constant wind velocity u is assumed in obtaining Eq. (2-14) and (2-15). This is not true for the induced motion of the particle as a result of blast winds. The wind velocity, u, is a function of overpressure, which is dependent on yield, ground range, and time. Hence, trajectories must be determined by computing the horizontal motion for a series of short time intervals, Δt, over each of which a constant wind velocity can be assumed. Towards applying Eq. (2-14) and (2-15) throughout the trajectory let us assume that at the end of the mth interval the velocity and horizontal displacement are $\dot{x}_m$ and x_m. From Eq. (2-14), setting $t = 0$ one has

$$C_{3m} = \frac{1}{\beta_m} (\dot{x}_m - u_m)$$

where u_m is the (assumed) constant wind velocity and β_m is associated with the (assumed) constant local air density. The remaining constant of integration C_{4m} is simply the horizontal displacement at the beginning of the time interval.

The displacement at the end of the time interval x_{m+1} is obtained from Eq. (2-15) and is

$$x_{m+1} = x_m + u_m \Delta t + \beta_m \log_e \left(1 + \frac{\dot{x}_m - u_m}{\beta_m} \Delta t\right) \quad (2\text{-}16)$$

A more directly useful form of Eq. (2-16) is given by

$$\Delta x_m = u_m \Delta t + \beta_m \log_e \left(1 + \frac{\dot{x}_m - u_m}{\beta_m} \Delta t\right) \quad (2\text{-}17)$$

where Δx_m is the increase in horizontal displacement at the time increment Δt.

In Eq. (2-17), it is assumed that u_m, β_m and $\dot{x}_m$ are determined at the beginning of this interval. In sequencing the successive intervals it is convenient to employ Eq. (2-14) to establish the velocity at the end of the time interval Δt. Thus, we have

$$\dot{x}_{m+1} = u_m + \frac{\dot{x}_m - u_m}{\beta_m + (\dot{x}_m - u_m)\Delta t} \quad (2\text{-}18)$$

Consideration must also be given to the increasing lag of the particle behind the shock front during flight, as shown in Fig. 2.5.

A description of the physical situation is as follows. Consider the instant at which the building is fragmented. The blast parameters are now inspected. Denote the weapon yield as W, ground range as R_o. Under these conditions we can evaluate the shock wave velocity, u, the air mass density ρ, the positive phase duration t_d, and the overpressure p at the instant the initial shock wave is R_o distance from ground zero; or in other words, just as the shock wave is exerting its influence on the particle. Now we can allow the action to continue until some small duration of time has lapsed, Δt. The shock front hasmoved a distance $u \Delta t$. From Eq. (2-15) we can find the particle movement, x_1. Furthermore, the particle has fallen behind the shock front because it has not been able to accelerate fast enough to keep up with it. At this point, we can evaluate a new u, ρ, t, and p. However, this must be done for the blast wave which is now acting on the particle. This requires taking into account an additional decay in overpressure. After these new "constants" are evaluated, we can again solve Eq. (2-15) for some time increment, Δt, and obtain the new distance the particle

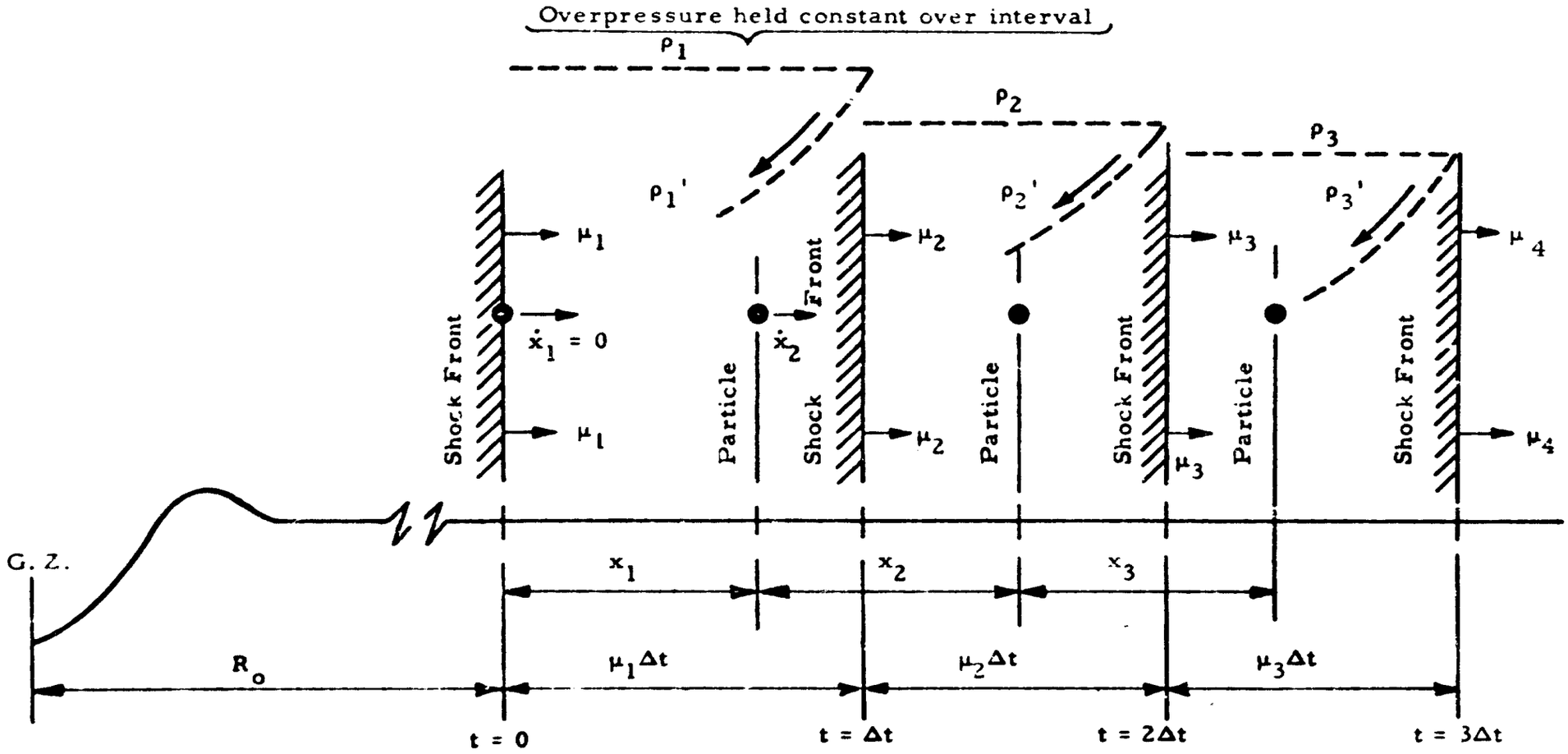

ρ is the overpressure computed at shock fronts

ρ' is the overpressure computed at particle position

Total distance particle is transported is

$$\sum_{i=1}^{\mu} x_i$$

R_o is initial ground range

μ is shock front velocity

$\dot{x}$ is particle velocity

Fig. 2.3 LAG OF PARTICLE BEHIND SHOCK FRONT

travels, x_2. So far the particle has traveled a total distance of $x_1 + x_2$, if we do not change Δt, the number of times we can increment is

$$n = \sqrt{\frac{2 h_o}{g}} \Big/ \Delta t$$

Where $\sqrt{\frac{2 h_o}{g}}$ is the fall time of a particle from height h_o, using the considerations outlined for each increment or solution of Eq. (2-15), the total distance the particle travels is:

$$D = \sum_{i=1}^{n} x_i$$

If we index the size of the particles to show that they are of different sizes, we have the total distance each particle travels by repeating the solution of Eq. (2-11) under these conditions, but for different sizes of particles. We obtain:

$$D_1 = \sum_{i=1}^{n} x_{1_i}$$

$$D_2 = \sum_{i=1}^{n} x_{2_i}$$

If we select k sizes:

$$D_k = \sum_{i=1}^{n} x_{k_i}$$

It is then possible to incorporate all this information into graphical form valid for the W_o, R_o in question, as depicted in Fig. 2.6.

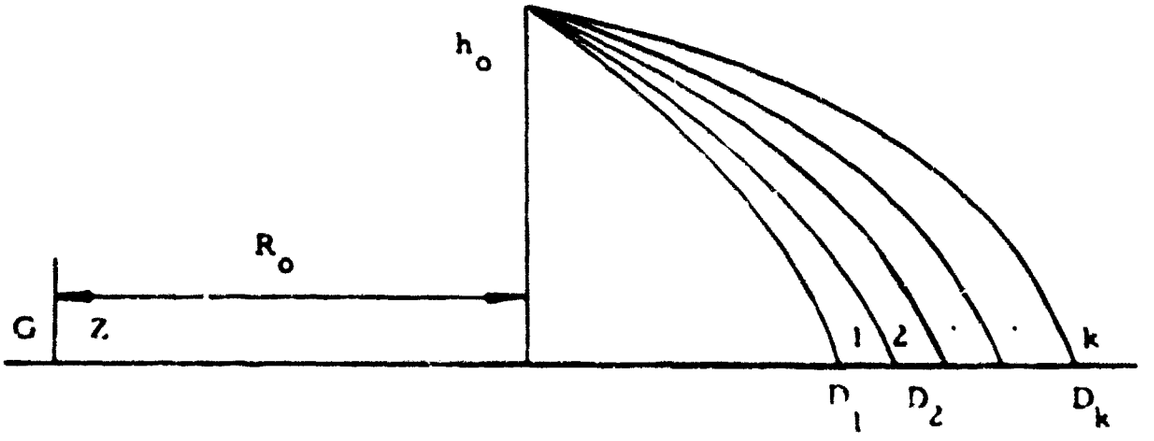

FIG. 2.6 TRAJECTORIES OF VARIOUS SIZED DEBRIS PARTICLES

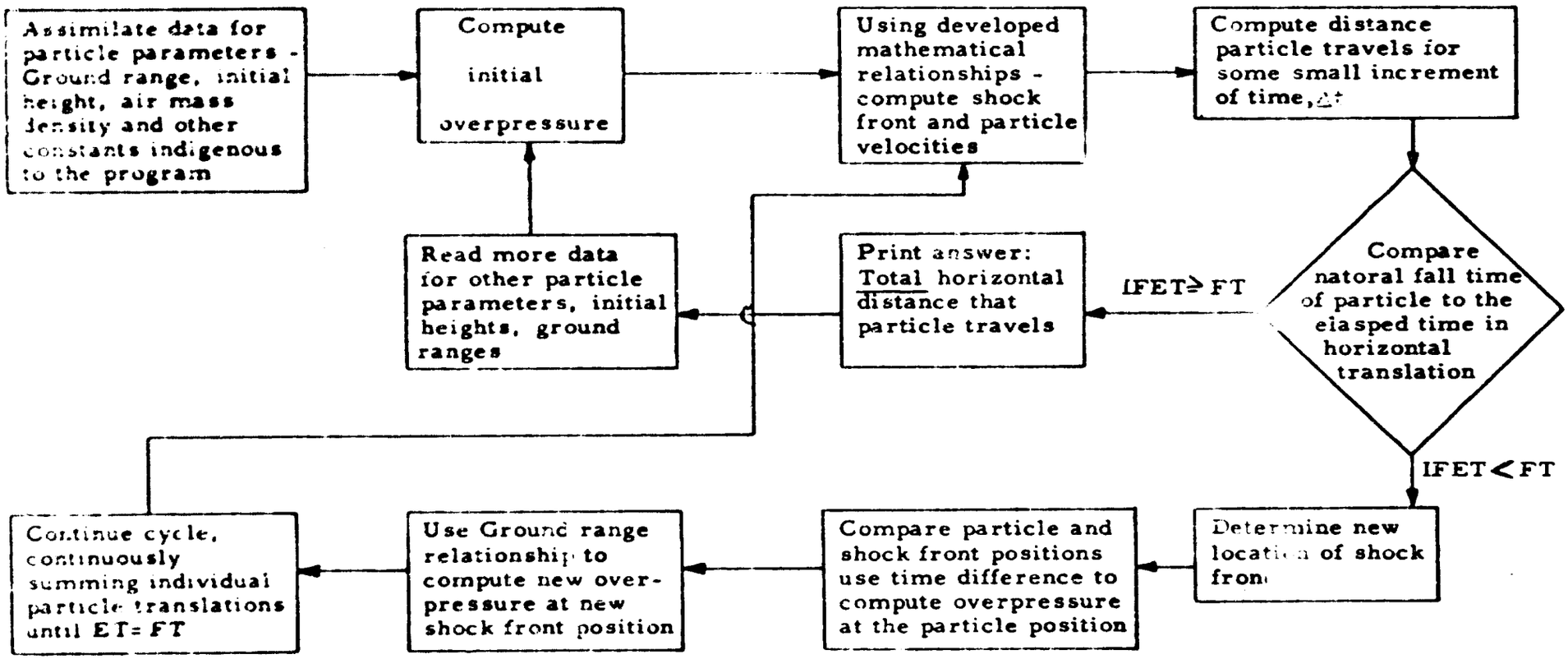

Note:
ET = Horizontal elapsed time
FT = Fall time

Fig. 3.7 COMPUTER FLOW CHART FOR PARTICLE TRAJECTORY CALCULATIONS

2.2.2 Terminal Velocities of Debris Particles

It is possible to obtain the velocities of the different size debris particles in an analogous manner utilizing Eq. (2-11). Appendix D contains trajectory curves for debris transport that consider four parameters; displacement, velocity, particle size, and starting height, for various overpressures due to 1 MT. One outstanding fact that presents itself is the extremely high terminal velocities that all particles have (e.g., in excess of 60 ft/sec for a 5 in. particle at 8 psi, 1 MT). This bombardment of debris is bound to have serious tertiary effects on both structural and human elements in an area of high debris concentration.

CHAPTER THREE

DYNAMIC FLEXURE EXPERIMENTS WITH BRITTLE BEAMS

3. PURPOSE

In the previous chapter, a unique fragmentation model was developed. During the course of formulating this theory a fundamental assumption was made. This was that the maximum dynamic stresses introduced into the various unit segments of the loaded beam were independent of the fracture characteristics of the segments. The experiments described below and the further analytical studies in Appendix C tend to verify the validity of the above assumption.

Another purpose in conducting the following experiments was to get a better qualitative feel for brittle elements under dynamic load. To facilitate this, extensive high speed photography was employed to record a variety of support and load conditions.

Finally, an attempt was made to investigate the fragment distribution of a cantilevered hydrostone beam under a uniform dynamic load.

3.1 Static Versus Dynamic Flexure in Brittle Materials

The classical flexure experiment with brittle beams is aimed at establishing static bending strength of a material (i.e., its modulus of rupture). Such tests are usually performed using three or four point bending on a simply supported beam specimen. In the case of three point bending, for example, maximum flexural stress occurs at the center of the span for a uniform beam (i.e., under the point of load), and fracture will initiate there too as the ultimate load is reached. This simple static test results in two pieces (fragments), and is consistent specimen to specimen with a scatter in the magnitude of the failure stress as influenced by severity of the critical flaws at the center of the span. In such a case as this, simple theory is adequate to predict the location of the failure section, but the actual material strength can only be predicted after consideration of the statistical nature of the material has been made. Weibull,[6] for example, has developed one such statistical theory which can be used to predict static material strength for a variety of stress states if certain "material parameters" are known.

When the case of dynamic flexure is considered the problem becomes a great deal more complicated. In the dynamic case, the elastic response of the beam is a function of its dynamic excitation (load-time history); an infinite number being possible. Thus, one begins by not having a very good idea of what the actual dynamic bending moment diagram might be. Since this quantity is time dependent and continually influenced by inertial forces, one is confined to predicting stresses for relatively simple cases unless he is prepared to undertake the numerical analysis done in Appendix C. When the problem of predicting dynamic stresses is combined with the dynamic effects of statistical flaw theory, prediction of the dynamic rupture characteristics in brittle beams becomes very complicated indeed. A number of investigators[9, 10] have been concerned with the dynamic response of reinforced concrete beams, but few have been concerned with the dynamic rupture behavior of brittle beams per se. English,[11] in 1951, reported a theoretical study of the rupture of brittle beams under impulsive loading. That study was intended to provide a pattern of the kind of fragmentation that would result from dynamic flexure, and was based primarily on the Griffith Flaw Theory,[12] and the Weibull Statistical Theory of Rupture.[6]

3.2 Material Properties

The brittle beams used in this study were cast of Hydrostone,* a white cementitious material which is similar to plaster of paris. The characteristics and some mechanical properties of the material are given below in Table 3.1. In this table, the static and dynamic values of tensile strength were measured using different specimen types and methods of test. Static tensile strength was measured by the use of a dog-bone type specimen in a direct pull test. Dynamic tensile strength was measured by the use of a stress wave technique described in detail in Reference 13. In this latter method a traveling longitudinal stress wave on a long slender free-free bar caused tensile fracture upon reflection of the first compressive pulse from a free end. By the use of suitably placed strain gages and dynamic recording, the ultimate fracture strain was monitored and converted to ultimate stress through a modulus of elasticity.

*Trade name - U. S. Gypsum Company.

Table 3.1

CHARACTERISTICS OF HYDROSTONE[+]

Specific Gravity	1.86
Unit Weight	116 lb/ft^3
Static Tensile Strength[++]	1020 psi
Static Modulus of Elasticity	2.73 x 10^6 psi
Dynamic Tensile Strength[++]	1730 psi
Dynamic Modulus of Elasticity	2.85 x 10^6 psi
Static Flexural Strength[+++]	1440 psi
Static Compressive Strength[++++]	6310 psi

[+]All material was mixed at maximum consistency with 0.4 percent sodate retarder added to provide workability.

[++]1/4 inch square cross section

[+++]1/2 inch square beams in pure bending

[++++]3 inch diameter cylinders in direct compression.

The dynamic modulus of elasticity used was calculated from observed values of the velocity of propagation of the longitudinal wave (1.28 x 10^5 in. per sec) and the mass density per unit volume of the material. The apparant disparity between the static and dynamic values of tensile strength reported in Table 3.1 can be attributed to the types of tests used. The direct pull test used for the static tensile strength measurements suffered from induced bending caused by eccentricity of loading. Hence, the measured static tensile strengths are lower than they would be if the parasitic bending effects were eliminated. The static and dynamic modulus of elasticity values agree within 6 percent.

3.3 Dynamic Flexure Experiments

The apparatus used in the dynamic flexure experiments of this study is pictured in Fig. 3.1. The device was essentially a steel frame with hardened steel pin roller supports which prevent the development of horizontal reaction forces. The supports were placed 5 in. center to center of supports. The beams used were about 6 in. in length, and 1/4 in. square.

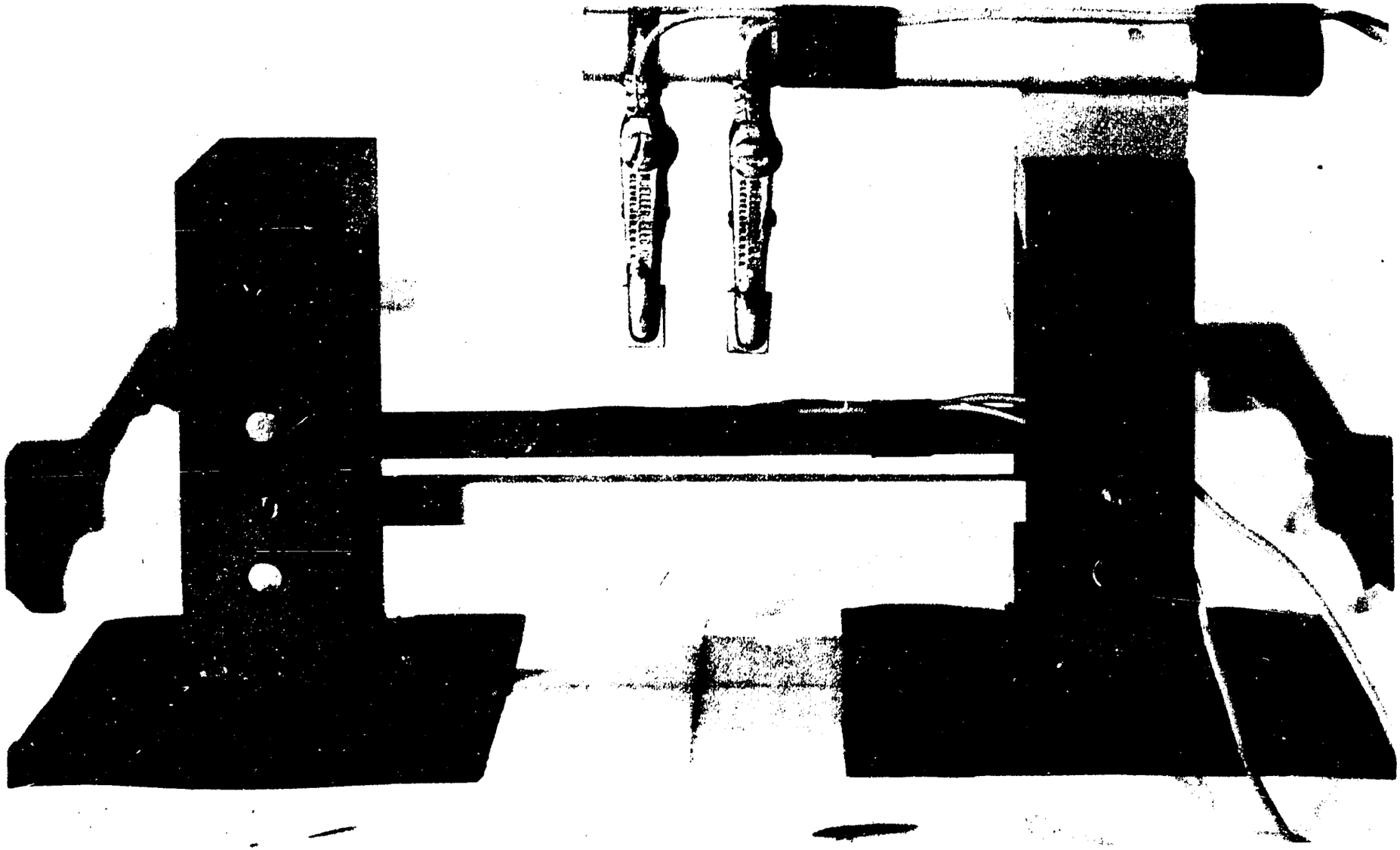

Fig. 3.1 APPARATUS FOR DYNAMIC FLEXURE EXPERIMENTS

With this arrangement an effective span to depth ratio of 20:1 was obtained. Experiments were performed by placing a beam in the flexural device, as shown in Fig. 3.1 and then a charge of lead azide was placed at the center of the span in a small gelatin capsule. The charge was ignited by use of a crimped nichrome "hot wire" operated from a battery.

For some of the experiments other end support conditions were investigated. For these cases other fixtures were constructed. For the case of the "fixed-fixed" beam, a device providing clamped ends was used. In the case of the cantilever beam, a clamp fixture at one end of the beam was used.

The simplest of photographic techniques was used during the experiments. A Fastex* high speed movie camera (approximately 7500 frames per sec) was aligned, sighted, and focused on the span of the beam between the steel support frame. Proper lighting behind the specimen through a frosted glass plate provided a clear image for photographing. A Goose* synchronizing unit was used to coordinate the camera with the explosive impulse. Initially, the camera was started from a switch and after 1/2 sec of running time, the explosive charge was detonated by the Goose. The entire experiment requires only 3/4 of a second. The first 1/2 sec period was used to allow the camera to get up to speed and the remaining 1/4 sec was used to detonate the explosive and record the dynamic event on film.

Figures 3.2 through 3.6 each show three successive frames from typical experiments. In Fig. 3.2, for example, the clear span between supports is plainly indicated. The flag bearing the symbols "3 SS" on the left lower corner of the frame indicates that a 3 mg charge of lead azide was used at the center of the span and that the beam was simply supported. The dark mass in the upper center of the frame is a cone shaped "smoke stack" which was used to remove the smoke which would otherwise obscure the photographs. The vertical bar in the background on the right side of the frame is a portion of a ring stand which was used to support the "smoke stack" and the ignition wire. The single frames are about 150 microsec apart.

*Trade names - The Wollensak Corporation.

The fracture which resulted in Fig. 3.2 was representative of a typical static break. One complete fracture occurred, at the center of the span (under the point of loading) and only two fragments were produced. This behavior was found to be reproducible and typical of all simply supported dynamic experiments where very small explosive charges were used.

The behavior which was found to be typical of the large load levels with simply supported beams is pictured in Fig. 3.3. In this case an explosive impulse of 30 mg of lead azide was used. The photograph reveals the extent of multiple fracturing which occurred at this high dynamic load level. From a strictly qualitative argument, the symmetry of the fractured pieces seems to indicated relatively simultaneous formation and stochastic independence of the failures. If this were not true, an antisymmetrical fragment pattern would result.

Experiments with fixed-fixed beams showed results similar to those of the simply supported cases. At low (Fig. 3.4) load levels, three breaks (four fragments) were observed. This is what again would be expected in the static case of a fixed-fixed beam since under center point loading, this beam will develop equal maximum bending moments at the center of the span (positive moment) and at the end supports (negative moment). For fixed-fixed beams having high load levels multiple symmetrical breaks nearly identical to those observed for the simply supported beam were found to occur. (Fig. 3.5)

One experiment was performed using a cantilevered beam and a high load level (30 mg). In this experiment, one end of the beam was charged and the charge was placed 1 in. from the free end (i.e. 4 in. from the clamped support). Figure 3.6 illustrates the dynamic behavior of the brittle cantilever for the loading imposed. In the photograph the free end of the beam is on the left side of the frame. The figure dramatically shows that localized fracture and multiple fragments are produced near the free end of the beam where the dynamic load was imposed.

Since the result shown in Fig. 3.6 is contrary to static analysis, a dynamic analysis was made with a lumped mass model as outlined in Appendix C. The results of this analysis confirm the behavior observed.

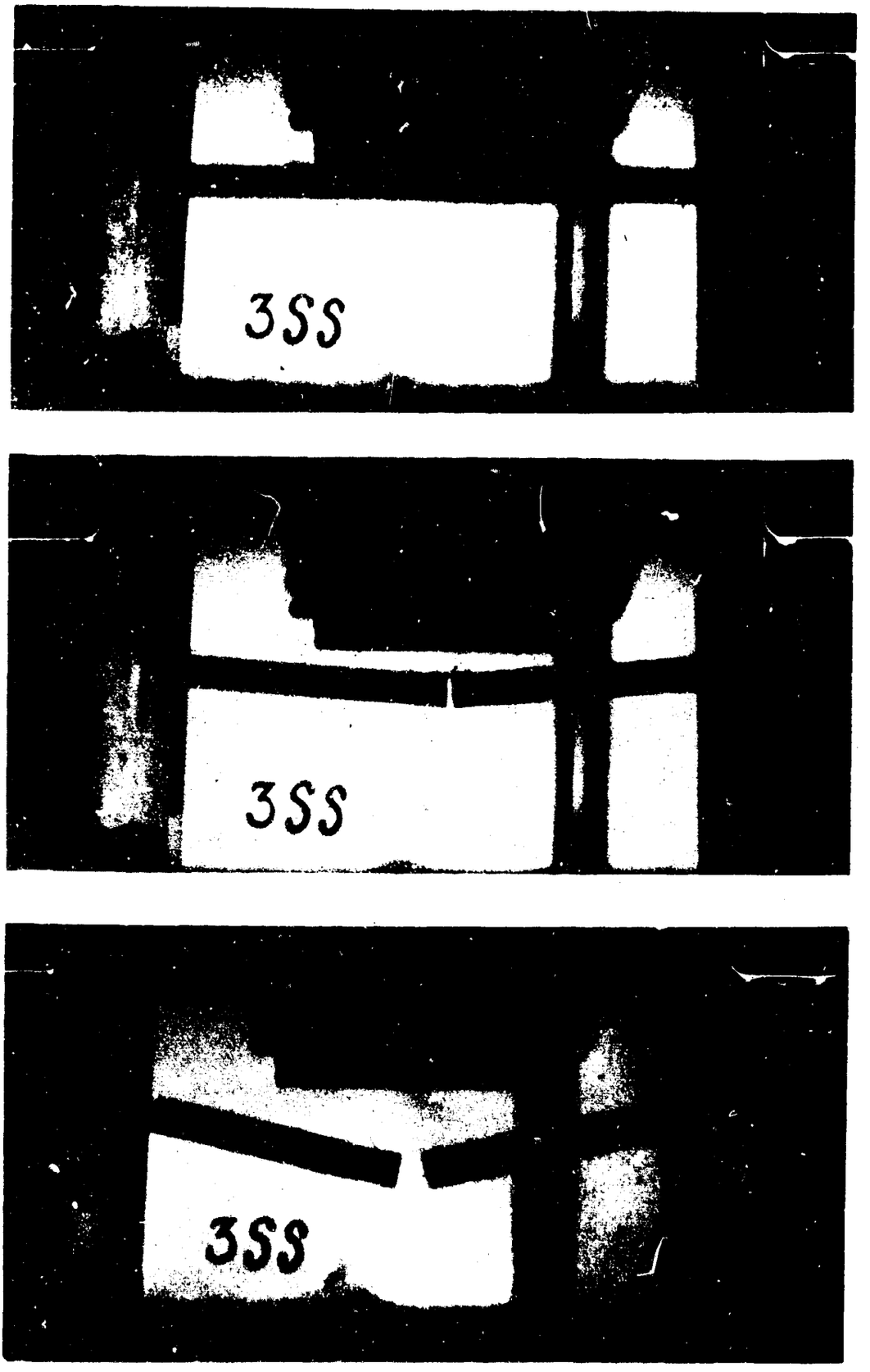

Fig. 3.2 SIMPLY SUPPORTED BEAM UNDER CENTER POINT DYNAMIC LOADING - 3 mg LOAD LEVEL

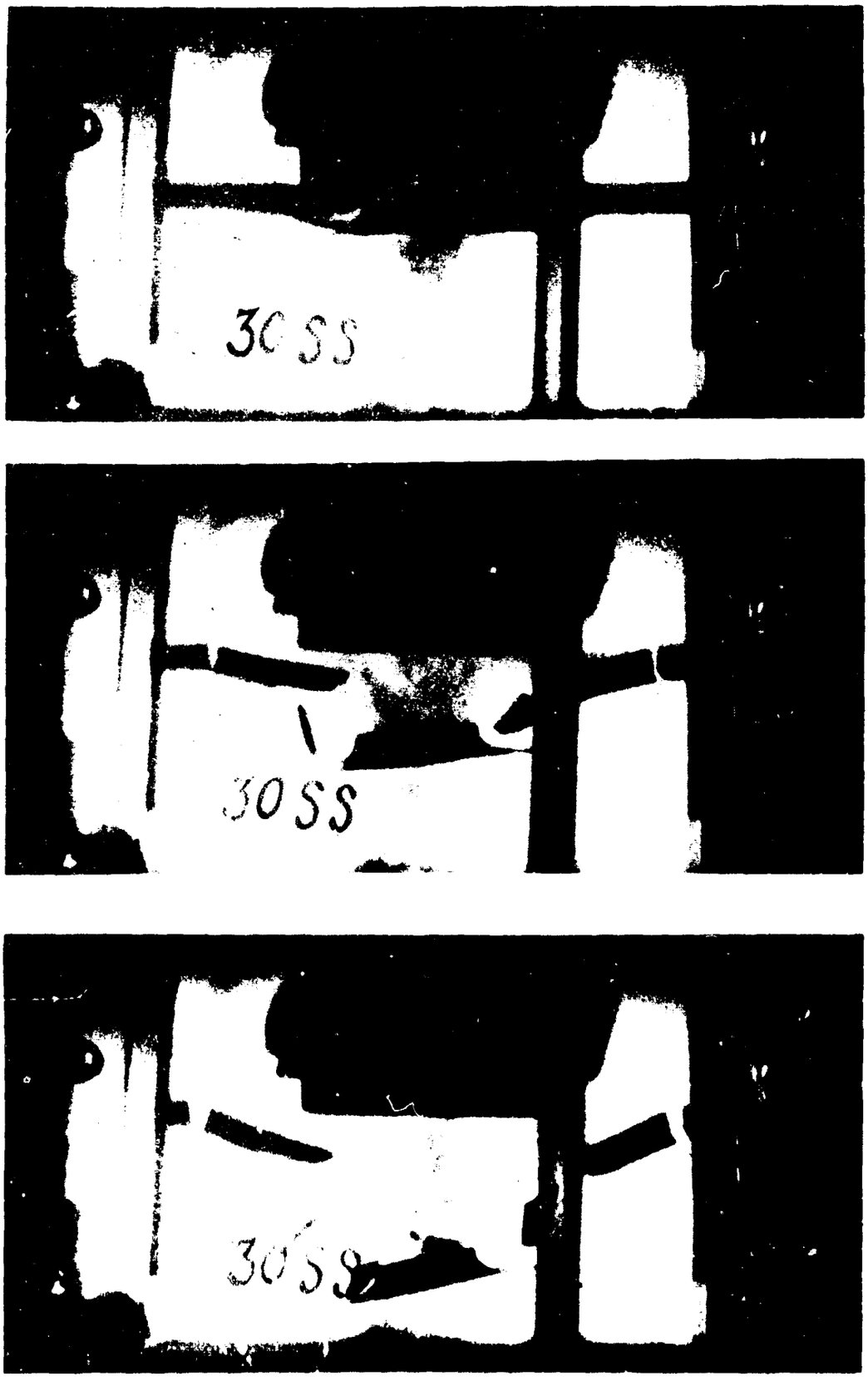

Fig. 3.3 SIMPLY SUPPORTED BEAM UNDER CENTER POINT DYNAMIC LOADING - 30 mg LOAD LEVEL

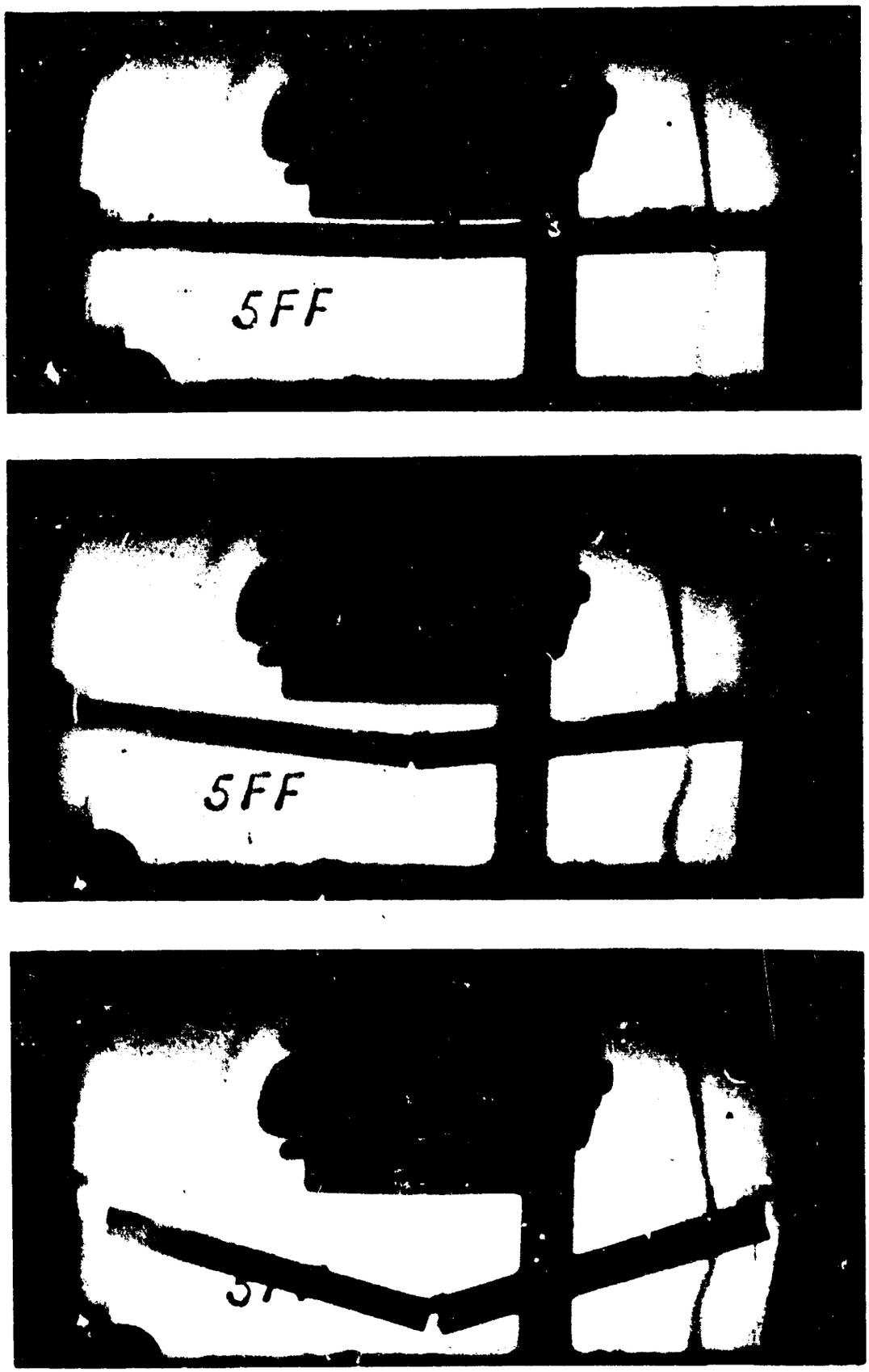

Fig. 3.4 FIXED ENDED BEAM UNDER CENTER POINT DYNAMIC LOADING - 5 mg LOAD LEVEL

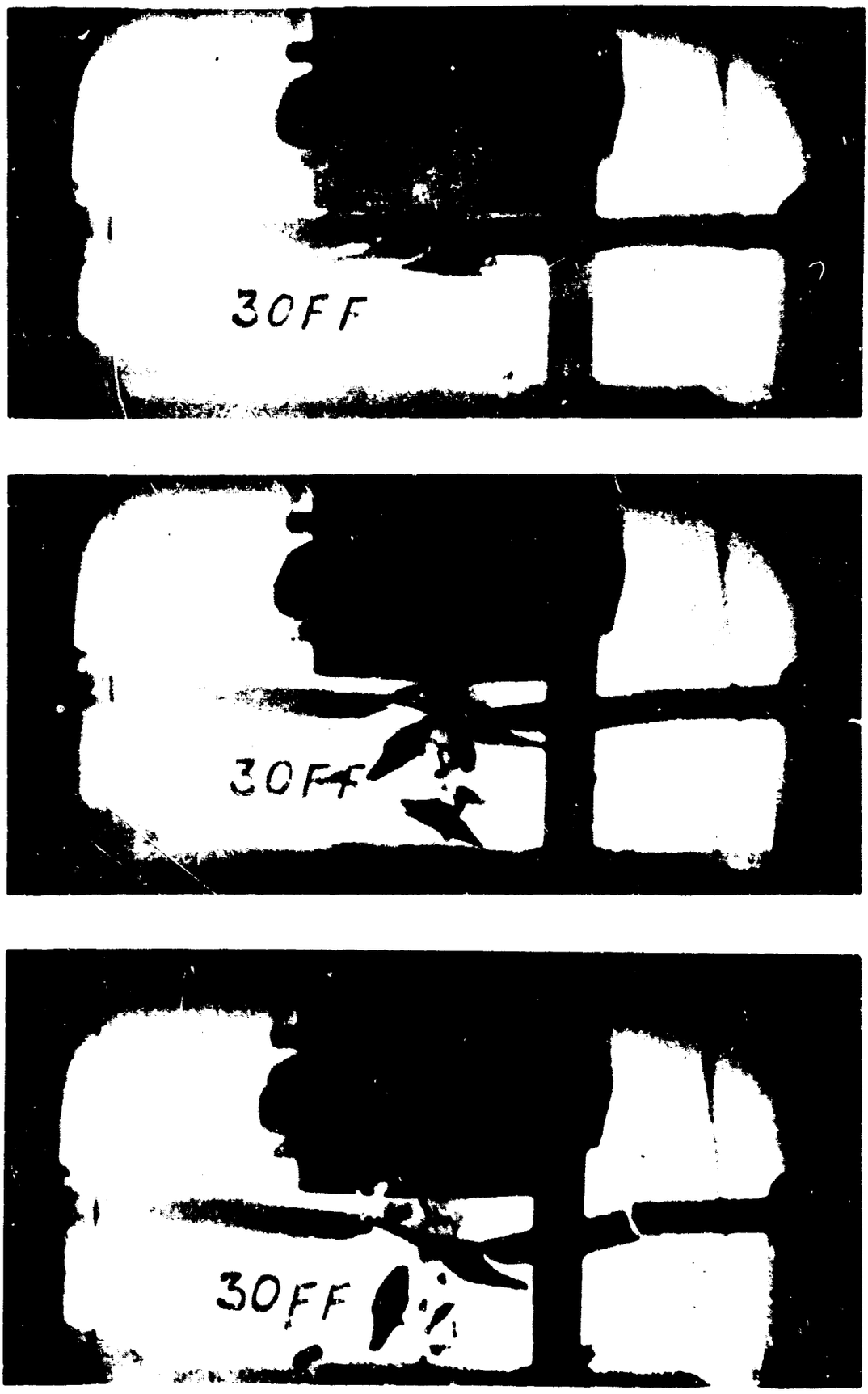

Fig. 3.5 FIXED ENDED BEAM UNDER CENTER POINT DYNAMIC LOADING - 30 mg LOAD LEVEL

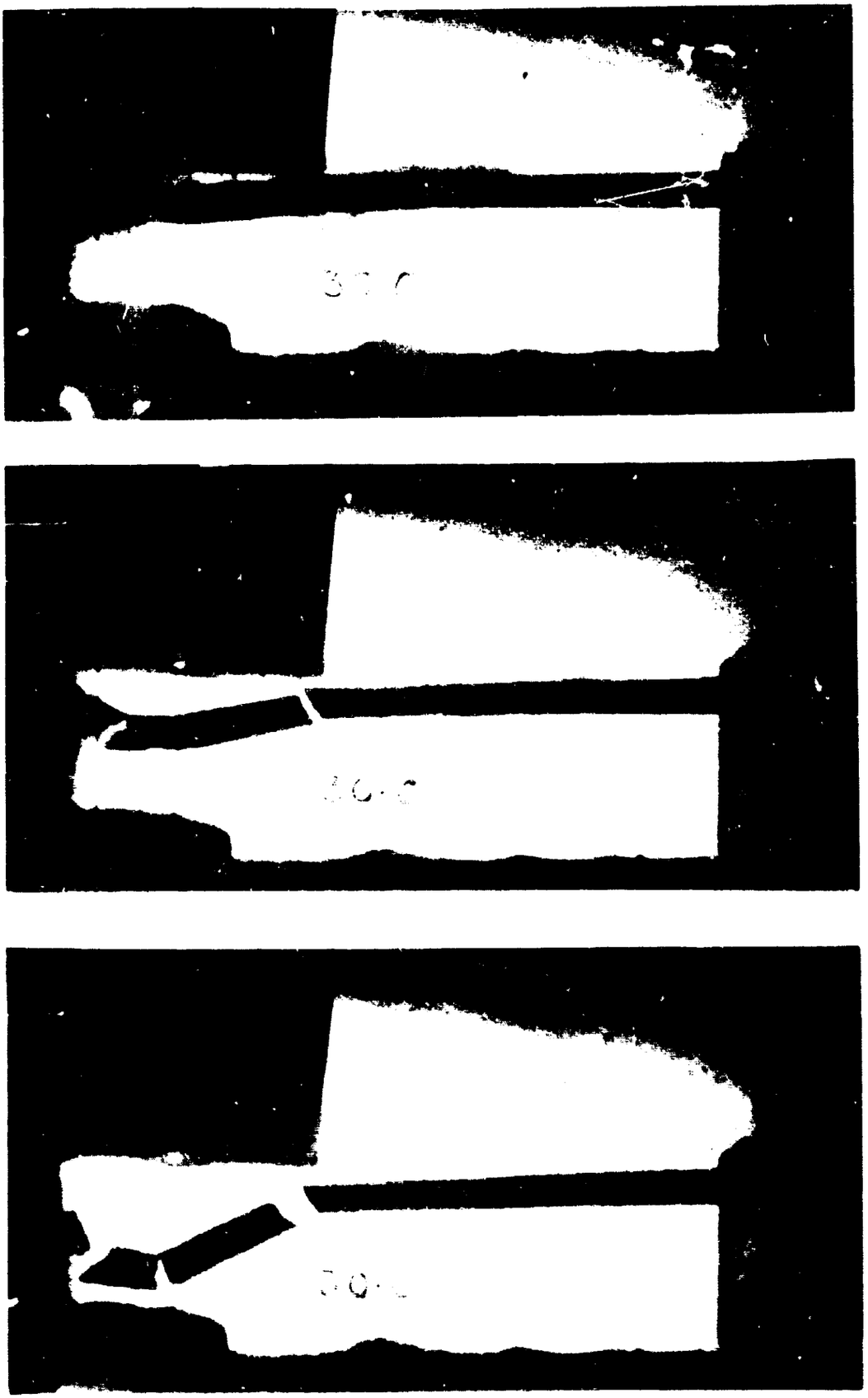

Fig. 3.6 CANTILEVER BEAM UNDER END POINT DYNAMIC LOADING - 30 mg LOAD LEVEL

It is interesting to note that for the load imposed the maximum allowable bending moment was exceeded in 0.1 microsec. Since the velocity of propagation was observed to be 1.28×10^5 in./sec and the masses were lumped 1/2 in. apart, the wave takes at least 6 microsec to reach the nearest adjacent masses. These masses, however, have long since exceeded their allowable maximum in bending. Thus it is now shown in a quantitative as well as qualitative manner that fracture may develop simultaneously and independently at more than one station along a brittle beam. This effect was shown for a concentrated loading. In the more practical case of uniform dynamic loading, this phenomena would be even more pronounced; not being constrained to a localized region.

3.4 Shock Tube Experiments

Shock tube experiments were carried out to determine the piece size distribution versus pressure relationship for fixed ended hydrostone beams under uniform dynamic pressure loadings. The experimental scheme is illustrated in Fig. 3.7. Beams 1/4 in. square and 6 in. long were mounted in a fixture which attaches to the open end of the shock tube. The fixture clamps both ends of the beams, providing a clear span of 5 in. on a "fixed-fixed" beam. A burst diaphragm containing an explosive charge at its center is installed some distance upstream at the static load section of the tube. The explosive charge is then hooked into the igniter circuit. Next, a static pressure, P_1, is placed in the static load section from an ordinary nitrogen gas bottle. When the tap switch in the igniter circuit is closed, the explosive charge bursts the diaphragm and the resulting shock wave travels down the tube and breaks the beams dynamically. An open-end shock tube was used to avoid the effects of wave reflection ordinarily encountered in closed ended shock tubes.

Dynamic pressures were measured by the use of piezoelectric pressure gages placed at the center and end of span. The output of these gages was displayed on a suitable oscilloscope, equipped with a scope-back Polaroid camera which made the dynamic recordings. Results of the dynamic pressure measurements showed very little difference between the pressures at midspan and at the fixed support. Based on this result the pressures measured in each experiment were averaged and taken as the uniform

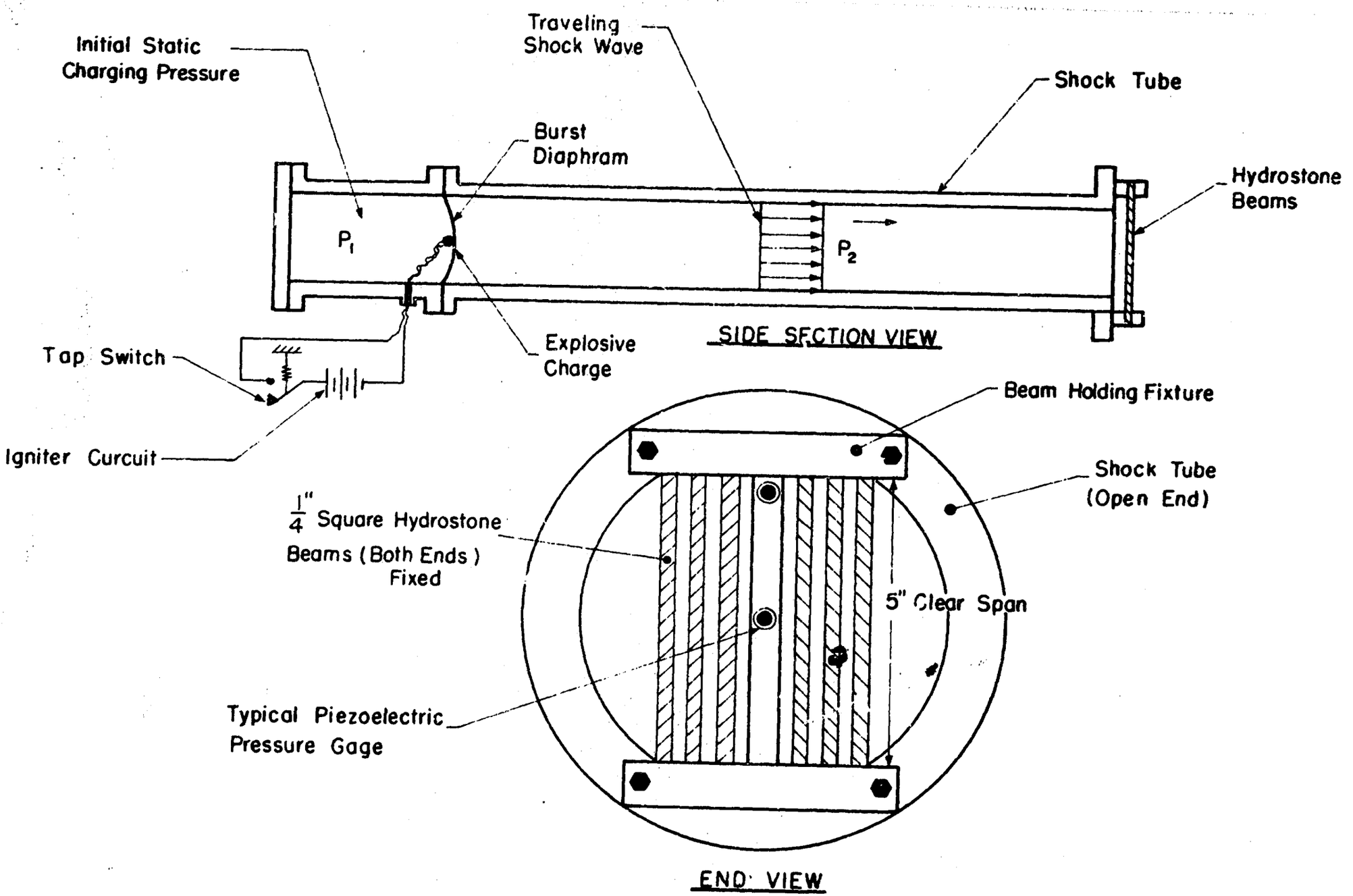

Fig. 3.7 EXPERIMENTAL APPARATUS FOR SHOCK TUBE TESTS

dynamic pressure over the clear span. Static loading pressures ranging from zero to 92 psi where used to charge the tube and the resulting average downstream pressures on the beams varied from 13.5 to 31.8 psi. The lowest pressures obtained resulted from the use of an explosive charge only, with no pressure in the static load section of the tube. Since only about 8 psi would be required to cause static failure in the beams, the minimum dynamic pressure loading greatly exceeds the pressure required to cause failure.

Results in the range 13.5 to 31.8 psi tend to confirm our intuitive and analytical observation that piecesize decreases with increasing load. This is shown in Fig. 3.8 which relates the mean fracture length for a ten unit beam to increasing load.

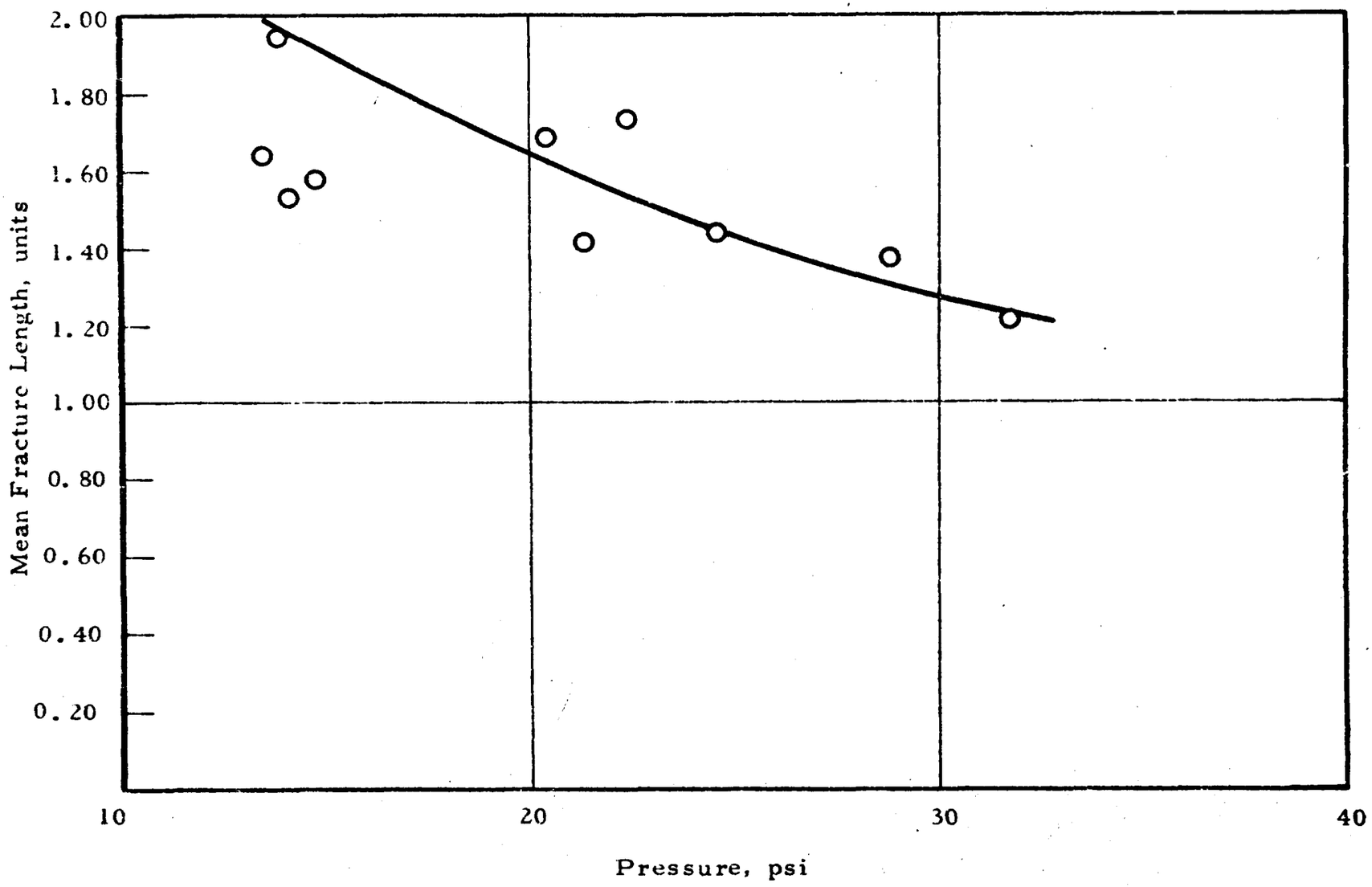

Fig. 3.8 MEAN FRACTURE LENGTH VERSUS PRESSURE

CHAPTER FOUR

TYPICAL STRUCTURAL APPLICATION OF DEBRIS MODELS

4. INTRODUCTION

This chapter deals with the application of the methods developed in the previous chapter to predict how debris resulting from a large multistory structure forms and is transported offsite.

4.1 Model Structure

The model structure to be analyzed is a 40 story curtain wall. The walls are faced with brick which is 6 in. thick. The total wall height is 340 ft and the panel height is 8-1/2 ft. The support structure of the wall will be considered infinitely ductile; thus, only the outside brick material in the panels will be considered as possible transportable debris.

Figure 4.1 illustrates the wall described above except that window openings will not be considered in the fragmentation analysis of an individual panel.

4.2 Loading

It is anticipated that within the fireball region of an atomic blast, total destruction will occur. For situations such as this, debris distribution may be made by the methods developed in the previous report.[1] This report is concerned with those regions which are characterized by only partial destruction. This partial distribution may include failure of exterior and interior walls, but excludes the total collapse and transition on an entire structure (i. e. floor panels, support structure, etc.). The loading that will be investigated will therefore be from about 8 psi to an overpressure region just short of total destruction (18 psi).

Figure 4.2 indicates the blast wave approach to the frontal face of the structure. It is seen that within the overpressure region of interest the structures will be well within the range of the mach stem. It is therefore felt that the pressure will be uniformly distributed across the frontal face of the building. Since each bay on each story will contain one window, the building should undergo diffraction type loading exclusively, at least for the walls.[2]

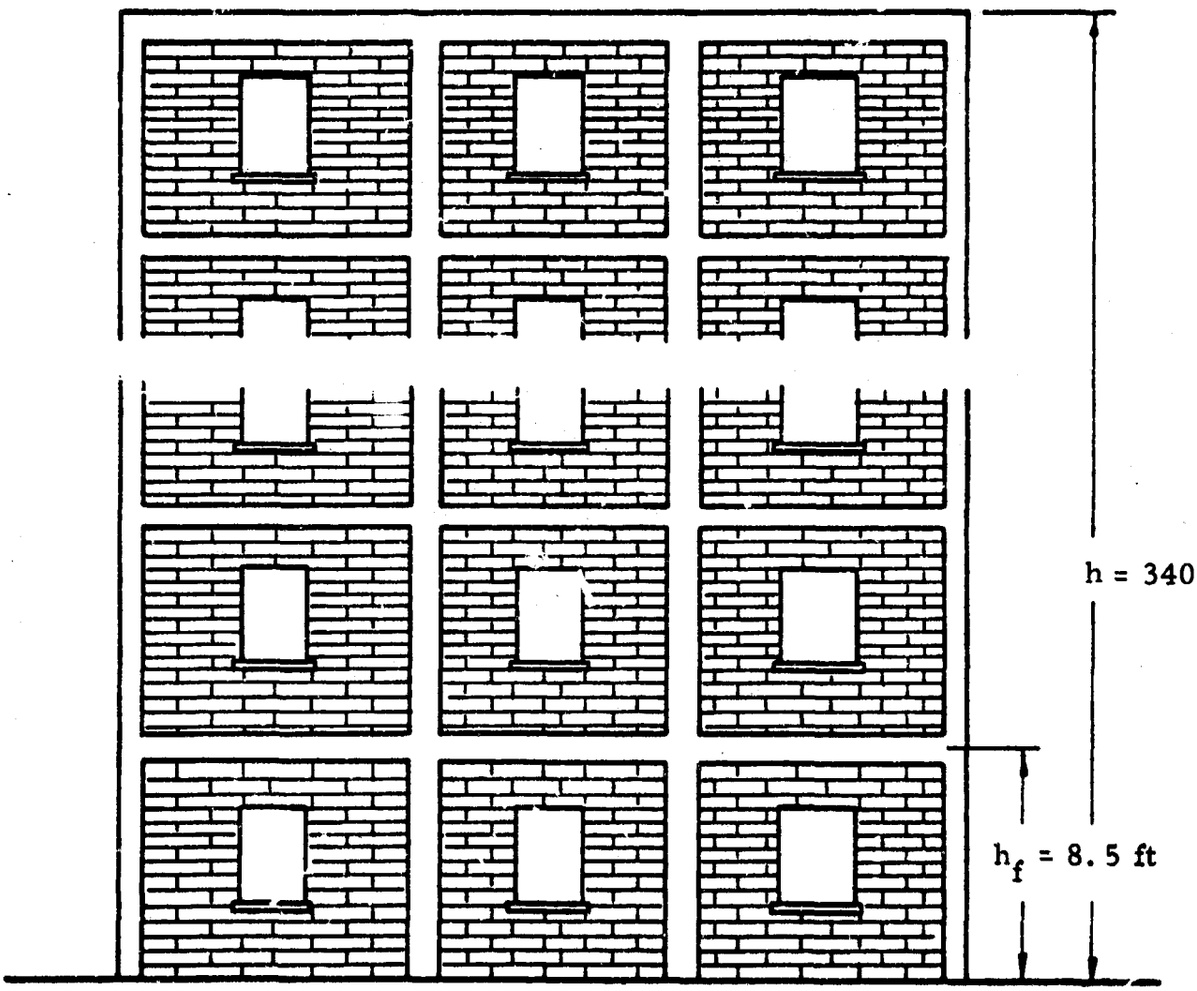

Fig. 4.1 TYPICAL STRUCTURE

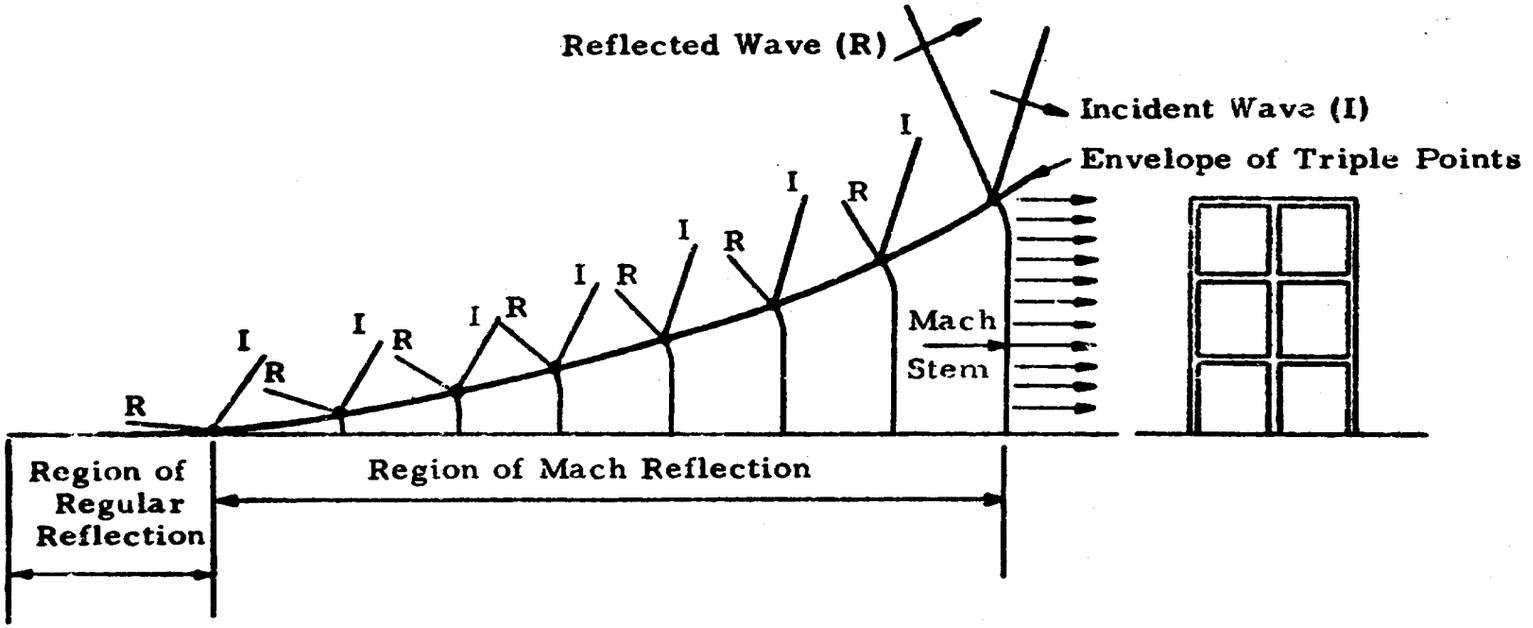

Fig. 4.2 SHOCK FRONT APPROACH TO STRUCTURE

The frontal wall may be expected to receive an overpressure in excess of twice the sideon pressure. This phenomenon occurs due to the fact that as the front of the blast wave strikes the face of the structure reflection takes place. As the blast wave moves forward, the front face reduces to the sideon pressure. The rear, or leeward face, of the structure will experience a pressure in the opposite direction to the pressure on the frontal face. This pressure will have a magnitude equal to the sideon overpressure. What then is the effective loading on the structure? This is depicted in Fig. 4.3 which illustrates the front wall of the structure fragmenting due to a load of twice the sideon pressure. The rear wall is fragmented by a load equal to the sideon overpressure. Although the shock wave caused fragmentation in opposite directions on the front and rear walls, the pressure acting on the leeward wall, from the rear, comes off when the shock front is past the front wall. The only force acting on the fragments will be due to the blast winds associated with the passing shock front. Debris resulting from the fragmentation of the side walls will not be included at this time.

4.3 Panel Fragmentation

Figure 4.4 is a beam analogy for the fragmentation of a masonry panel (i.e., the panel is bounded by the enclosing floors and is between two columns). Failure of a masonry wall panel has been shown to be characterized by the "arching effect"[7] along most of its length (except near the column supports). By expanding the fragmentation distribution of a rigid beam along this "arching length" most of (at some load levels all) the panel's masonry material will be accounted for. In those cases where the "arching effect" only acts for some distance which is short of the panel's total length, the remaining material could be characterized by another beam, cantilevered, on each of the ends adjacent to the columns, and this beam's fragmentation distribution could be expanded between the enclosing floors. The panel to be considered in the following application will have its fragmentation analysis based on the entire panel material acting as a rigid beam of length equal to the panel height (i.e. 8 1/2 ft) and cross section equivalent to the thickness squared (i.e., 6 in. by 6 in.). The results of this analysis of the masonry rigid beam is exhibited in Fig. 4.5 and is analogous to the results depicted in Fig. 2.4 for the cantilevered hydrostone beam.

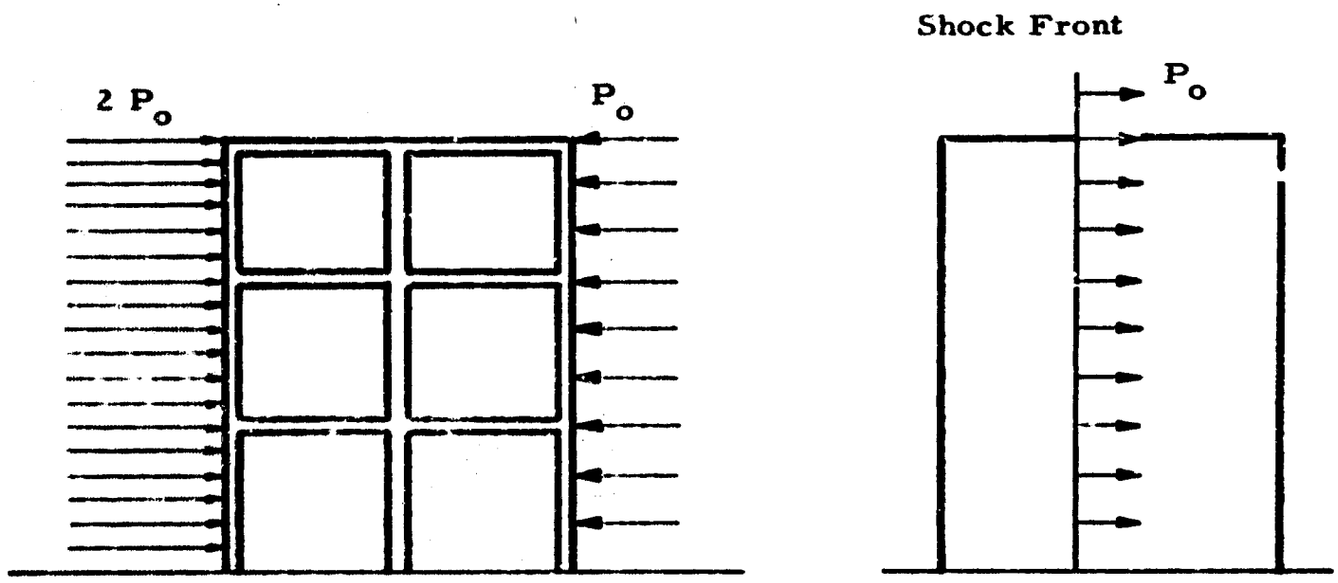

(a) Before Fragmentation

(b) After Fragmentation

Fig. 4.3 LOADING ON WALLS PARALLEL TO SHOCK FRONT BEFORE AND AFTER FRAGMENTATION TAKES PLACE

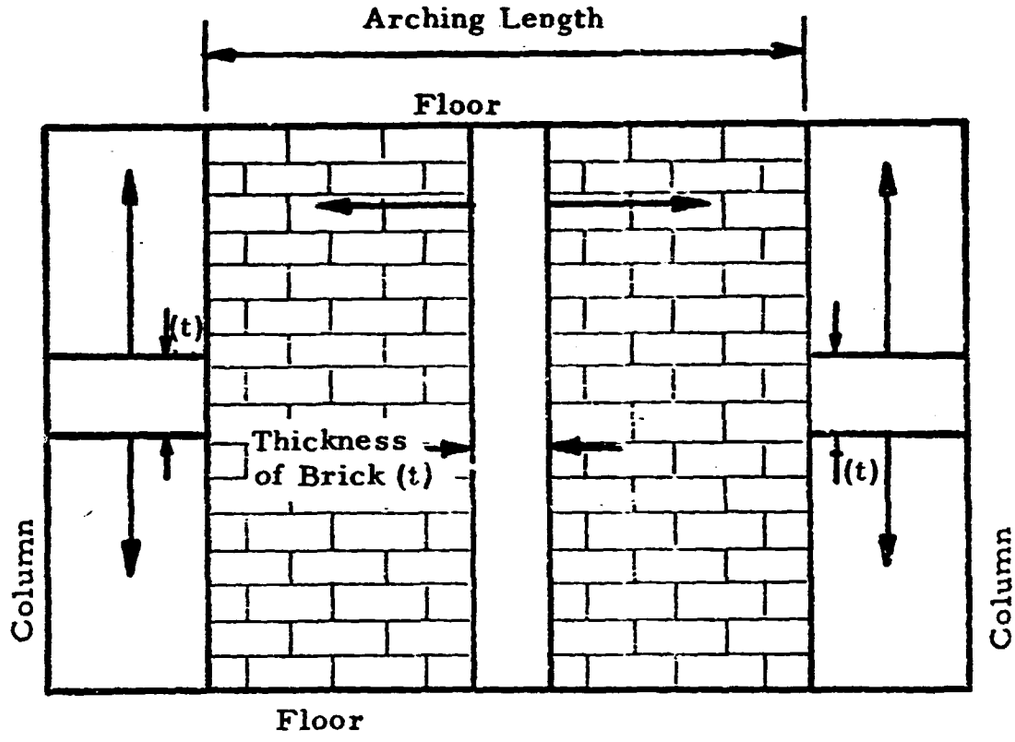

Fig. 4.4 BEAM ANALOGY FOR A MASONRY PANEL FAILURE

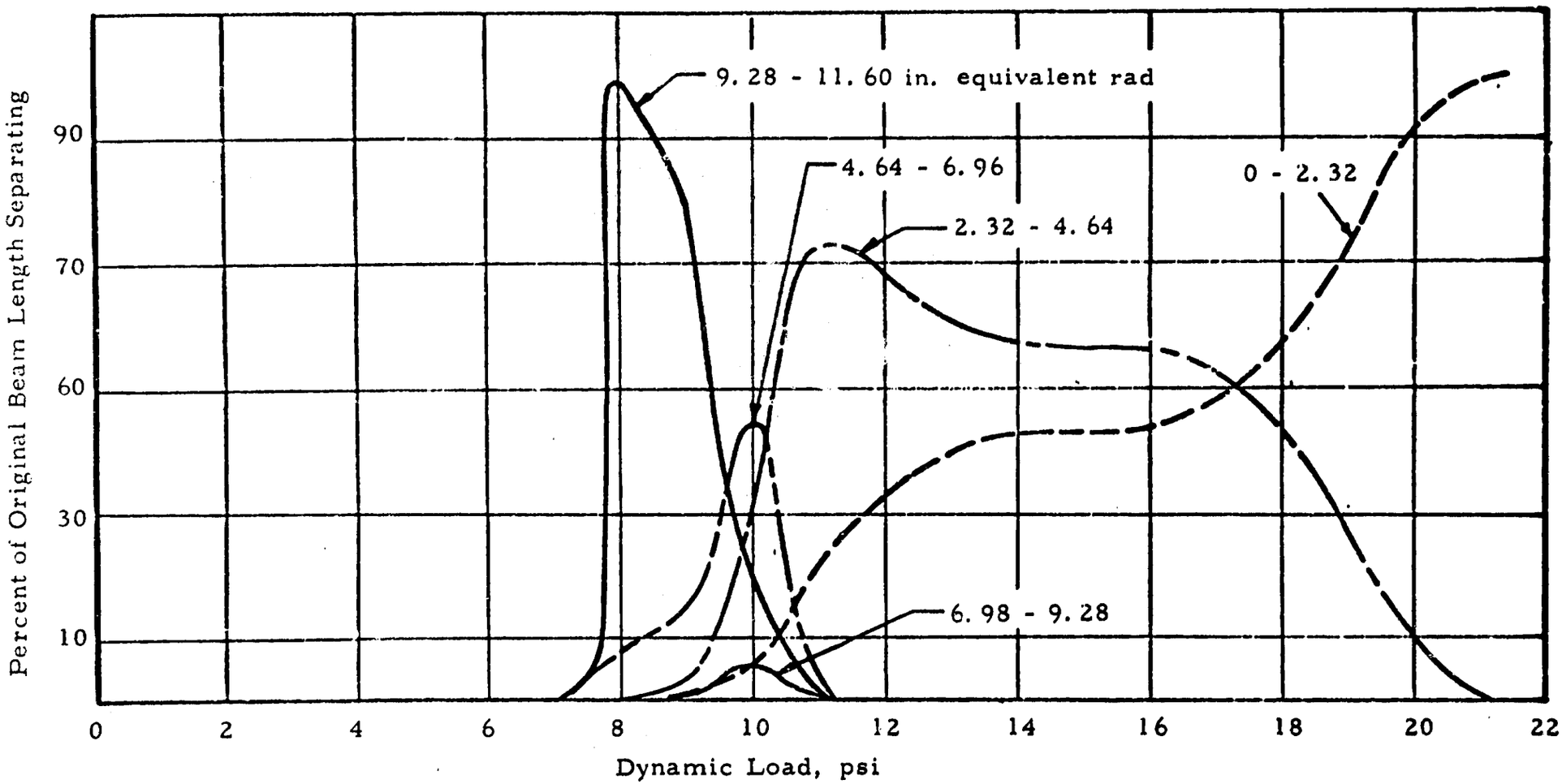

Fig. 4.5 FRAGMENTATION CURVE FOR MASONRY PANEL

4.4 Orientation of Structure with Respect to the Shock Front

The initial distribution studies will not consider any orientations other than the frontal wall being incident to the shock wave. It is understood that orientation will play a large role in determining debris distributions, from both a loading and transport standpoint. This report will not, however, include this effect.

4.5 Fragmentation Results

Figure 4.5 is the fragmentation curve for the masonry panel analyzed as a rigid masonry beam and discussed in Section 4.3 above. The number of trials, n, used in the fragmentation analysis was again 15. The curve indicates that fragmentation occurs at about 8 psi and total pulverization (i.e. only the smallest size interval, 0-2.32 in., is present) is achieved at about 20 psi. Weibull parameters for the masonry beam were determined by experience consistent with the strength of the material. (i.e., $m = 6$, $\sigma_o = 448.0$, and $\sigma_u = 381.0$)

4.6 Transport of Fragment Sizes

The curves in Fig. 4.6 describe the model panel's fragmentation and transport characteristics at a 10 psi overpressure range. It is thus possible to find the expectation of obtaining a particular size particle a given distance from its preblast position.

4.7 Debris Distribution Profiles

The information supplied in Fig. 4.6 is sufficient, along with some knowledge of the wall dimensions, to develop a debris profile. The procedure employed is to uniformly distribute the material from each story height over its transported distance. For example, at 10 psi the particles of size range 2.32 - 4.64 in. equivalent spherical radius at the 40th story travel 345 to 515 ft horizontally from their original position before striking ground. We thus distribute 32 percent (i.e. the percentage of material between 2.32 and 4.64 in. radius at 10 psi) of the wall material for one panel over an area of length 170 ft and unit width. The height of this distributed material may be determined by dividing the percentage of fragments of size 2.32 - 4.64 in. radius by the unit width area over which the material distributes.

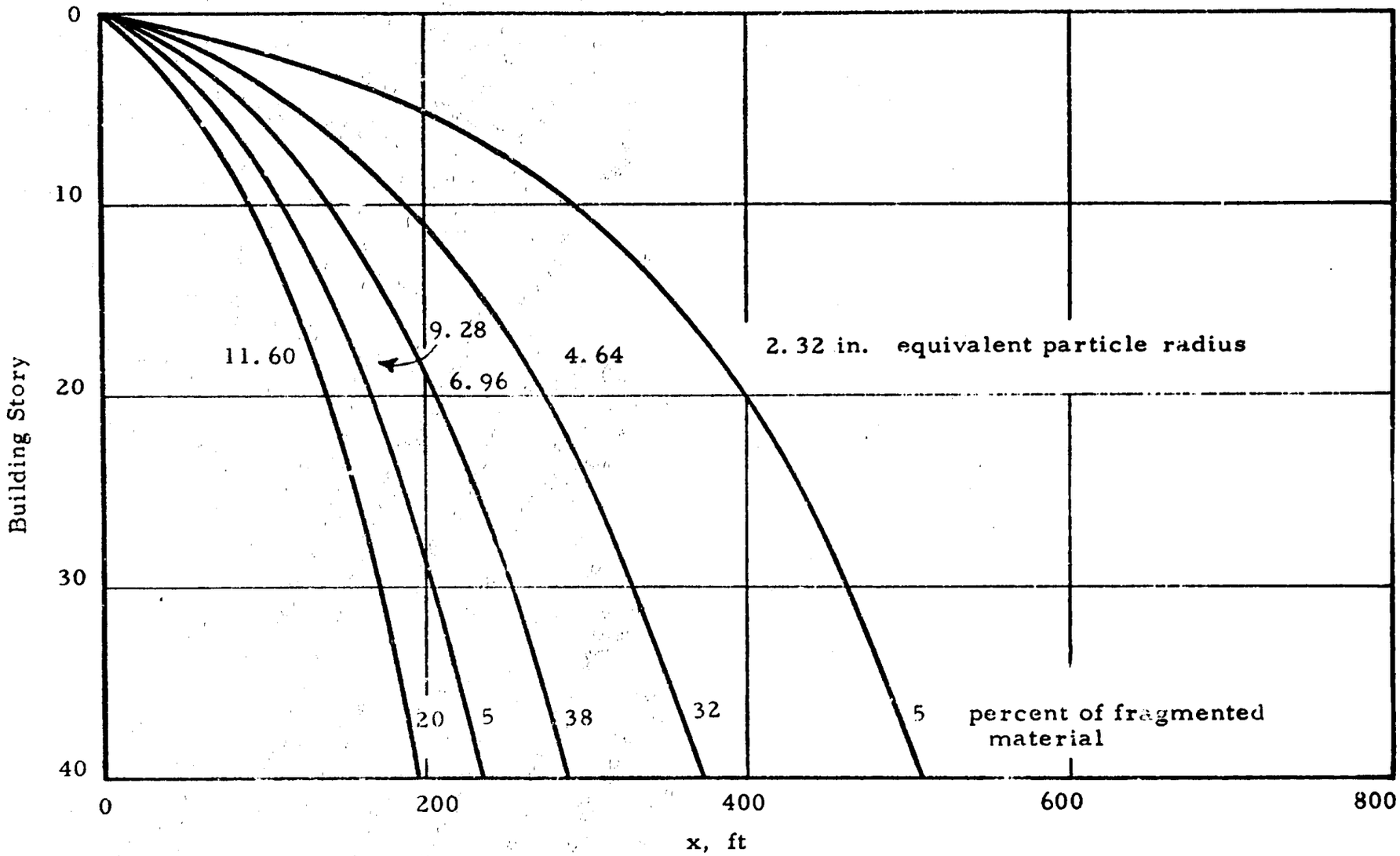

Fig. 4.6 FRAGMENTATION AND TRANSPORT CHARACTERISTICS FOR MODEL PANEL

The above procedure for determining debris height implies a unit volume of material at the 40th story level (i.e., the panel at this level is 1 ft long by 1 ft thick). Thus the debris height is "normalized" for a unit panel volume, however, the actual thickness of the panel, utilized later in determining actual debris heights, is implied (i. e., 6 in.) implicitly by the development of the Weibull parameters used in the fragmentation analysis. If we repeat the procedure for all size ranges at a given story and then at each story of the wall, then by superimposing all these individual debris depths upon one another we obtain a normalized debris profile. The profiles are normalized in the sense that we must multiply the debris depth by the volume of material in the panel at one story level. (i. e., 8 1/2 ft high by 1/2 ft thick by 1 ft wide minus a correction for window openings). The super position procedure is illustrated in Fig. 4. 7.

Appendix E contains profiles for a range of wall heights and in some cases fragmentation criteria were varied over a constant wall height to illustrate the sensitivity of the debris profile to fragment particle size. The three cases of fragmentation criteria were:

a) 100 percent small particles 0-2. 32 in. in radius.

b) The panel fragmentation behavior at 10 psi as calculated by the methods developed in Chapter II and illustrated in Fig. 4. 5 for the masonry beam.

c) 100 percent large particles 9. -28 - 11. 60 in. in radius.

The critical characteristics of these curves are specified in Table 4. 1. The parameters X^* and y^* are the same as illustrated in Fig. 1. 3. Again, in order to relate the y^* to actual debris height it must be multiplyed by the unit width volume of panel material at one story level. (i. e. 8 1/2 ft by 1/2 ft corrected for any wall aperatures).

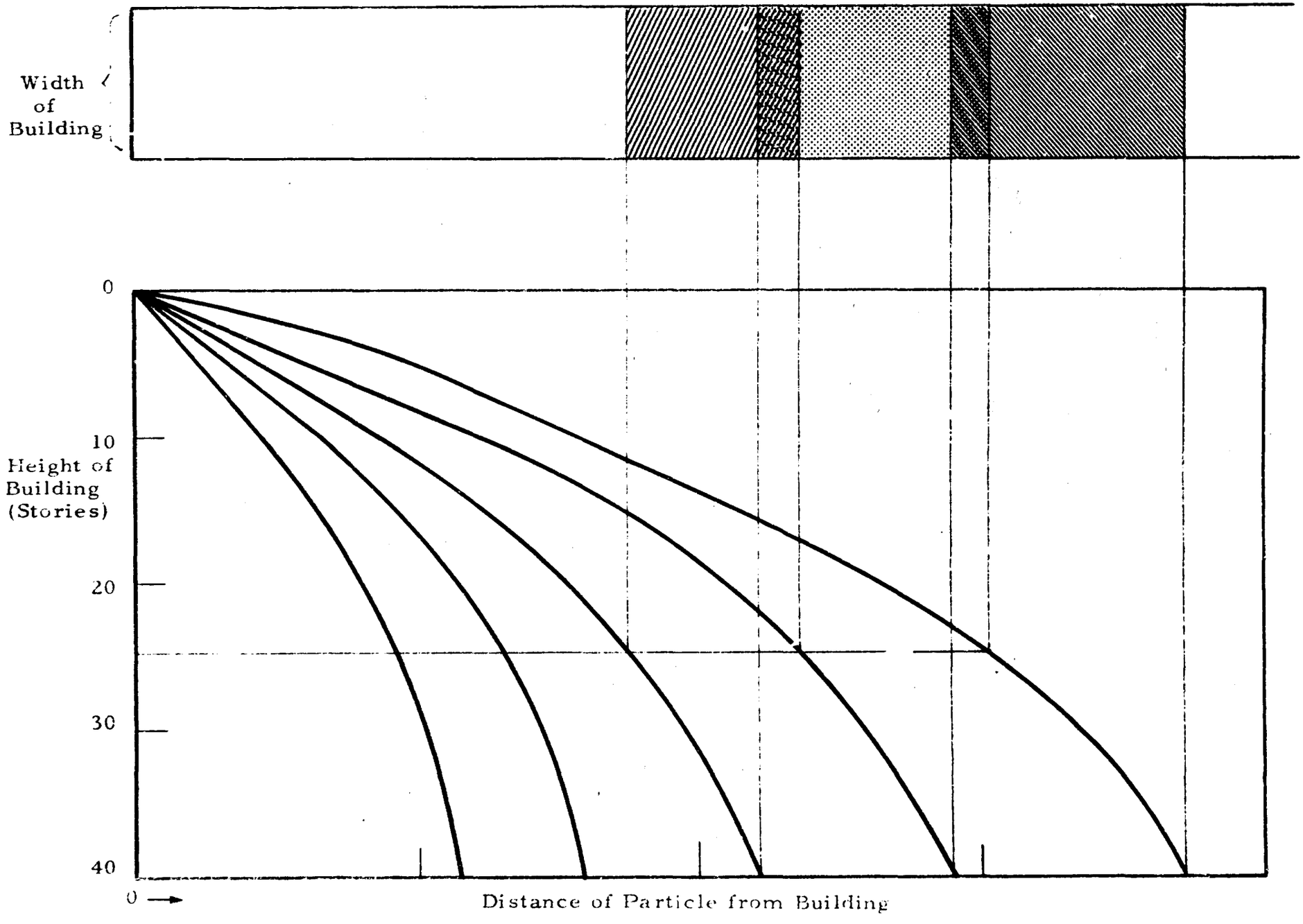

Fig. 4.7 CONSTRUCTION OF DEBRIS PROFILES

Table 4.1

SENSITIVITY OF DEBRIS CONTOURS TO BUILDING HEIGHT AND PARTICLE SIZE

Building Height	All Small		Predicted		All Large	
	x^*	y^*	x^*	y^*	x^*	y^*
40	514	0.003	200	0.036	200	0.085
35	496	0.0027	180	0.035	180	0.080
30	460	0.0023	165	0.032	130	0.075
25	425	0.019	155	0.029	- -	- - -
20	400	0.015	135	0.026	130	0.060
15	350	0.012	125	0.023	125	0.055
10	300	0.009	75	0.018	90	0.045
5	175	0.006	50	0.015	40	0.040

CHAPTER FIVE

CONCLUSIONS AND RECOMMENDATIONS

5. SUMMARY

The work in the first four chapters of this report completes this phase of the debris study. It is significant to note that it is now possible to predict the deposition of offsite debris with a one-to-one correspondence between the original structural material and its final rubble form for brittle wall elements. This debris model is based upon a fragmentation theory that is derived from a statistical approach to the strength of brittle materials. The validity of the theory has been verified by the dynamic experiments of Chapter Three. The fragmentation model was outlined for a variety of end conditions and is a significant computational improvement over the method previously developed.[1]

Debris profiles of hypothetical masonry wall panels were generated utilizing a simple distribution procedure. The results of this study indicate the validity of the general procedure for obtaining the debris profile for a single building.

5.1 Conclusions

1. Debris may be divided into two categories, offsite and onsite. Onsite debris prevents no impedance to logistic activity other than localized shelter rescue operations.

2. In order to characterize offsite debris profiles, the piecesize distribution of the fragments must be known. This is in order to characterize the particle's trajectory.

3. Low level dwellings must be included as potential debris producing structures. Even elements at 10 ft above ground may be transported significant distances (e.g. into the street) at moderate overpressure levels (10 psi).

4. In general, smaller particles from higher initial heights will be transported greater distances than larger particles at lower heights. As overpressure increases the size of the particle fragmenting will be smaller.

5. Particles fragmenting and being transported offsite from their original position will have an extremely high terminal velocity (i.e., at least 50 ft per sec). For this reason, offsite debris must be considered an extremely dangerous secondary effect of blast. This effect must be evaluated in light of its damage producing capabilities to structures as well as a casualty producing mechanism to unsheltered populence.

6. The assumption that the maximum dynamic stresses introduced into the various unit segments are independent of the fracture characteristics has been shown both experimentally (Chapter Three) and analytically (Appendix C). This establishes the theoretical development of the fragmentation model.

7. The statistical strength characteristics of typical unit segments have been expressed by their cumulative distribution function, F(p). This function gives the probability of fracturing the unit at a load magnitude equal to or less than p and for computational purposes has been expressed in Weibull form. It is to be emphasized that this form was chosen for convenience. At present, Weibull parameters are not known for many common construction materials and must be determined as outlined in Appendix B.

8. Debris profiles from multistory walls may be generated as outlined in Chapter Four. As one may see from Appendix E the profiles are typically unimodal in shape and of course are very sensitive to piecesize distribution. For walls at 5, 10, 15 stories in height profiles exist for each of three piecesize distributions, all large, predicted, and all small. It is interesting to note that the large particles generally lend most of the shape to the predicted size profile. That is, up to the peak the large size particles predominate. This, of course, is in part due to the method of developing these profiles. Large particles are distributed over much less area than small ones and hence tend to produce much greater depths.

9. The profiles in Appendix E. have their ordinate normalized with respect to volume and packing. (Packing corresponds to a void ratio of 1.0 in Appendix E.) If the ordinate were multiplied by the unit width volume of material at one story height and then again by a suitable void ratio, then the profile would express the true depth of the building's transported debris at all points along its transported distance.

5.2 Recommendations

After reading this report one can see that the balance covers only one area as outlined in Chapter One (i. e., brittle wall elements). In addition, the analytical methods of fragmentation and subsequent transport did not consider either the effects of orientation of the structure to the blast or shielding of one building by another. It is therefore recommended that any follow on study should:

1. Continue to develop analytical methods for additional structural materials and elements as well as complete structures. These analytical models should be suitably verified by appropriate experimental investigation.
2. The individual building debris contours must be combined to give a cumulative debris contour for an entire subarea of contiguous structures.
3. Effects of blast orientation and structural shielding should be accounted for in specifying the load on the structure.
4. Finally, all methods developed should be combined to yield a single computational model, as outlined in Chapter One.

REFERENCES

1. Ahlers, E. B., "Debris Clearance Study," IIT Research Institute, for the Office of Civil Defense, OCD-PS-62-202, Subtask 3322-A, September 1962.

2. Glasstone, S., (Editor), "The Effects of Nuclear Weapons," revised edition, prepared by the U. S. Department of Defense and published by the U. S. Atomic Energy Commission, Supt. of Documents, U. S. Government Printing Office, Washington 25, D. C., April 1962.

3. Brode, H. L., "Point Source Explosion in Air," Report AECU-3517, the Rand Corporation, December 3, 1956.

4. Raynham, C. J. SES 100 Ton TNT Blast Trial, "Model Studies of the Movement of Debris from Brick Panels which Fail Under the Action of a Blast Wave," AWRE Report No. E7/63, August 1961.

5. Uspensky, J. V., Introduction to Mathematical Probability, McGraw Hill Book Company, Inc., 1937.

6. Weibull, W., "A Statistical Theory of the Strength of Materials," Ingeniorsvetenskapsacademein, Handlingar No. 151 and 153, 1939.

7. McDowell, E. L., McKee, K. E., and Sevin, E., "Arching Action Theory of Masonry Walls," Journal of the Structural Division, Proceedings of the ASCE, Paper 915, Vol. 82, March 1956.

8. Ungar, A., "Logistical Study of Debris Removal," IIT Research Institute, for the Office of Civil Defense, OCD-PS-64-50, Subtask 3322-A, August 1964.

9. Abbott, B. W., "Dynamic Tests of Reinforced Concrete Beam-Columns," M. S. Thesis, Massachusetts Institute of Technology, Department of Civil Engineering, May 1961.

10. Yang, C. Y., Reinschmidt, K. F. and Hansen, R. J., "Stress Propagation in Reinforced Concrete Columns," Symposium on the Use of Computers in Civil Engineering, Vol. I, pp. 53.21-53.27, Lisbon, Portugal, 1962.

11. English, J. M., "Rupture of Brittle Beams Under Impulsive Loading," Report No. 51.14, Department of Engineering, University of California (Los Angeles), December 1951.

12. Griffith, A. A., "The Phenomena of Rupture and Flow in Solids," Phil Trans. Roy. Soc., Series A, No. 221, pp. 163-198, March 1927.

13. Abbott, B. W. and Cornish, R. H., "A Stress Wave Technique for Determining the Tensile Strength of Brittle Materials," Experimental Mechanics, April 1965, Vol. 5, No. 4.

APPENDIX A

COMPUTATIONS OF STATIC STRESS DISTRIBUTIONS FOR DIFFERENT END CONDITIONS

Fixed-Free

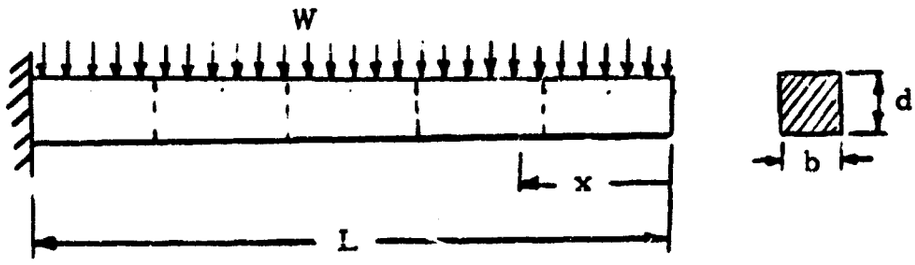

Fig. A. 1 CANTILEVER BEAM UNIFORMLY DISTRIBUTED LOAD

For the beam in Fig. A. 1,

$$M_x = \frac{wx^2}{2} \qquad 0 < x \leq L$$

$$\sigma_x = \frac{M_x C}{I} \qquad C = \frac{d}{2}$$

$$\sigma_x = \frac{3wx^2}{bd^2} \qquad I = \frac{bd^3}{12}$$

but $w = P_s b$ where P_s is the static load

and $P_s = \frac{P_d}{K}$ where P_d is the applied dynamic load and K is the dynamic load factor. Therefore,

$$\sigma_x = \frac{3P_d x^2}{Kd^2}$$

Simply Supported

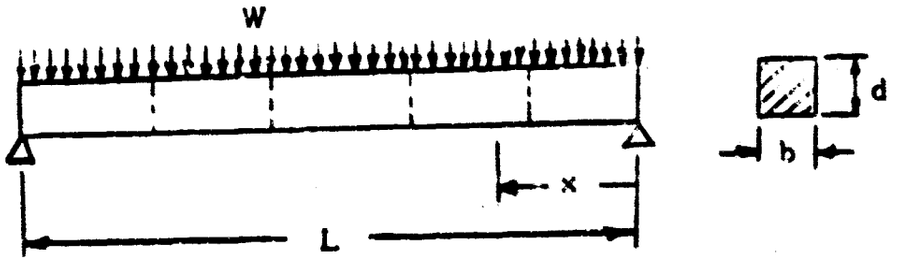

Fig. A. 2 SIMPLY SUPPORTED BEAM-UNIFORMLY DISTRIBUTED LOAD

The beam shown in Fig. A. 2 has a moment distribution for $0 < x \leq L$ of:

$$M_x = \frac{w\,x}{2}(L-x)$$

Since

$$\sigma_x = \frac{M_x C}{I} \quad \text{and} \quad I = \frac{b d^2}{12}; \quad C = \frac{d}{2}$$

Then

$$\sigma_x = \frac{3\,wx\,(L-x)}{b d^2} = \frac{3\,P_d x(L-x)}{K d^2}$$

Fixed-Fixed

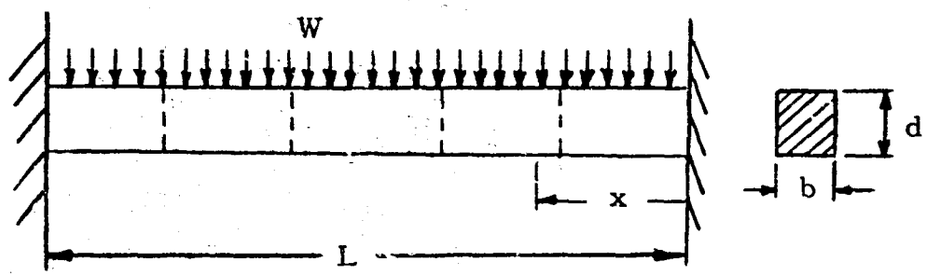

Fig. A. 3 BEAM FIXED AT BOTH ENDS-UNIFORMLY DISTRIBUTED LOAD

For the beam shown in Fig. A. 3,

$$M_x = \frac{w}{12}(6\,Lx - 6x^2 - L^2) \qquad 0 < x \leq L$$

Therefore

$$\sigma_x = \frac{M_x C}{I} = \frac{W(6\,Lx - 6x^2 - L^2)}{2\,b\,d^2}$$

$$\sigma_x = \frac{P_d(6\,Lx - 6x^2 - L^2)}{2\,K\,d^2}$$

APPENDIX B

DETERMINATION OF STATISTICAL STRUCTURAL PARAMETERS

The statistical strength characteristics of a typical unit segment are described by its cumulative distribution function, F(P). This function gives the probability of fracturing the unit at a load magnitude equal to or less than the applied loading. The distribution function may be determined by physically testing many unit segments or by appealing to one of the "weakest link" statistical fracture theories. Of these, Weibull's is the most popular theory now in use.

One method for determining the values of Weibull's statistical parameters m, σ_u and σ_o is the graphical method. The method can be applied for any type of test, however, for illustrative purposes a rectangular beam under pure bending will be considered here.

Let N be the number of nominally identical specimens whose fracture strengths have been determined. The fracture strengths are ordered in increasing magnitude such that

$$\sigma_1 < \sigma_2, \cdots, \sigma_{n-1} < \sigma_n, \cdots\cdots, \sigma_{N-1} < \sigma_n \tag{1}$$

Corresponding to the fracture strength σ_n of rank n, the cumulative probability of failure F_n is given by

$$F_n = \frac{n}{N+1} \tag{2}$$

For a rectangular beam under pure bending, Weibull's expression for the cumulative probability of failure is, for $\sigma \geq \sigma_u$,

$$F(\sigma) = 1 - \exp\left[\frac{V}{2(m\ \ 1)}\left(\frac{\sigma - \sigma_u}{\sigma}\right)\left(\frac{\sigma - \sigma_u}{\sigma_o}\right)^m\right] \tag{3}$$

where σ is the maximum fiber stress. This equation may be rewritten as

$$\log\log\left(\frac{1}{1-F}\right) + \log\sigma = (m+1)\log(\sigma-\sigma_u) - m\log\sigma_o + \log\frac{V}{2(m+1)} \tag{4}$$

It can be seen that a plot of this distribution function will be linear in a system of rectangular coordinates in which

$$\log\log\left(\frac{1}{1-F}\right) + \log\sigma$$

is the ordinate and $\log(\sigma - \sigma_u)$ is the abscissa.

Also, m+1 will be the slope of the distribution in these coordinates.

Thus the determination of the Weibull parameters proceeds as follows. A guess is made for the value of σ_u. A plot of

$$\log \log \left(\frac{1}{1 - F_n} \right) + \log \sigma_n \text{ versus } \log (\sigma_n - \sigma_u)$$

is made and fitted with a curve. If the curve is concave up, the value of σ_u should be decreased (however, a negative σ_u is physically unreasonable) and if the curve is concave down, the value of σ_n should be increased. This process is pursued until the resulting curve is (or may be approximated by) a straight line. This value of σ_u is the correct one. The value of m is determined as the slope minus one. Taking V to be the total volume of the beam in the same units of length as appearing in the stresses σ and σ_u, the value of σ_o may be determined by inserting the coordinates of a point on the line into Eq. (4).

APPENDIX C

A DYNAMIC ANALYSIS OF A CANTILEVER UNDER AN IMPULSIVE LOAD

For the beam shown below a concentrated load P is applied at an arbitrary distance (a) from the free end.

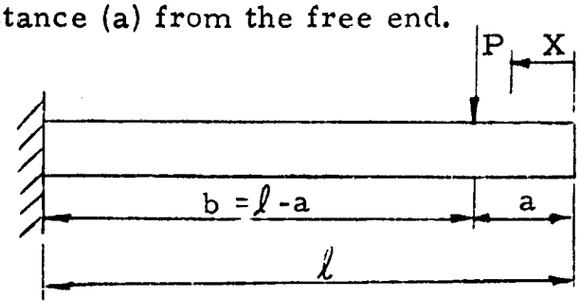

Fig. C.1 CANTILEVER UNDER ARBITRARY CONCENTRATED LOAD

From elementary beam theory the deflection x distance from the free end is:

$$y = \frac{P(\ell - x)^2}{6EI}(3b - \ell + x) \qquad (C\text{-}1)$$

We now let f_{ij} represent the deflection at point x_i due to a unit load (P = 1) at point x_j. Then using Eq. (C-1) and letting (a) represent x_j, x replace x_i and P = 1

$$f_{ij} = \frac{(\ell - x_i)^2}{6EI}(3(\ell - x_j) - \ell + x_i), \qquad i \geq j \qquad (C\text{-}2)$$

Formula (C-2) generates the lower triangular portion of the flexibility matrix $[F]$. Let the cantilever in Fig. C-1 be approximated by n equally lumped masses as shown below and loaded at

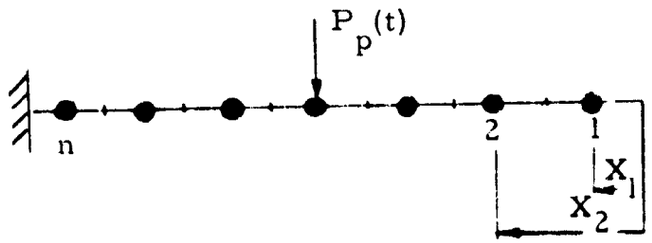

Fig. C.2 LUMPED MASS APPROXIMATION

mass number p. Then each lumped mass is

$$m = \frac{\rho \ell}{n}$$

where ρ is the beam mass per unit length.

The equilibrium equations which represent Fig. C. 2 are

$$\{P_p\} - m [I] \{\ddot{Y}\} = [k] \{Y\}$$

or

$$\{\ddot{Y}\} = \frac{1}{m} \{P_p\} - \frac{1}{m} [k] \{Y\}$$

let

$$\{\overline{P}_p\} = \frac{1}{m} \{P_p\} \text{ and } [\overline{k}] = \frac{1}{m} [k]$$

Thus

$$\{\ddot{Y}\} = \{\overline{P}_p\} - [\overline{k}] \{Y\} \qquad \text{(C-3)}$$

where $[k] = [F^{-1}]$ stiffness matrix, order n x n

$[I]$ = Identity Matrix, order n x n

$\{\ddot{Y}\}$ = Acceleration Vector, order n x n

$\{Y\}$ = Displacement Vector, order n x n

$$\{P_p\} = \begin{bmatrix} 0 \\ 0 \\ \vdots \\ P_p \\ 0 \\ 0 \end{bmatrix} \begin{matrix} 1 \\ 2 \\ \\ p \\ \\ n \end{matrix} = \text{Load Vector, order n}$$

Equation (C-3) represents a system of second order differential equations with the load P at mass p a function of time. This problem is an initial value one with the following conditions:

$$Y = 0 \text{ at } t = 0$$

and

$$\dot{Y} = 0 \text{ at } t = 0$$

The initial value problem was solved using a Runge-Kutta numerical integration scheme. At any time, t, the moment at point i, M_i, is

$$M_i = \begin{cases} \sum_{j=1}^{i-1} m \ddot{y}_j (x_i - x_j) + \frac{m}{8} \ddot{y}_i \, dx, & i \leq p \\ \sum_{j=1}^{i-1} m \ddot{y}_j (x_i - x_j) + \frac{m}{8} \ddot{y}_i \, dx - P_p (x_i - x_p), & i > p \end{cases}$$

Figure C.3 indicates the load-time history corresponding to a 30 mg charge which was used for $P_p(t)$. Figure C.4 shows the nondimensional bending moment diagram M/M_o versus x for various t.

where $$M_o = \frac{\sigma_B^o b d^2}{6}$$

and σ_B is the dynamic tensile stress.

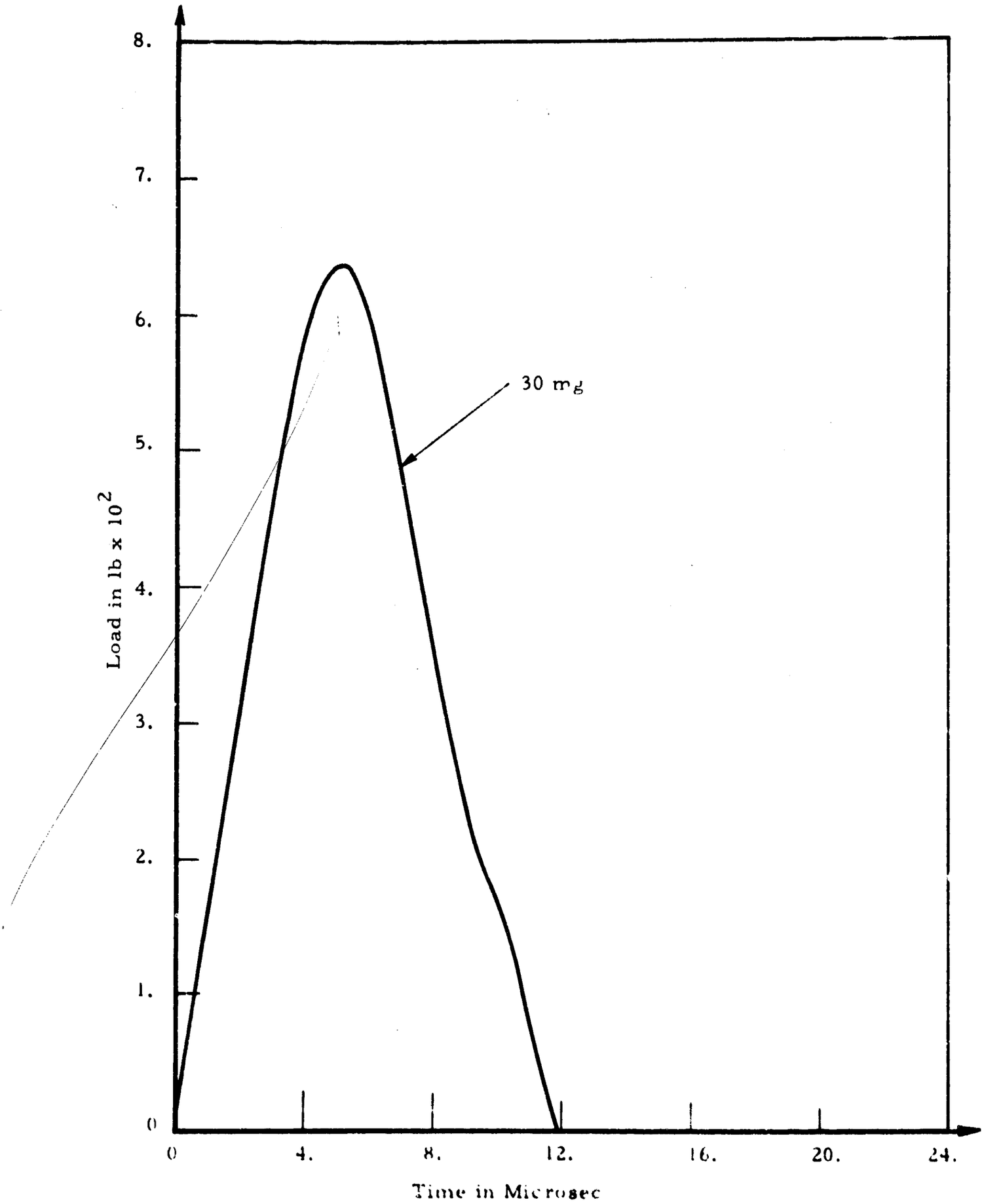

Fig. C. 3 LOAD-TIME HISTORY FOR 30 MG LEAD AZIDE CHARGE

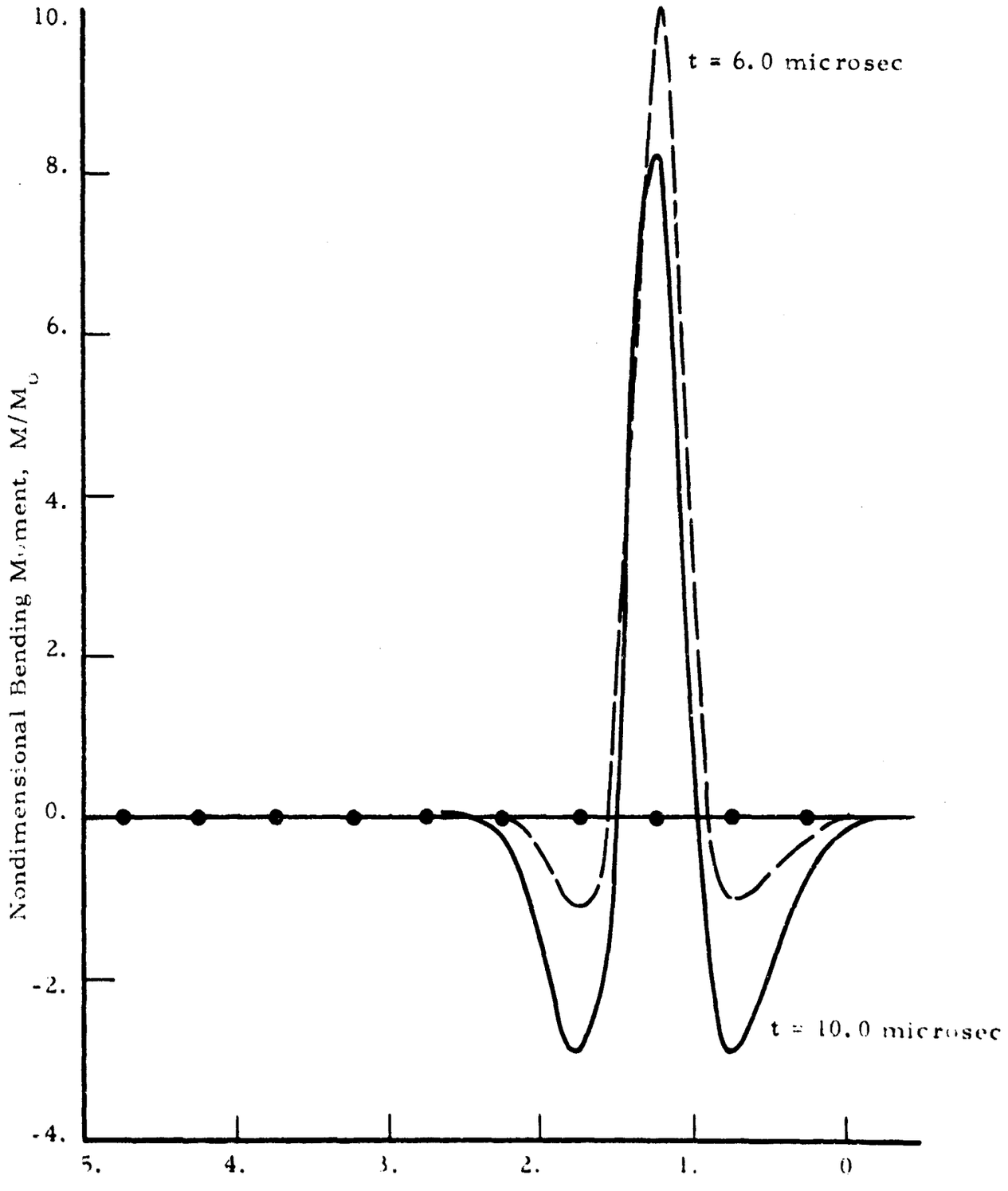

Fig. C.4 DYNAMIC BEAM BENDING MOMENT

APPENDIX D

FRAGMENTATION AND TRANSPORT CURVES FOR W = 1 MT

Trajectory calculations relating distance traveled to impact velocity for various initial heights were carried out, according to the method described in Section 2.2. The procedure utilized equivalent spherical fragment sizes corresponding to the results of the masonry fragmentation study of Chapter Four. Spherical fragments were selected for this analysis since drag effects are identical for all orientations of the sphere; whereas little is known of drag effects of irregular material at random orientation or during rotation. The effect of this assumption is to average out the effects of large and small projected areas from the irregular objects.

A value of 1.0 was used for the drag coefficient, C_d. This is an approximate value in the velocity range the particles travel. The selected value of the material density was 135 lb per ft^3, which is in the range of most masonry building materials.

Results of the calculations performed on the IBM 7094/1401 digital computer are plotted in the following figures.

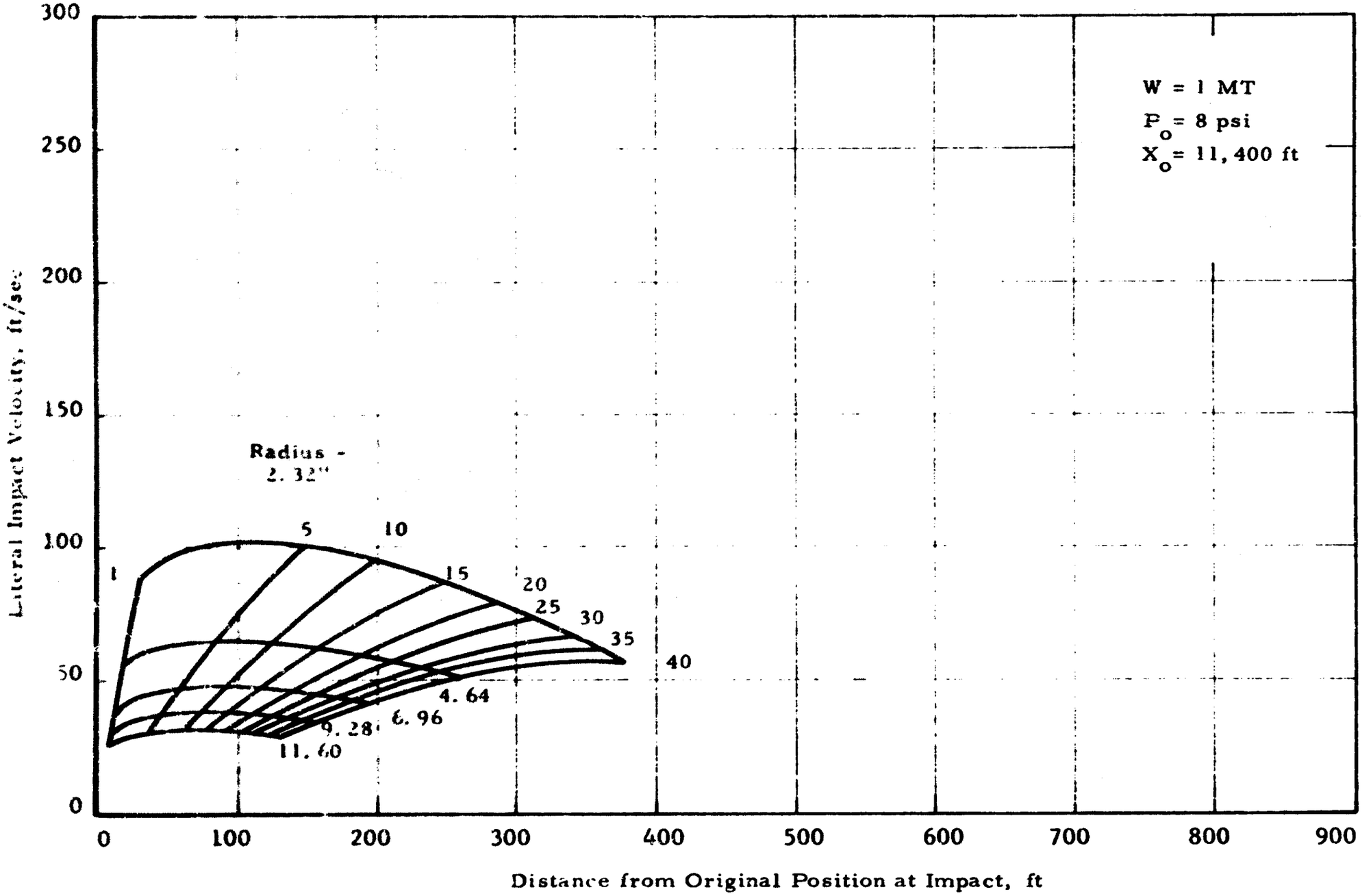

Fig. D.1 TRANSPORT CURVES AT 11, 400 ft FROM 1 MT SURFACE BURST

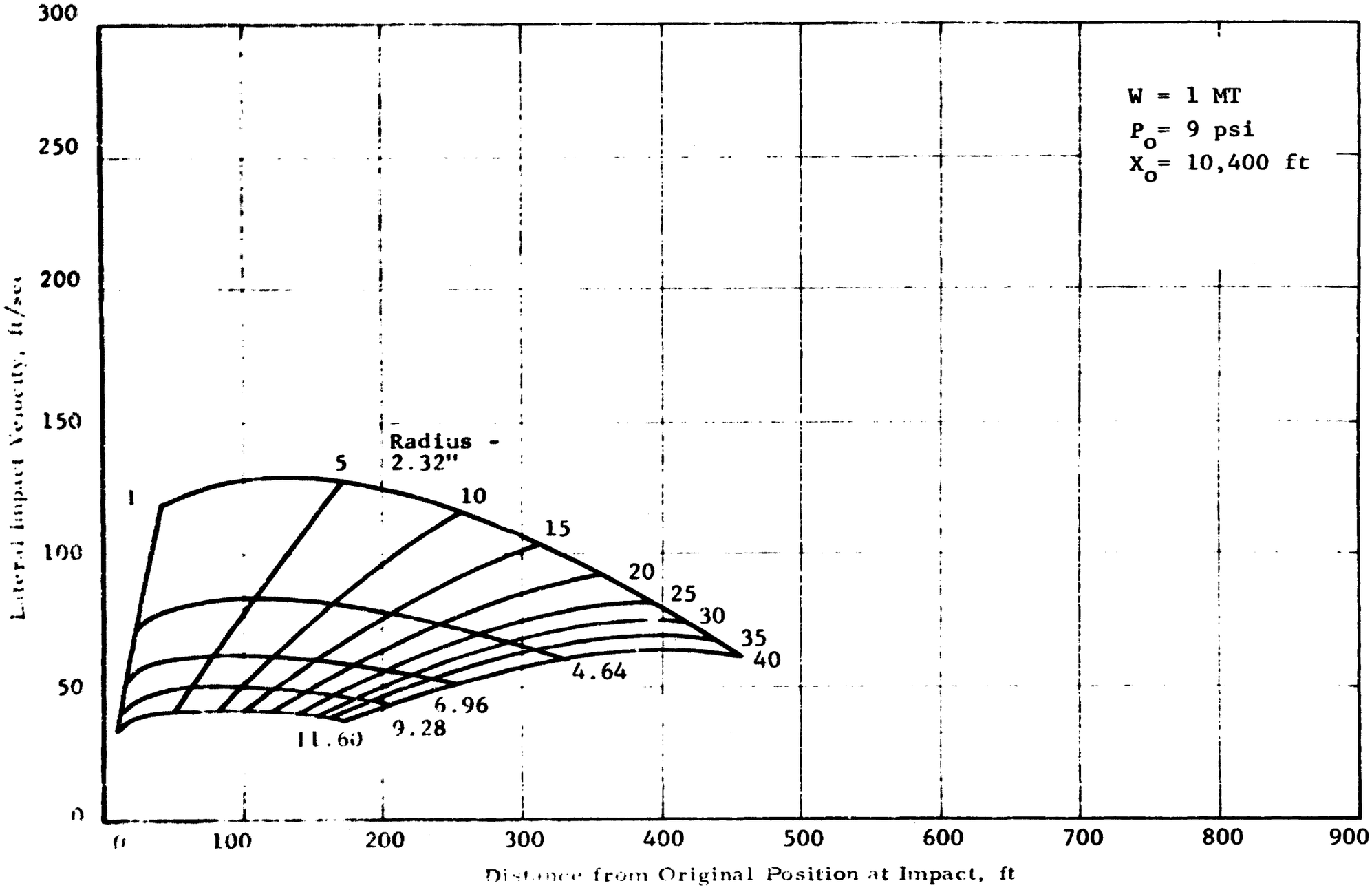

FIG. 9. [illegible] CURVES AT 10,400 ft FROM 1 MT SURFACE BURST

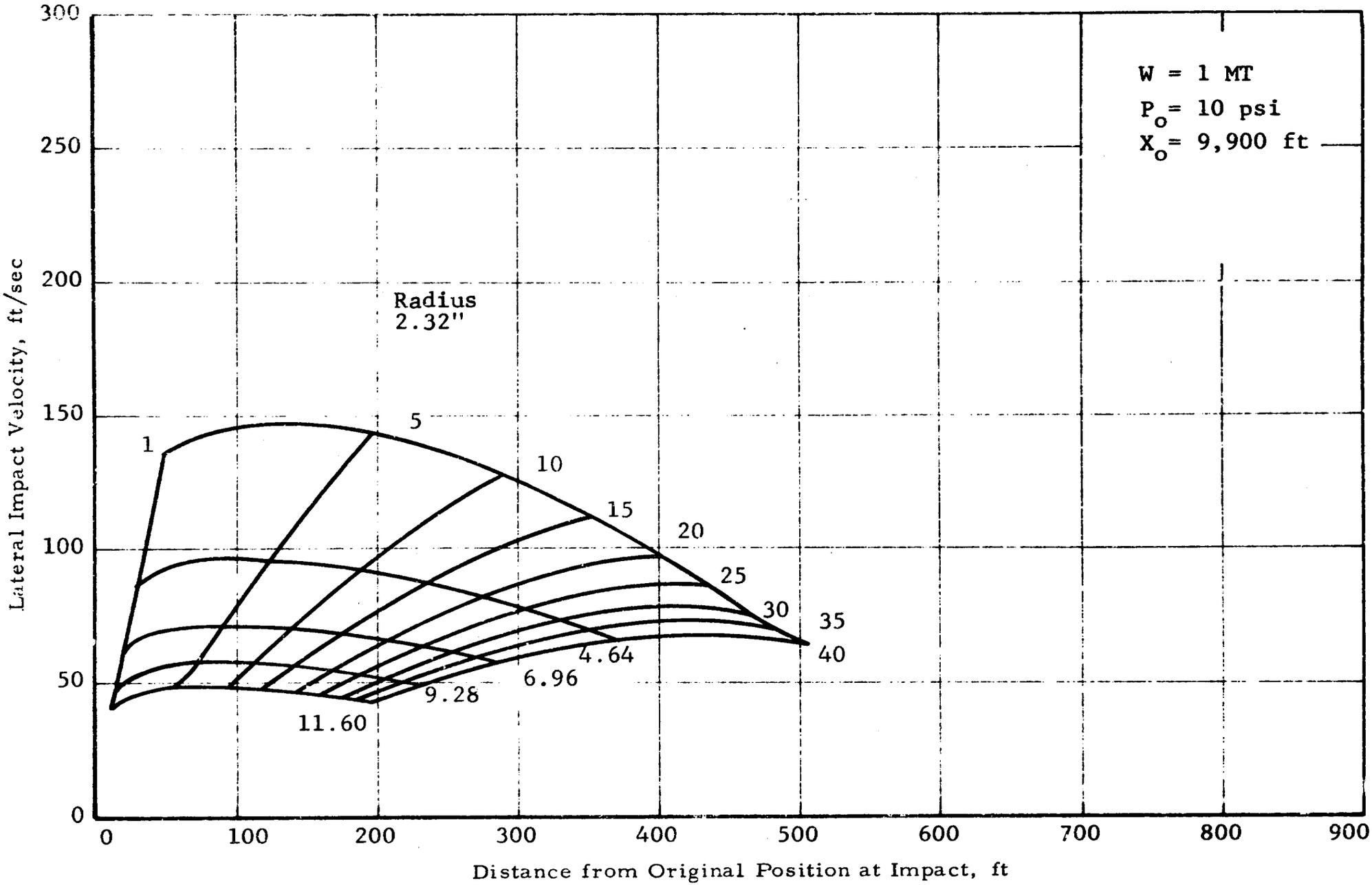

Fig. D. 3 TRANSPORT CURVES AT 9,900 ft FROM 1 MT SURFACE BURST

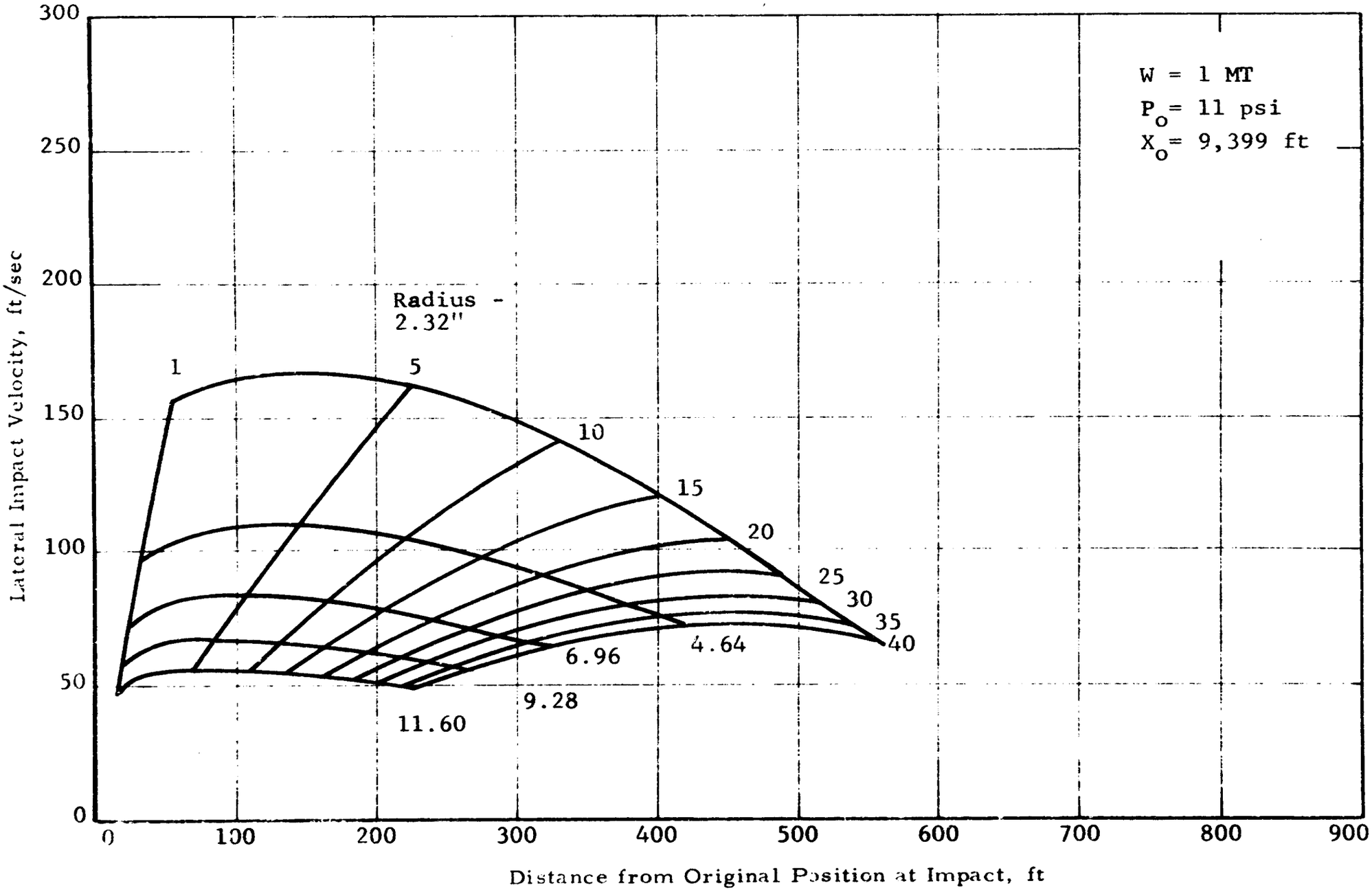

FIG. D.4 TRANSPORT CURVES AT 9,400 ft FROM 1 MT SURFACE BURST

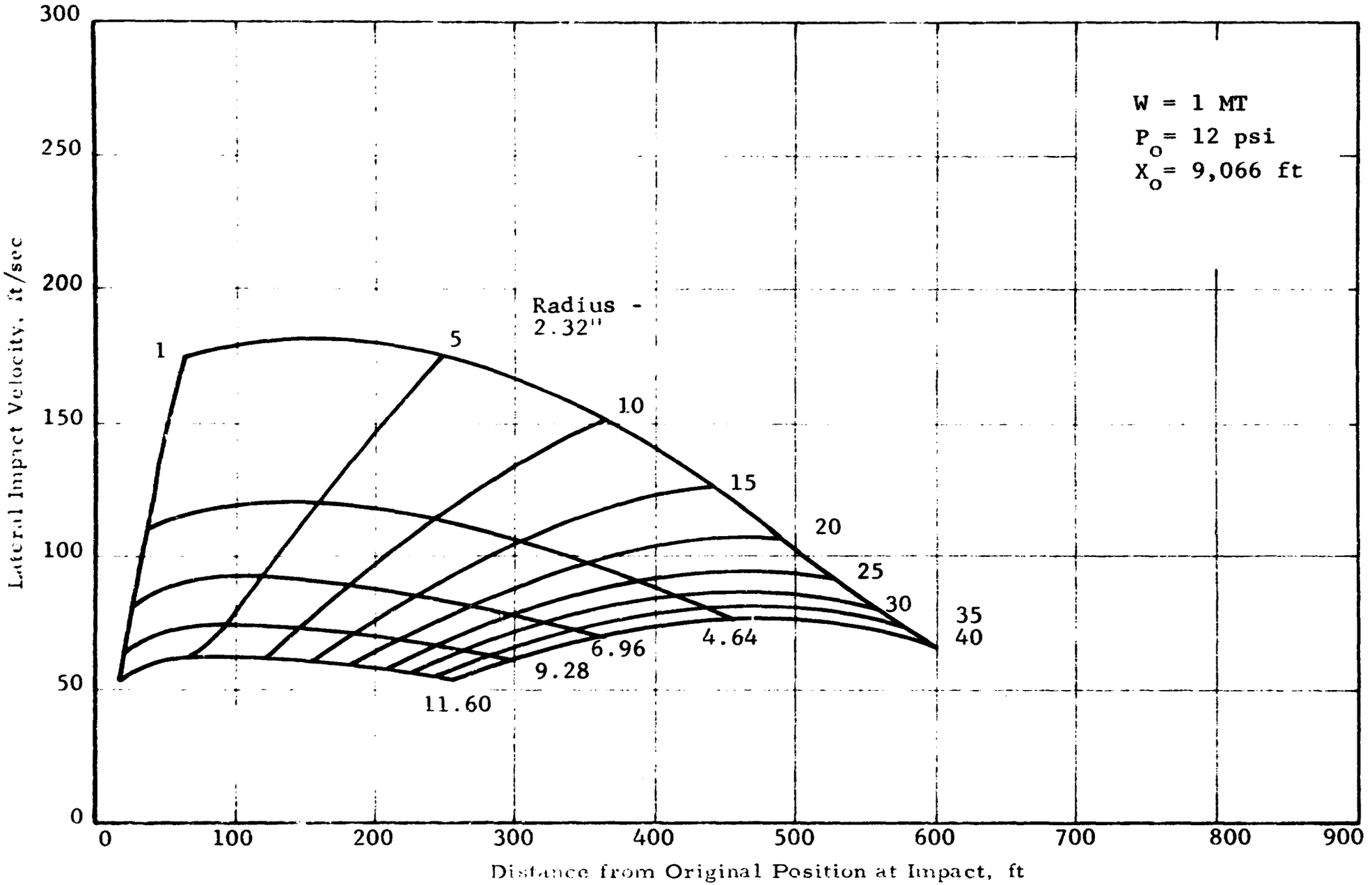

Fig. 12.5 TRANSPORT CURVES AT 9,066 ft FROM 1 MT SURFACE BURST

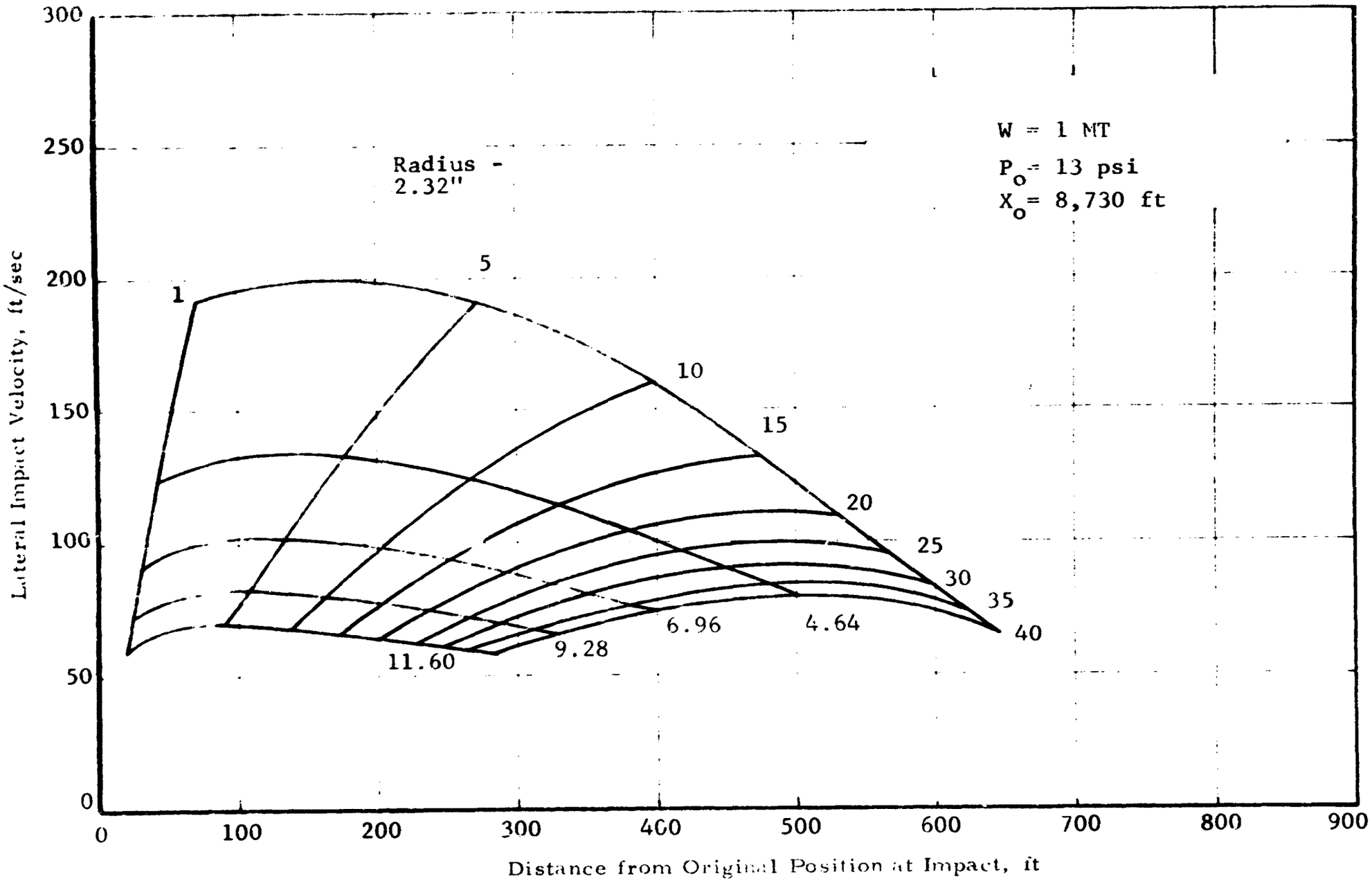

FIG. D.5 TRANSPORT CURVES AT 8,733 ft FROM 1 MT SURFACE BURST

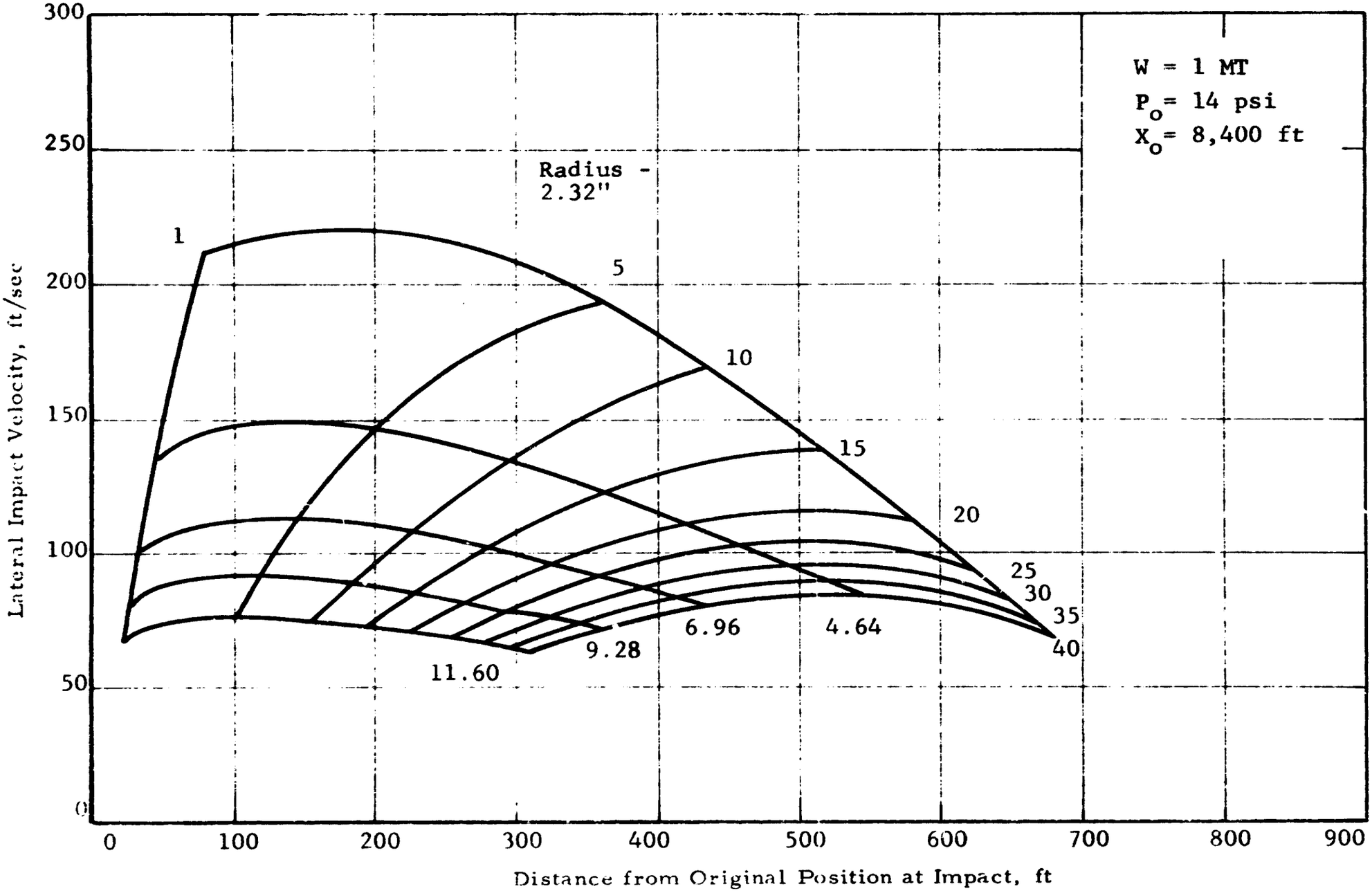

Fig. D.7 TRANSPORT CURVES AT 3,400 ft FROM 1 MT SURFACE BURST

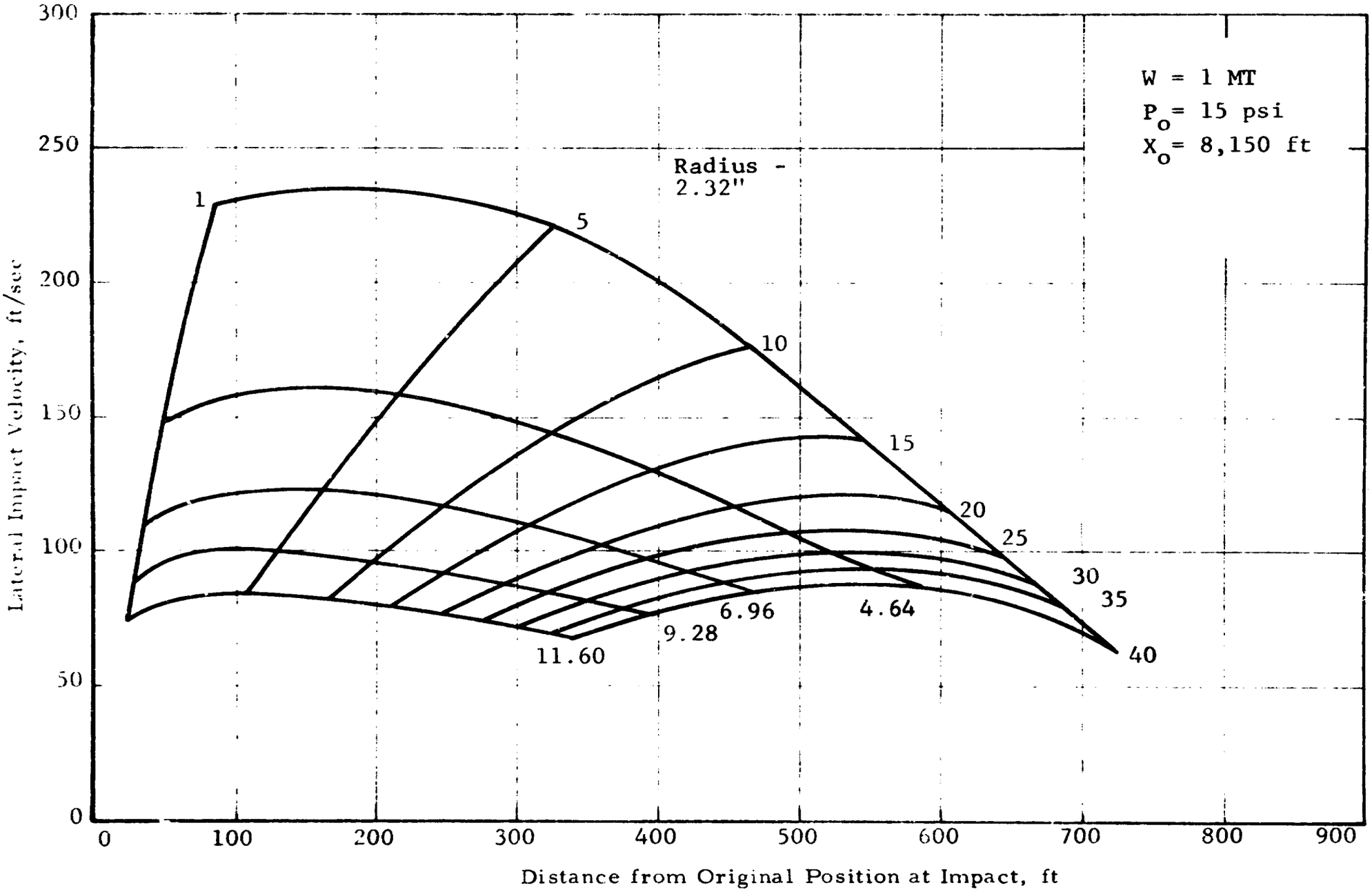

Fig. D. 8 TRANSPORT CURVES AT 8, 150 ft FROM 1 MT SURFACE BURST

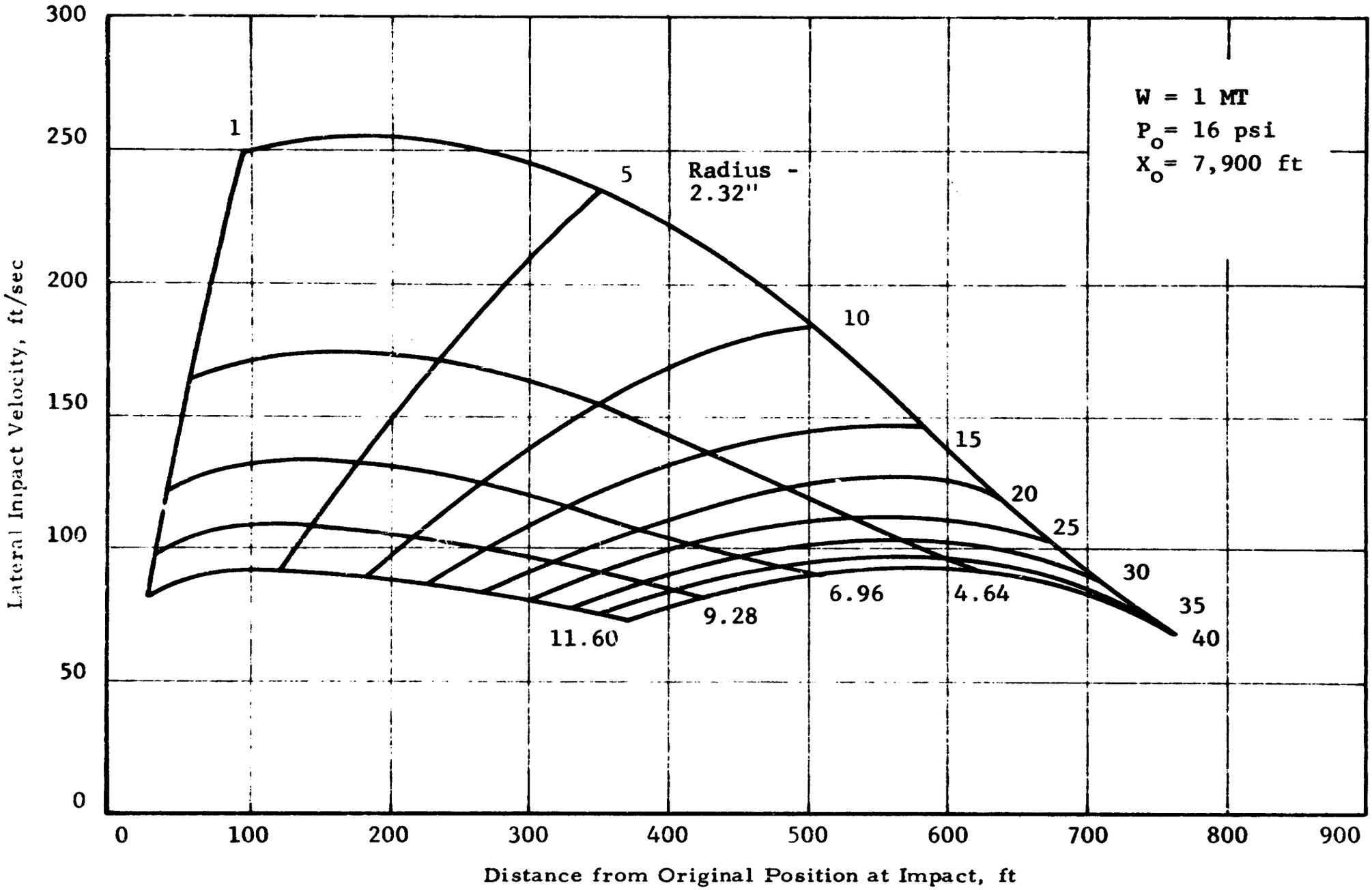

Fig. D. 9 TRANSPORT CURVES AT 7,900 ft FROM 1 MT SURFACE BURST

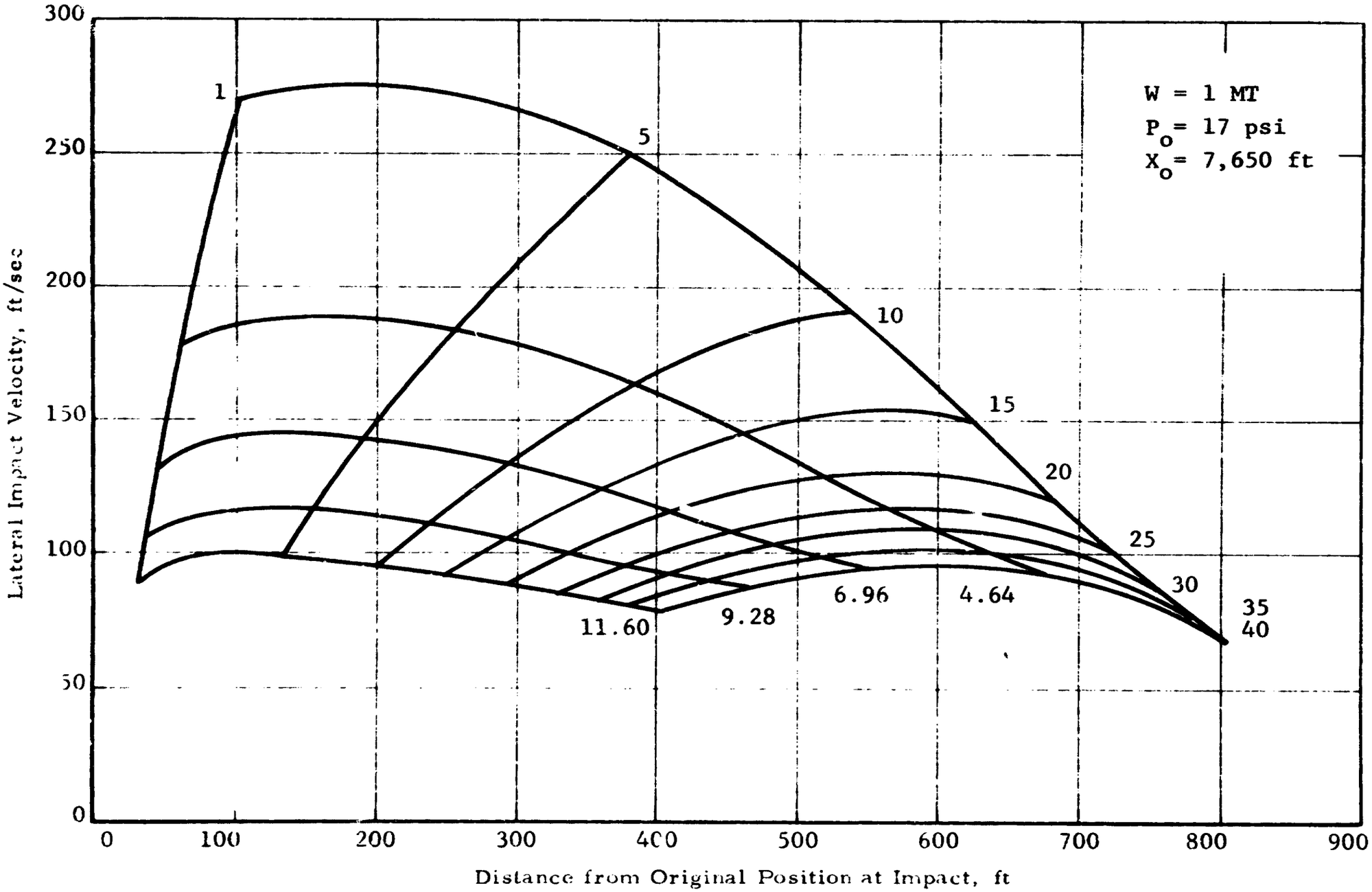

Fig. D.10 TRANSPORT CURVES AT 7,650 ft FROM 1 MT SURFACE BURST

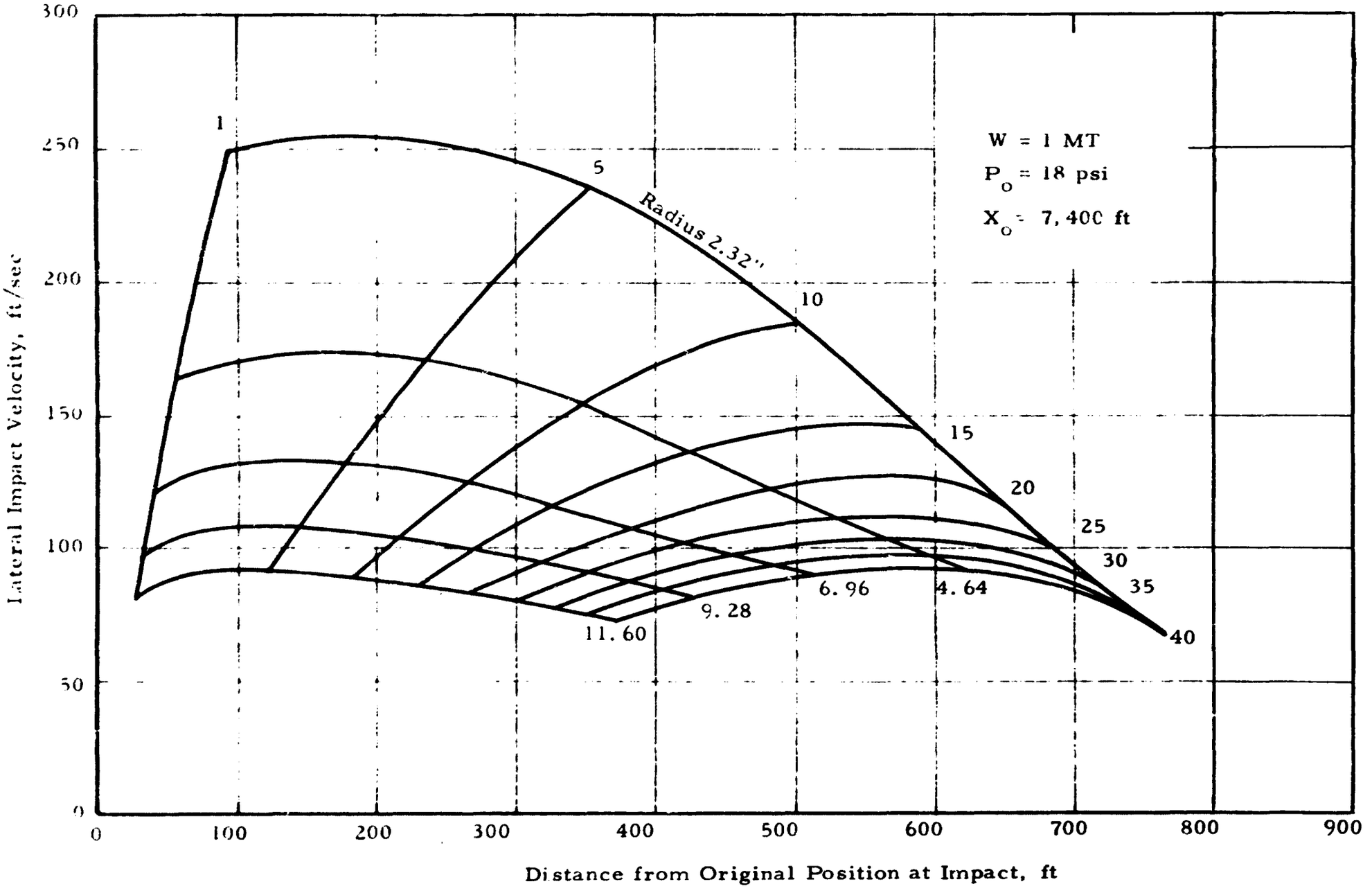

Fig. D.11 TRANSPORT CURVES AT 7,400 ft FROM 1 MT SURFACE BURST

APPENDIX E

DEBRIS PROFILES FOR HYPOTHETICAL WALL; W = 1 MT

Debris profiles were developed for the example wall as outlined in Chapter Four. In addition to varying the height of the wall, the fragment piecesize distribution was also varied in some cases.

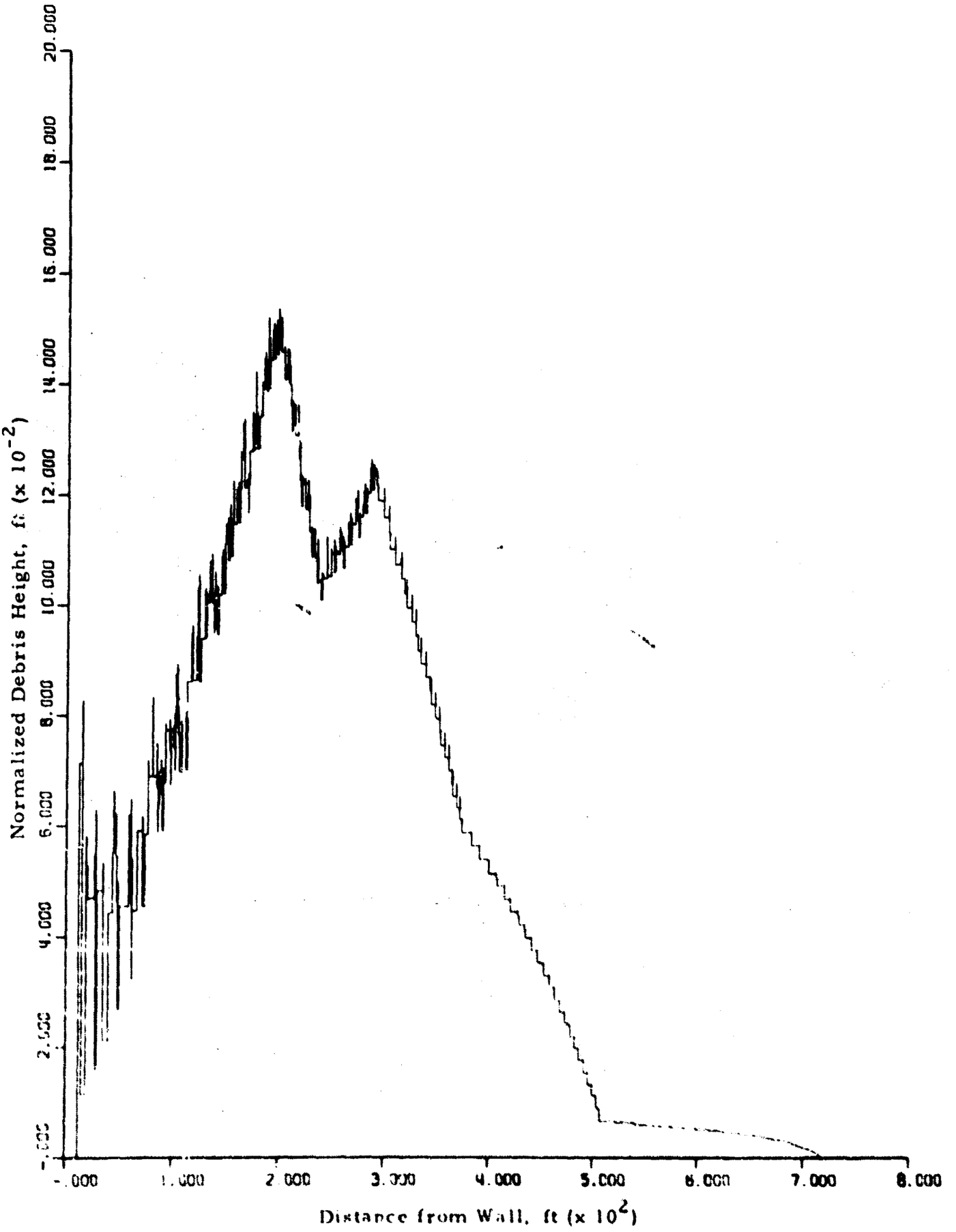

Fig. E.1 DEBRIS PROFILE FOR A WALL HEIGHT OF 40 STORIES EXPOSED TO 10 psi AT 1 MT

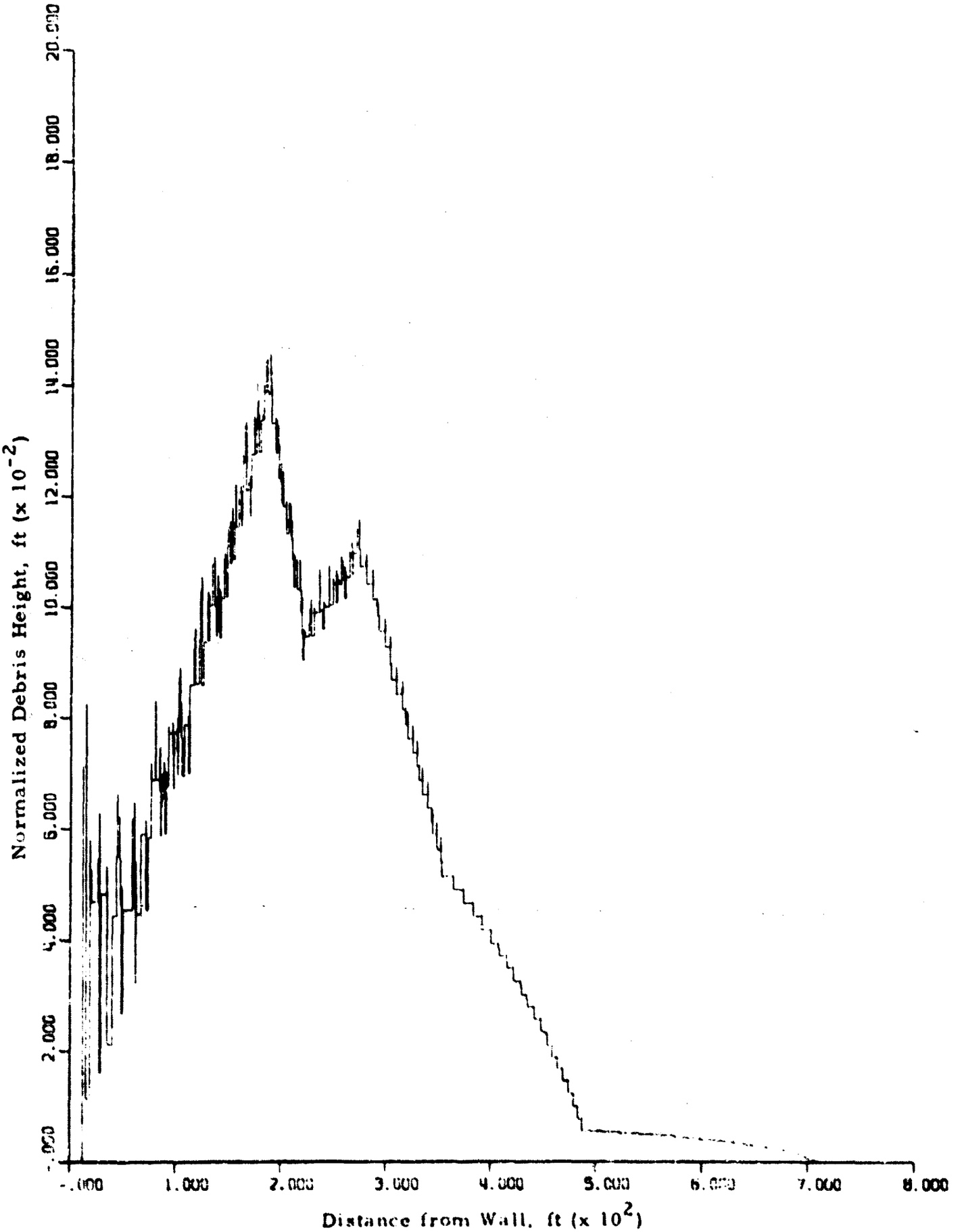

FIG. E.2 DEBRIS PROFILE FOR A WALL HEIGHT OF 35 STORIES EXPOSED TO 10 psi AT 1 MT

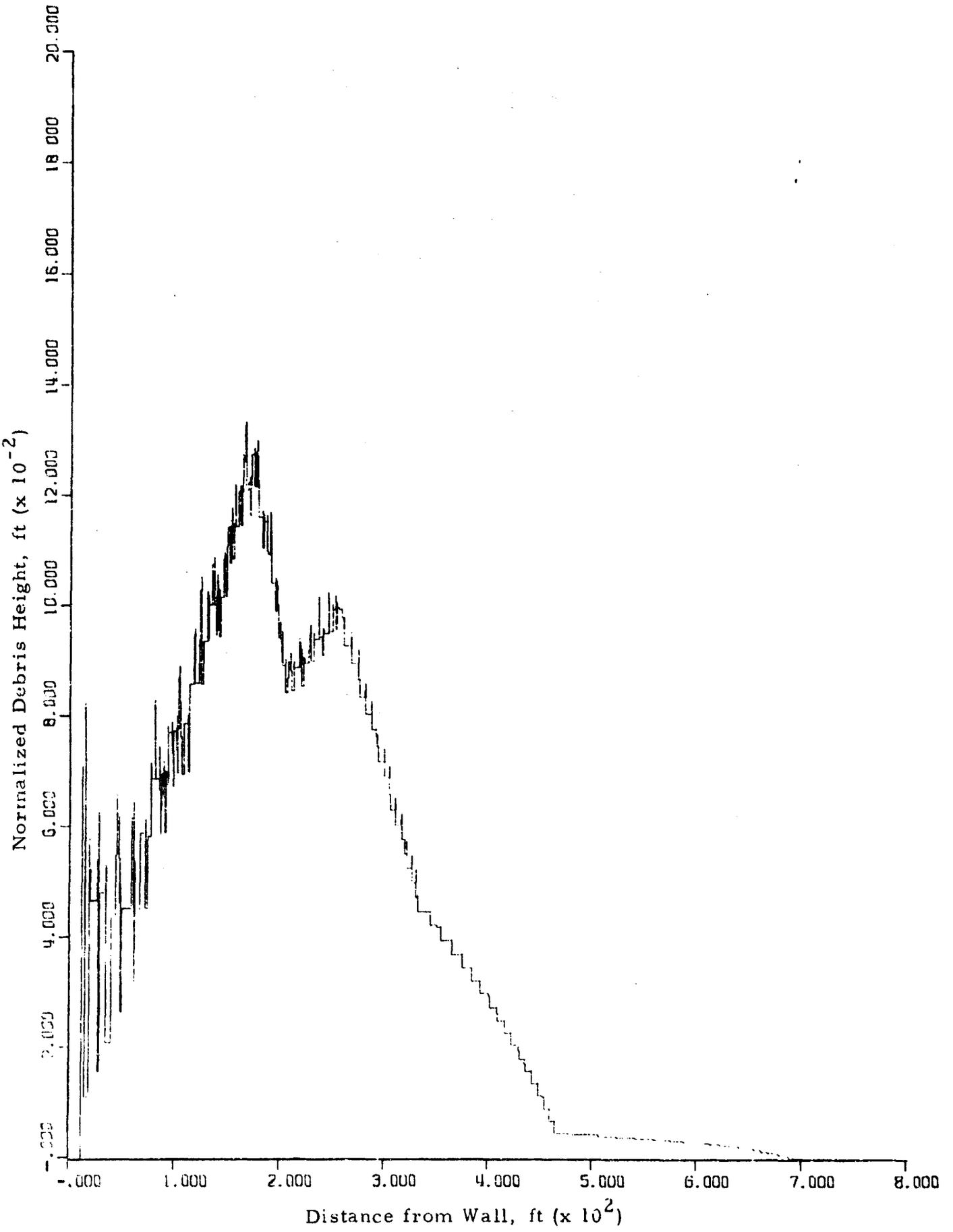

Fig. E. 3 DEBRIS PROFILE FOR A WALL HEIGHT OF 30 STORIES EXPOSED TO 10 psi AT 1 MT

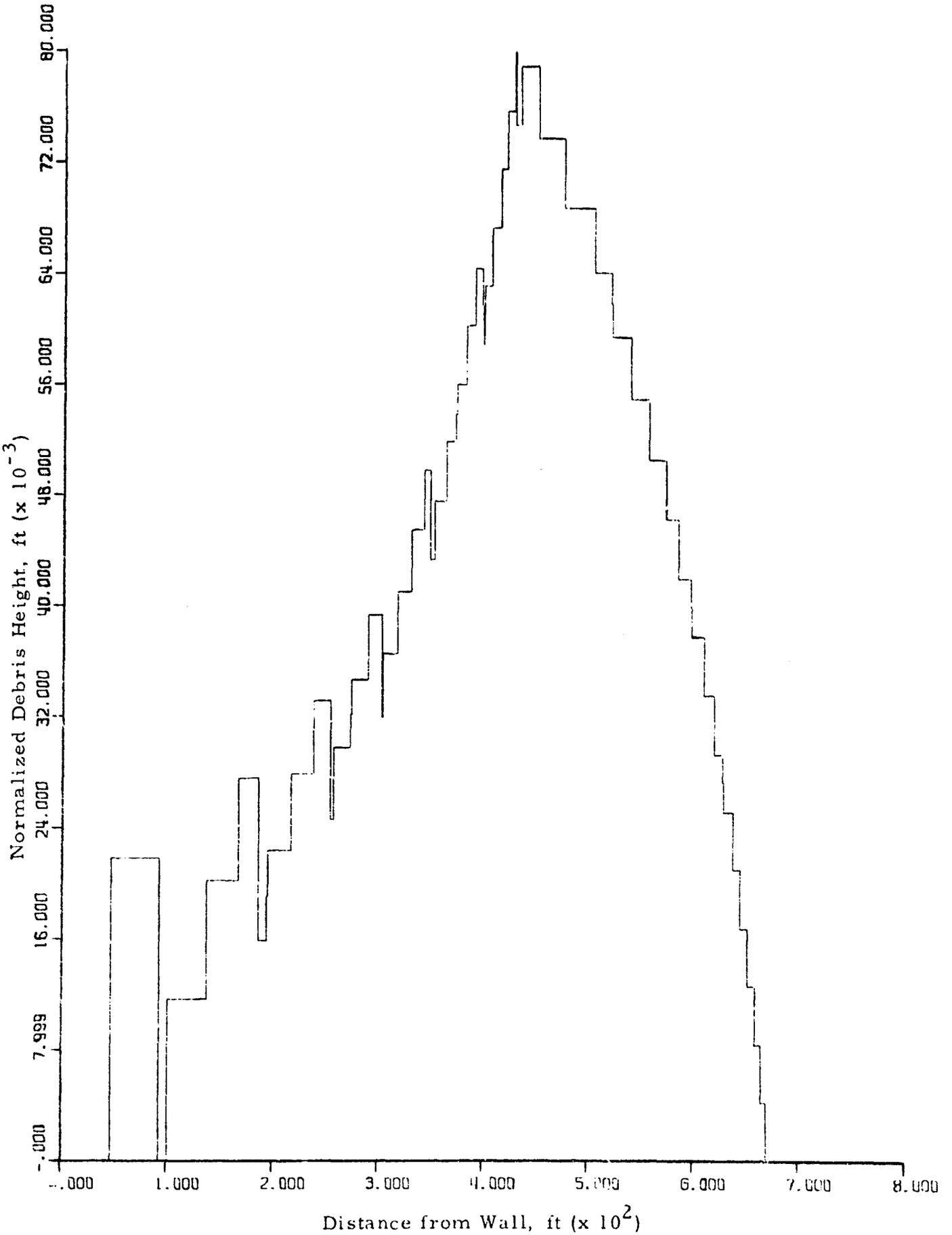

Fig. E.4 DEBRIS PROFILE FOR A WALL HEIGHT OF 25 STORIES EXPOSED TO 10 psi AT 1 MT (All Small Particles)

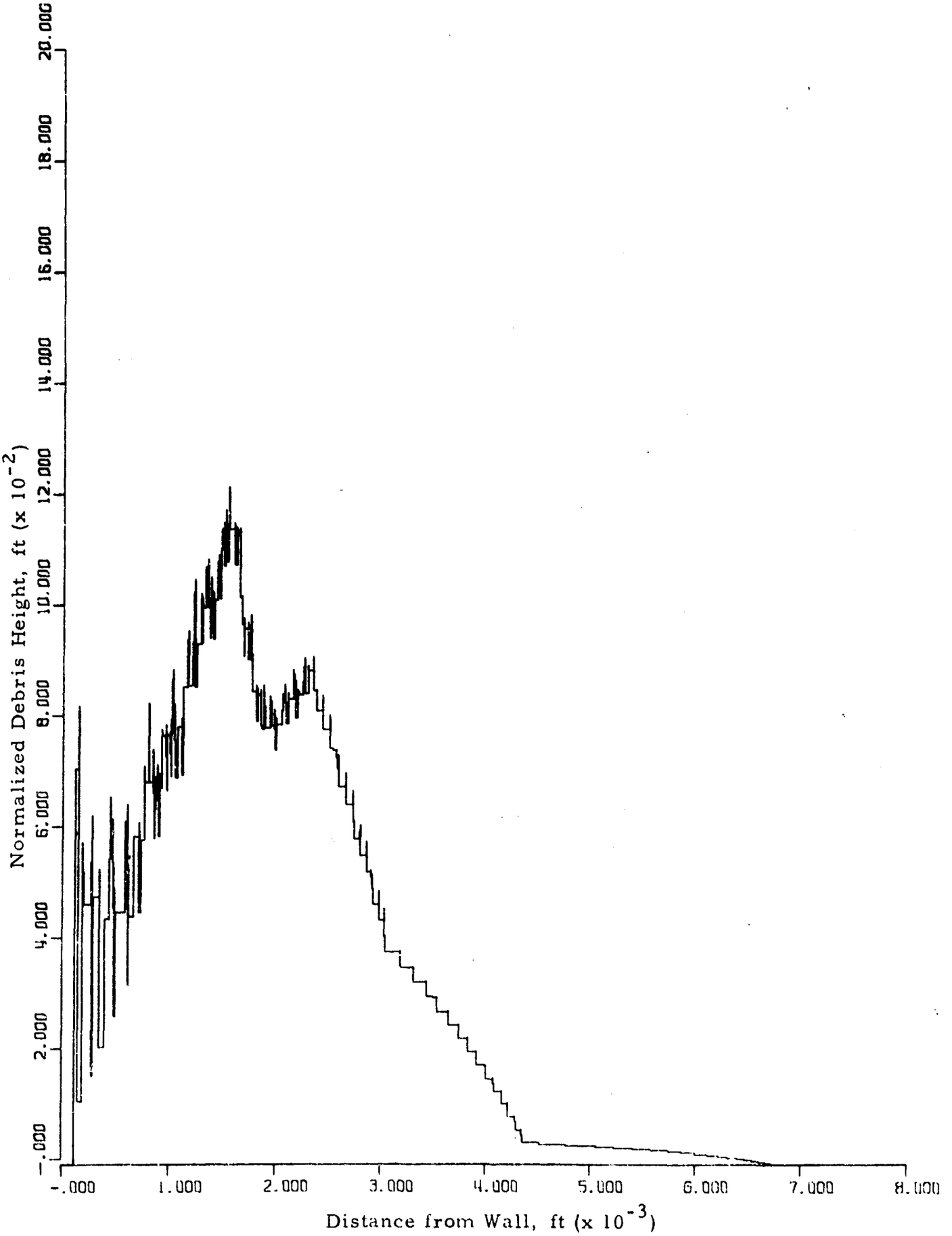

Fig. E. 5 DEBRIS PROFILE FOR A WALL HEIGHT OF 25 STORIES EXPOSED TO 10 psi AT 1 MT

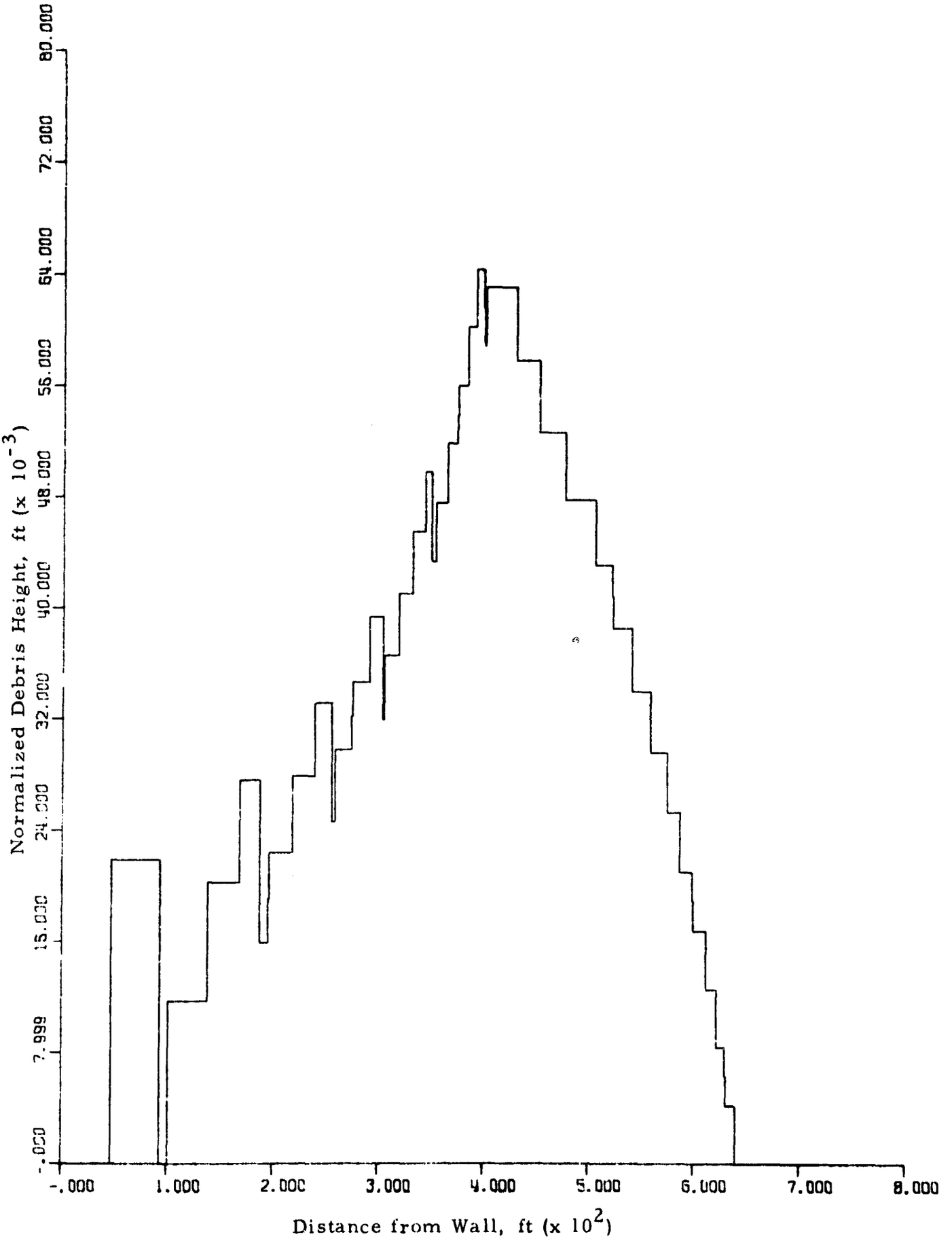

Fig. E. 6 DEBRIS PROFILE FOR A WALL HEIGHT OF 20 STORIES EXPOSED TO 10 psi AT 1 MT (All Small Particles)

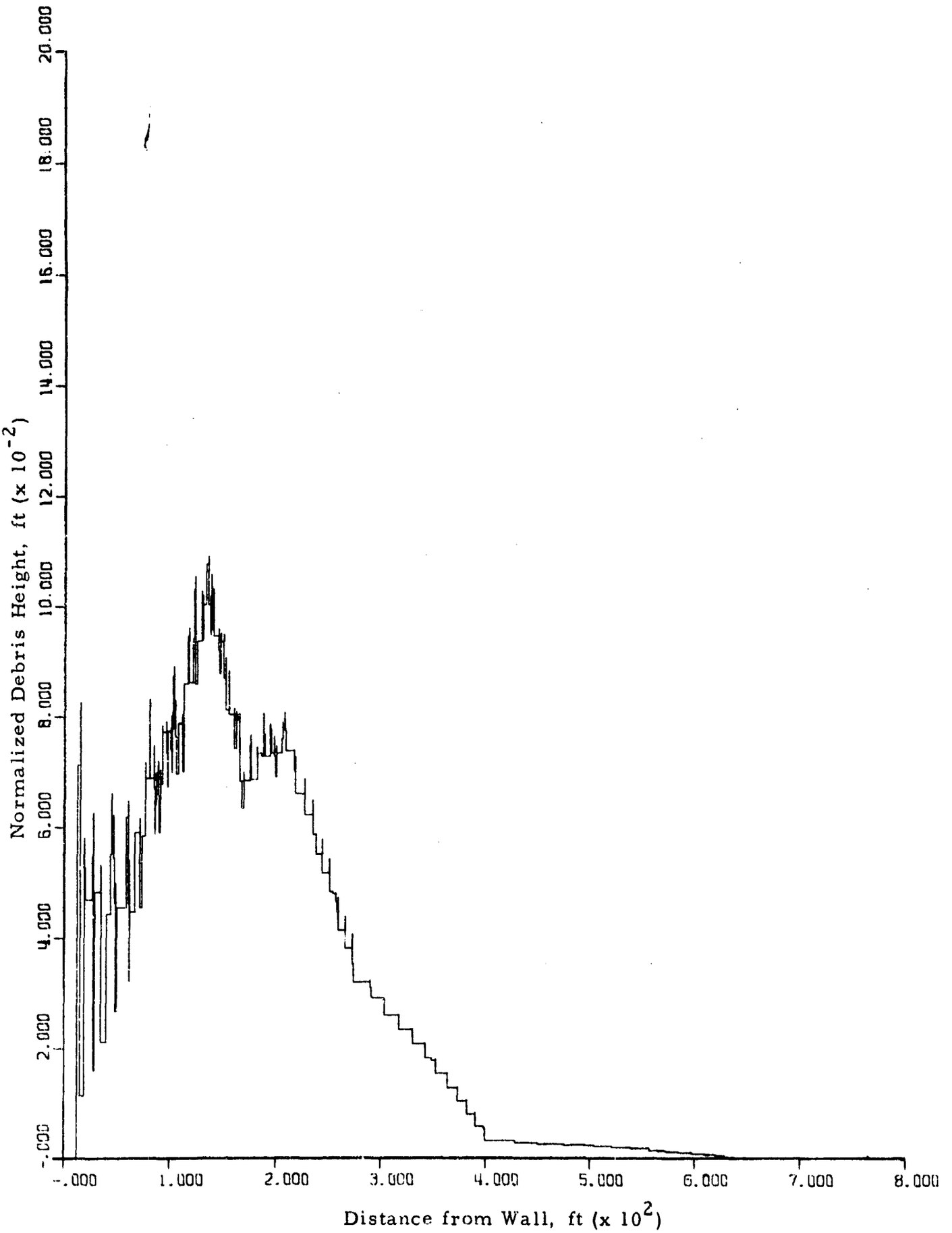

Fig. E. 7 DEBRIS PROFILE FOR A WALL HEIGHT OF 20 STORIES EXPOSED TO 10 psi AT 1 MT

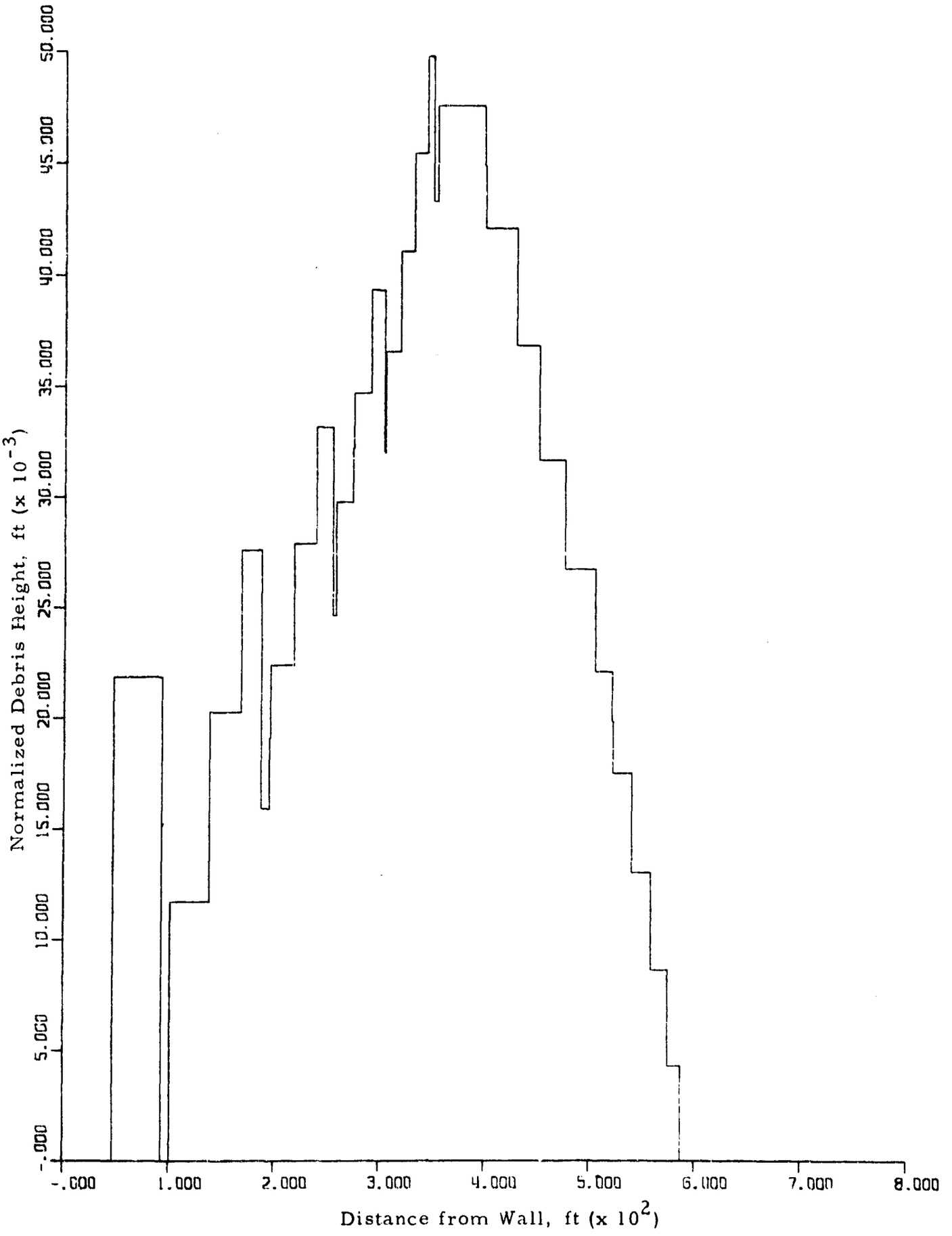

Fig. E. 8 DEBRIS PROFILE FOR A WALL HEIGHT OF 15 STORIES EXPOSED TO 10 psi AT 1 MT (All Small Particles)

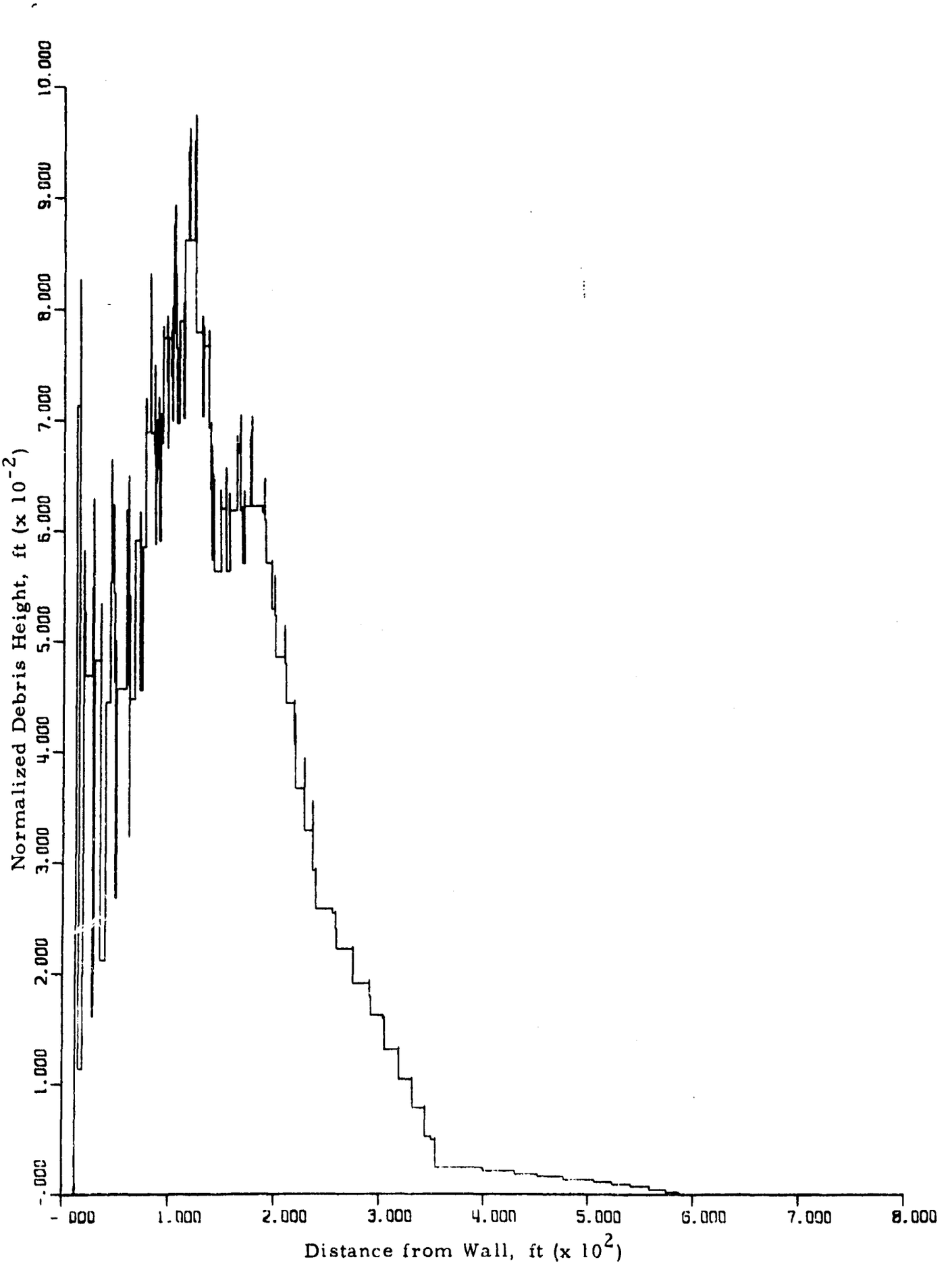

Fig. E. 9 DEBRIS PROFILE FOR A WALL HEIGHT OF 15 STORIES EXPOSED TO 10 psi AT 1 MT

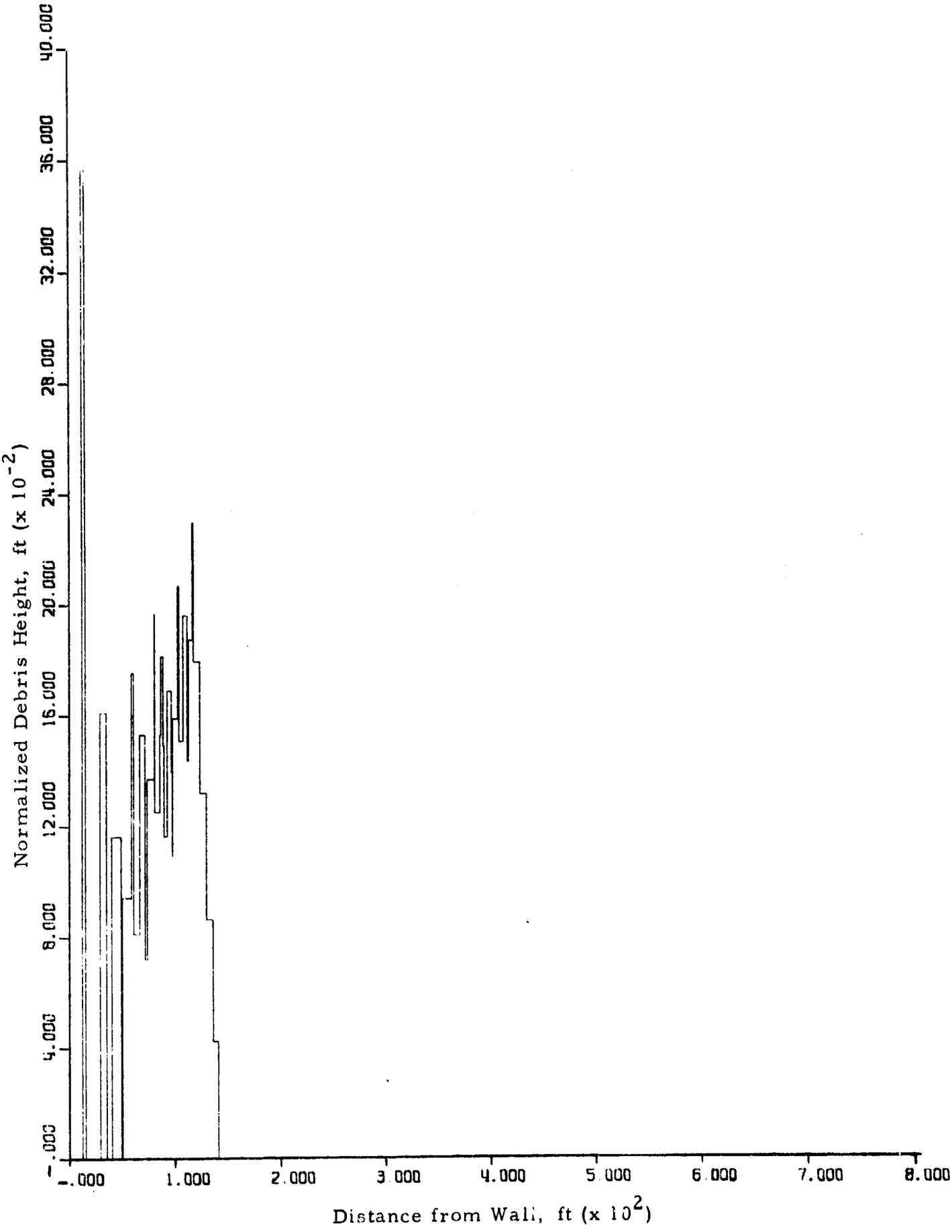

Fig. E.10 DEBRIS PROFILE FOR A WALL HEIGHT OF 15 STORIES EXPOSED TO 10 psi AT 1 MT (ALL Large Particles)

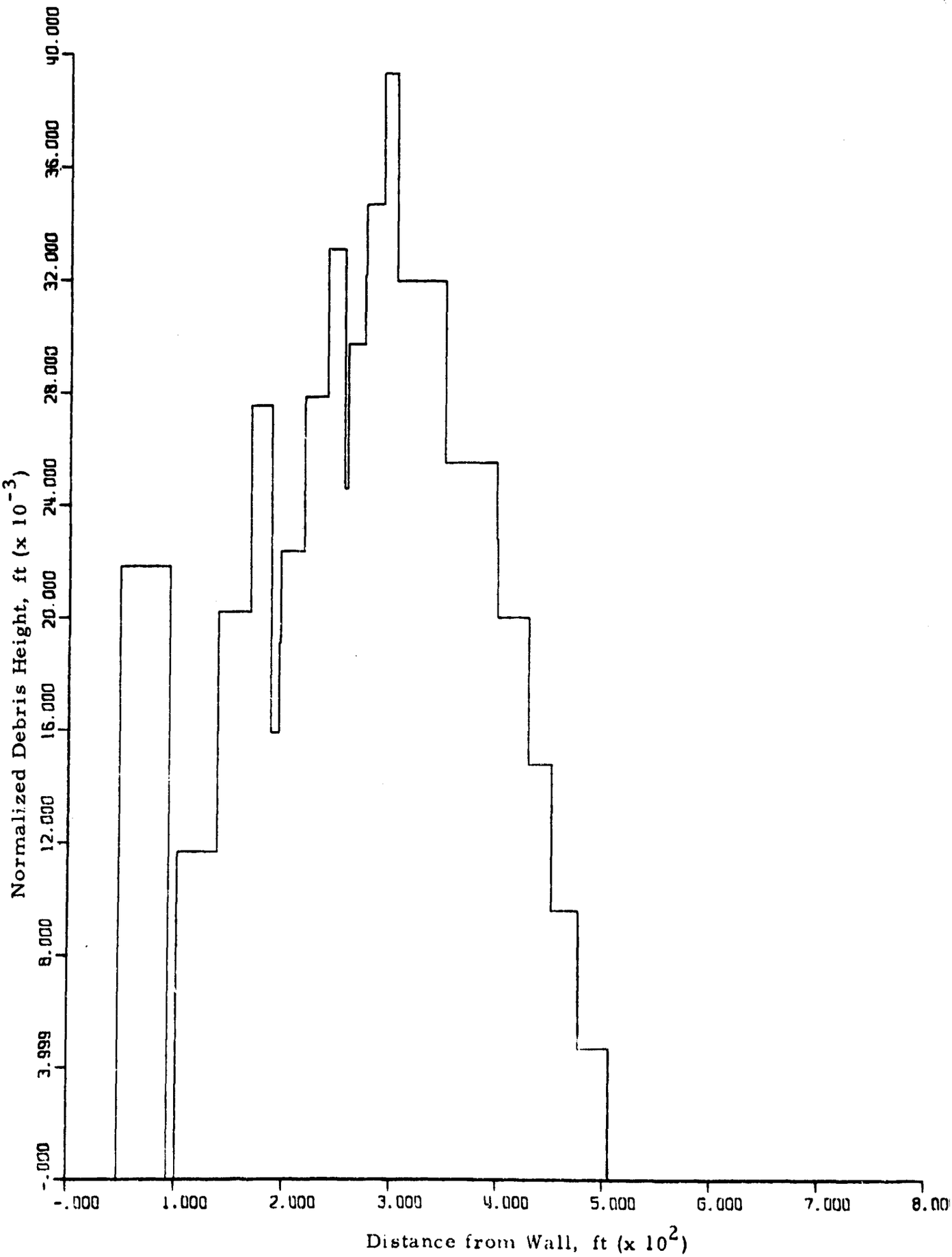

Fig. E.11 DEBRIS PROFILE FOR A WALL HEIGHT OF 10 STORIES EXPOSED TO 10 psi AT 1 MT (All Small Particles)

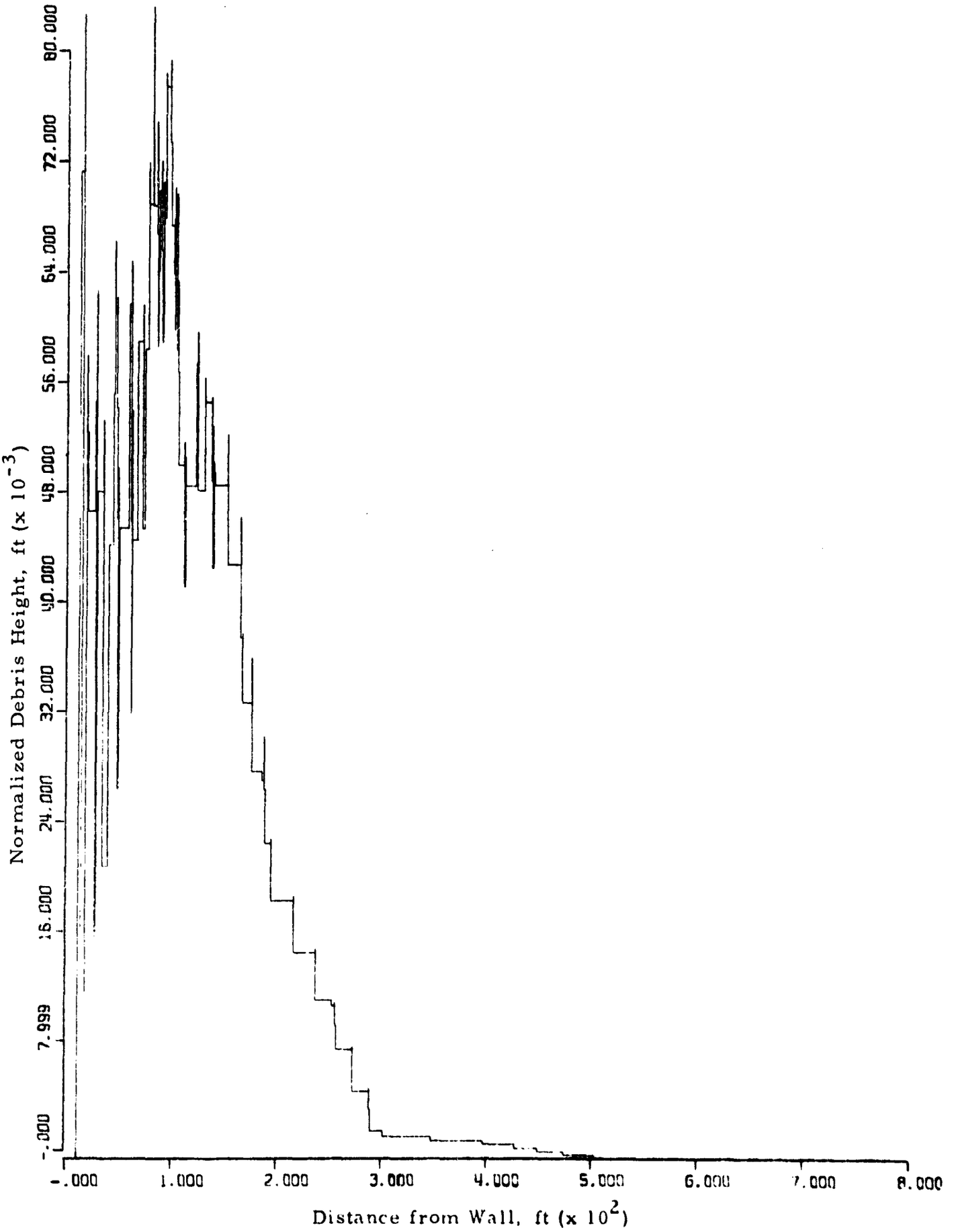

Fig. E.12 DEBRIS PROFILE FOR A WALL HEIGHT OF 10 STORIES EXPOSED TO 10 psi AT 1 MT

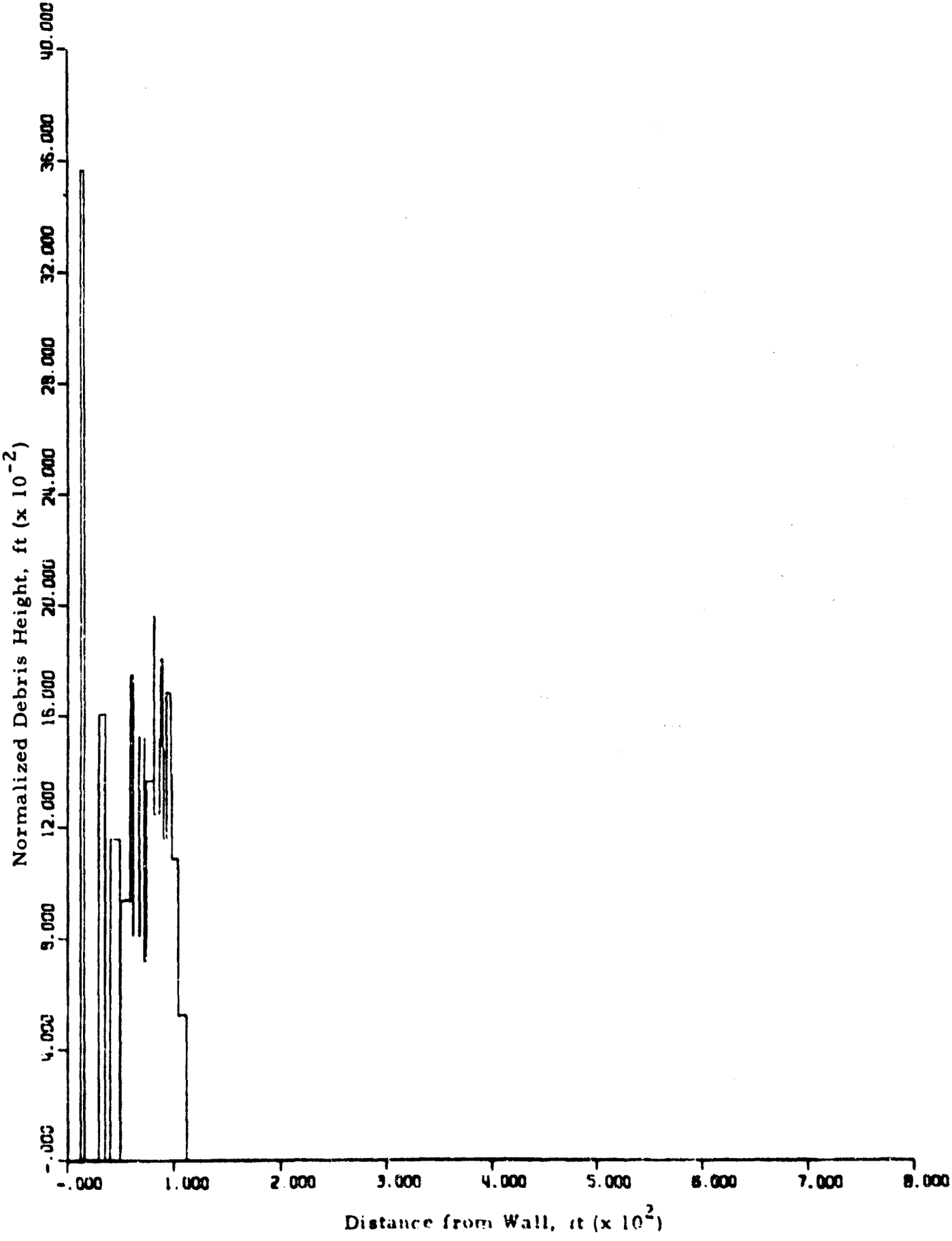

Fig. E.13 DEBRIS PROFILE FOR A WALL HEIGHT OF 10 STORIES EXPOSED TO 10 psi AT 1 MT (All Large Particles)

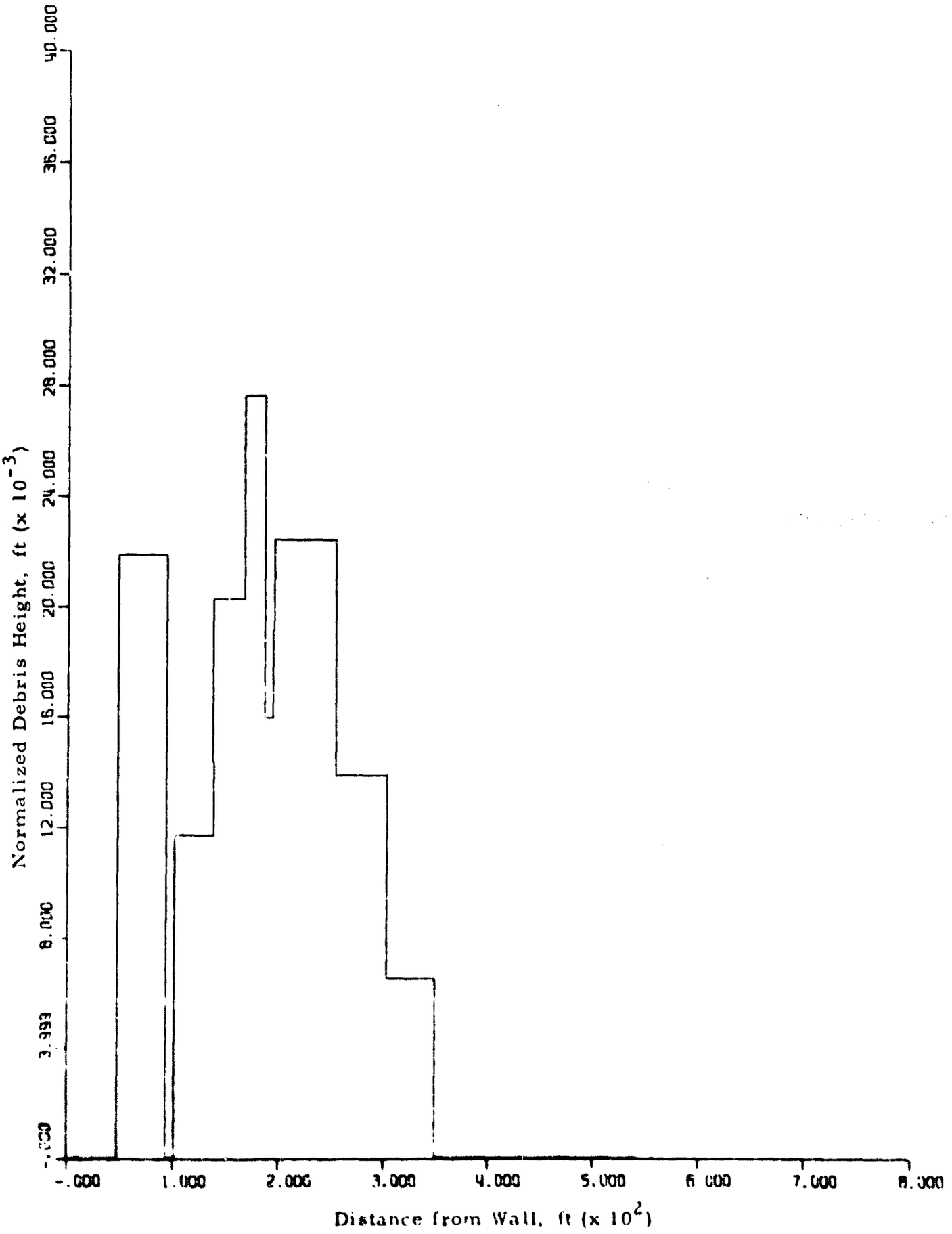

Fig. E.14 DEBRIS PROFILE FOR A WALL HEIGHT OF 5 STORIES EXPOSED TO 10 psi AT 1 MT (All Small Particles)

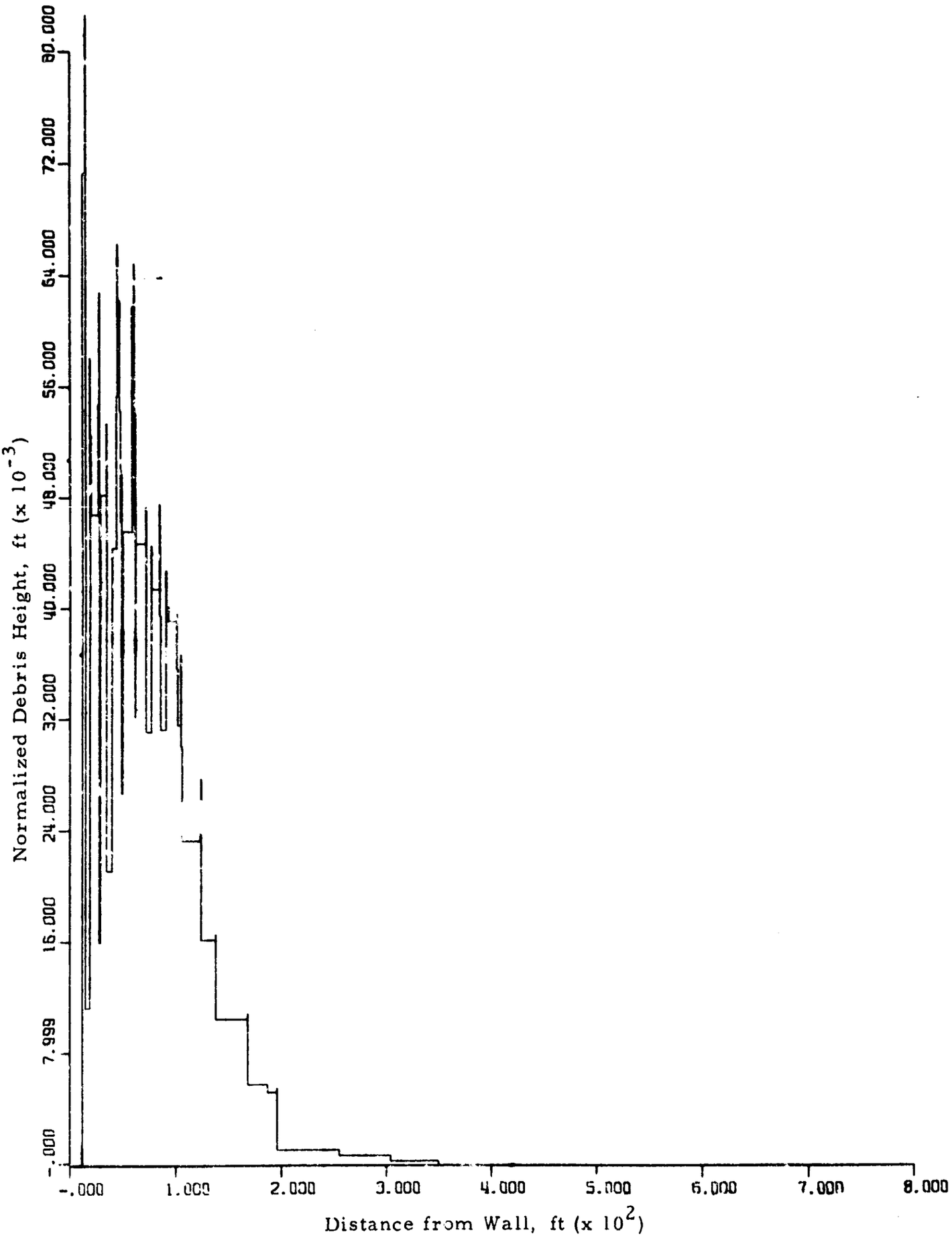

Fig. E.15 DEBRIS PROFILE FOR A WALL HEIGHT OF 5 STORIES EXPOSED TO 10 psi AT 1 MT

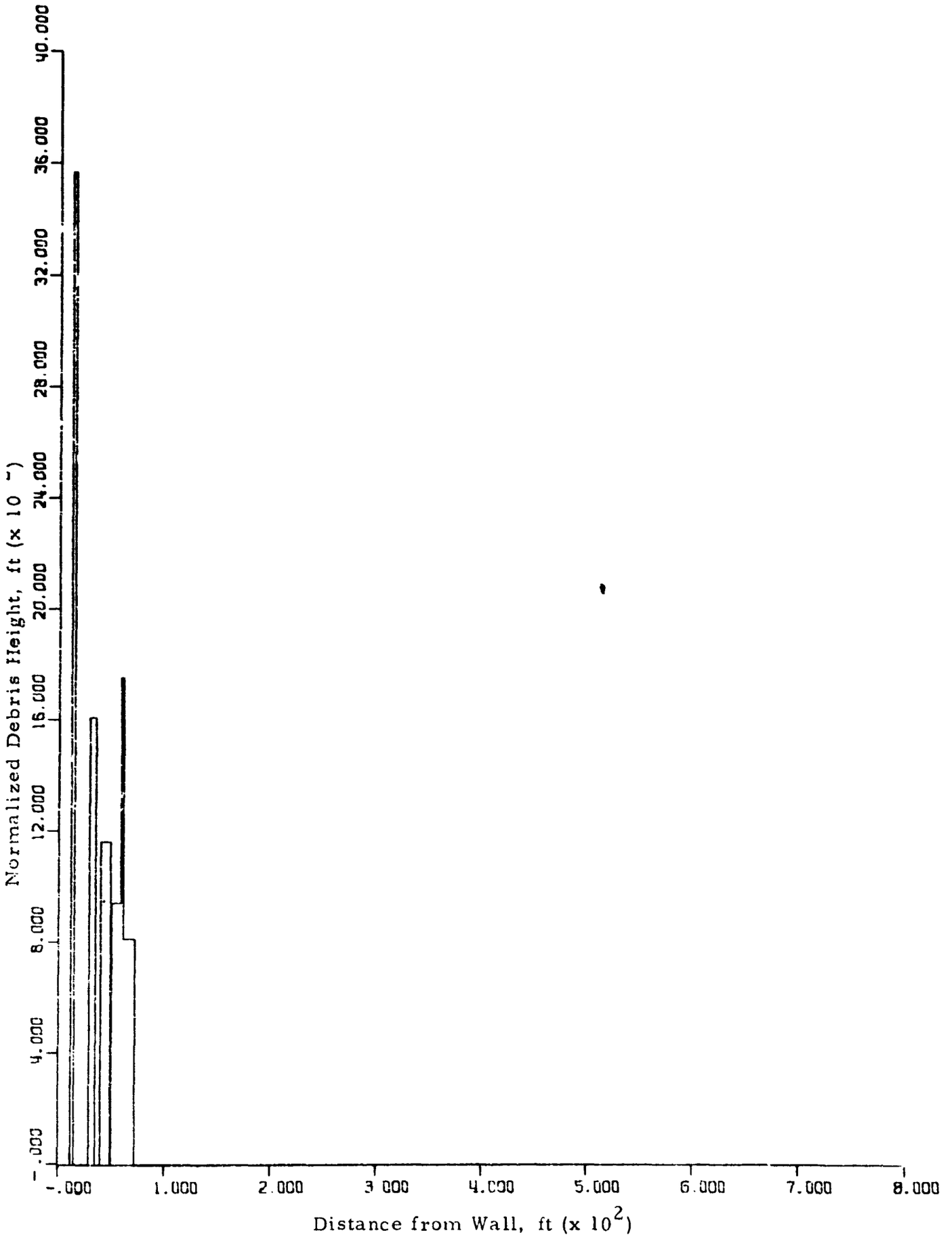

Fig. E.16 DEBRIS PROFILE FOR A WALL HEIGHT OF 5 STORIES EXPOSED TO 10 psi AT 1 MT (All Large Particles)

Unclassified

Security Classification

DOCUMENT CONTROL DATA - R&D

(Security classification of title, body of abstract and indexing annotation must be entered when the overall report is classified)

1. ORIGINATING ACTIVITY (Corporate author)	2a. REPORT SECURITY CLASSIFICATION
IIT Research Institute 10 West 35th Street Chicago, Illinois	Unclassified
	2b GROUP N/A

3. REPORT TITLE

"Debris Distribution"

4. DESCRIPTIVE NOTES (Type of report and inclusive dates)

Final Report and Summary March 1966

5. AUTHOR(S) (Last name, first name, initial)

Feinstein, David I.

6. REPORT DATE	7a. TOTAL NO. OF PAGES	7b. NO. OF REFS
March 1966	115	13

8a. CONTRACT OR GRANT NO.	9a. ORIGINATOR'S REPORT NUMBER(S)
OCD-PS-64-50, Work Unit 3322B b. PROJECT NO.	M6066
c.	9b. OTHER REPORT NO(S) (Any other numbers that may be assigned this report)
d.	N/A

10. AVAILABILITY/LIMITATION NOTICES

Distribution of this document is unlimited.

11. SUPPLEMENTARY NOTES	12. SPONSORING MILITARY ACTIVITY
	Office of Civil Defense Washington, D. C.

13. ABSTRACT

This study is a continuation of the "Debris Clearance Study." That study developed methods of estimating gross debris accumulation in various types of urban areas, based on total structural demolition and uniform distribution of the debris over a given size area. The present study makes use of several of the tools developed in the previous report and expanded herein to more accurately predict the debris distribution. Structural fragmentation is defined for a particular set of blast and structural parameters. The trajectories of the transportable material are calculated, and the distribution of this material is found by size as well as mass. In order to establish the credibility of the fragmentation theories which were developed, a series of experiments were conducted on brittle beams under dynamic loading. A sample problem is worked out that utilizes the above techniques on a hypothetical building to illustrate how the building's debris distribution may appear under various conditions of building height and fragment size distribution.

DD FORM 1 JAN 64 1473

Unclassified

Security Classification